Finite Drift Orbit Effects in a Tokamak Pedestal

by

Grigory Kagan

M.S. Physics, Advanced School of General and Applied Physics (2005)

Submitted to the Department of Physics in partial fulfillment of the requirements for the degree of Doctor of Philosophy in Physics

at the

MASSACHUSETTS INSTITUTE OF TECHNOLOGY

September 2009

Author.....

Department of Physics

August 26, 2009

Certified by.....

Peter Catto

Senior Research Scientist, Plasma Science and Fusion Center

Thesis supervisor

Certified by.....

Miklos Porkolab

Professor, Department of Physics

Thesis Co-Supervisor

Accepted by.....

Thomas Greytak

Professor, Associate Department Head for Education

Finite Drift Orbit Effects in a Tokamak Pedestal

by
Grigory Kagan
M.S. Physics, Advanced School of General and Applied Physics (2005)

Submitted to the Department of Physics on May 19th, 2009
in partial fulfillment of the requirements for the degree of
Doctor of Philosophy in Physics

Abstract

This thesis aims at better understanding of the tokamak pedestal, which is a defining feature of the so-called "High Confinement Mode" or "H Mode" of tokamak operation. This region is characterized by a drastic plasma density drop over a relatively short radial distance, typically of order of the poloidal ion gyroradius (ρ_{pol}). Experiments demonstrate that H Mode plasmas have superior transport properties compared to other known regimes, making them important for practical fusion energy generation. However, the nature of this improvement is still poorly understood and this thesis provides key new insights.

According to experiments and simulations, plasmas in a tokamak are turbulent and therefore their physics can only be addressed with a formalism that retains short perpendicular wavelengths such as gyrokinetics. To be applicable in the pedestal, the formalism must also be capable of treating background scales as short as ρ_{pol} and conveniently accounting for the effects of finite ion drift orbits whose size scales with ρ_{pol} as well. To this end, we develop a special version of gyrokinetics that employs canonical angular momentum in place of the standard radial gyrokinetic variable. Using this formalism to find the leading order ion distribution function we conclude that the background ion temperature profile in the H Mode regime cannot have a steep ρ_{pol} wide pedestal similar to the one observed for the plasma density.

Having obtained this result, we next deduce that a strong electric field is inherently present in a subsonic pedestal to sustain ion pressure balance, making the ExB drift enter the leading order streaming operator in the kinetic equation. We proceed by analyzing novel features that the existence of the pedestal introduces in collisionless zonal flow, the dominant mechanism controlling the anomalous transport. In particular, we find that due to the electric field modifying ion orbits, the zonal flow residual in the pedestal is enhanced over its core value. This allows us to suggest a new scenario for the pedestal formation.

Since the turbulence level is lowered, we are led to consider neoclassical mechanisms of plasma transport by retaining collisions in our gyrokinetic equation. Then, we observe that the ExB drift entering the gyrokinetic equation makes the neoclassical ion heat conductivity sensitive to the pedestal electric field. Next, with the help of the same technique we evaluate the neoclassical poloidal ion flow. Importantly, we predict that once the equilibrium electric field goes beyond a certain value this flow changes its direction. This result elucidates the discrepancy between the conventional banana regime predictions and recent experimental measurements of the poloidal impurity flow performed at Alcator C-Mod.

Thesis Supervisor: Peter J. Catto
Title: Senior Research Scientist, Theory Head and Assistant Director, PSFC

Thesis Co-Supervisor: Miklos Porkolab
Title: Professor of Physics, Director, PSFC

Acknowledgements

When I started a Ph.D. program at MIT I did not think that it would be over any time soon. Now that I am about to submit this thesis, I feel sorry for not making my Ph.D. period longer. Wherever I find myself in the future, I will miss this school, this city, and these people.

The research summarized in this thesis would never be carried out without fine mentorship of Peter Catto. Peter combines broad and deep expertise in plasma physics with a warm and truly humane attitude and intelligence with patience. He personifies the gold standard of an advisor, which I shall follow if I am ever to supervise a student myself. I am also indebted to Miklos Porkolab, who taught me that in any research project theoretical creativity must be accompanied with physical relevance. Finally, I thank Jeffrey Freidberg for his sympathy and long conversations about career paths.

In addition, I am grateful to my officemates Felix Parra Diaz, Antoine Cerfon and Matt Landreman for always fruitful discussions. I also thank my fellow MIT students who came to support me at my defense, as well as Alexey Zykov and Nikolay Iosifov who made all the way from New York to feed them.

Table of Contents

1 Introduction

The focus of this thesis is in the physics of a tokamak, the most developed version of fusion reactors employing magnetic confinement of plasmas. The idea of such a device was initially proposed by Sakharov and Tamm in 1953 and since then many experimental and theoretical tokamak studies have been conducted. Along the way, a widely recognized break-through was the experimental discovery of the so-called High Confinement Mode or H Mode [1] in which energy transport from plasma in the core of a tokamak is significantly reduced. The distinctive feature of this regime as compared to the Low Confinement Mode or L Mode that had been known before is the existence of the pedestal, the region in which plasma density drops significantly over a relatively short radial scale length.

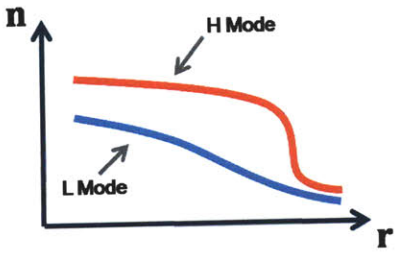

Fig 1.1. Density profiles in H and L modes

The most obvious advantage of the H Mode is higher plasma energy content. Indeed, as shown on Fig 1.1, the area below the profile with a pedestal is greater than that below the smoother L Mode curve. More importantly, it was observed that anomalous transport becomes noticeably lower as a tokamak switches from L to H Mode. This transport is due to the so-called drift wave turbulence that is inevitably present in any fusion reactor due

to the enormous change between the core plasma temperature, which must be as high as a million degrees to initiate the nuclear fusion reaction, and the reactor walls, which can only tolerate plasma at about 1000°C. Evidently, in H Mode such microturbulence is well controlled and hence, understanding the mechanism of attaining and sustaining this regime is crucial for practical fusion power generation.

A great number of studies are concerned with the mechanism of the L-H transition which is still poorly understood. Here we instead concentrate on the physics of the pedestal itself considering it as given. Such an approach, however, will allow us to make reasonable conjectures about the formation of this region of a tokamak. In other words, in this thesis we start with an existing steep density profile, such as sketched in Fig 1.1, and then investigate the consequences. Then, having the self-consistent model of a pedestal in hand we are able to speculate on a possible scenario for the L-H transition.

Theoretical modeling of the H Mode is complicated by existence of two different background scales with the larger one relevant to core plasmas and the shorter to the pedestal region. Therefore, for a formalism aiming at studying such a regime it is desirable to encompass both of these scales in an uncoupled manner. Also, to address the issue of turbulent transport the formalism must be capable of retaining perturbations with wavelengths ranging from the ion Larmor radius to the size of a tokamak. To this end, we have developed a special version of gyrokinetics , an approach that has been successfully

used for describing tokamak core plasmas [2-8], but is not conveniently applicable to sharp density regions in its conventional form.

The original idea of using gyrokinetic variables was proposed by Catto in 1978 [9] who suggested a new way of eliminating the fast Larmor motion scale from the kinetic equation. The need for this elimination took on added importance once it became clear that choosing the time step below the cyclotron period would make the computation time unrealistically large. The technique that had been employed before then is called drift kinetics and based on splitting the yet unknown distribution function into two pieces with one evolving on the cyclotron period time scale and the other being slowly varying. The key point of gyrokinetics is that we can conveniently retain the rapidly oscillating dynamics by introducing a certain change of variables. While giving the same physical results as drift kinetics in the case of perturbation wavelengths much greater than the ion gyroradius, this new technique is more elegant and significantly reduces the amount of analytical work in the process.

More importantly, the gyrokinetic formalism allows retaining the perturbations with perpendicular wavelengths comparable to the ion gyroradius, a feature that drift kinetics does not have. Hence, it soon became a vital instrument in turbulent studies. Nowadays, it has been successfully implemented in codes such as GYRO [6] and GS2 [3] or GTC [5] that are aimed at investigating the fusion relevant plasmas. In addition, its first application in astrophysics has recently appeared [10].

The distinctive feature of the gyrokinetic formalism developed in this thesis is employing the canonical angular momentum in place of usual radial variable. Obviously, this choice makes direct use of the axisymmetry of a tokamak. Furthermore, it naturally separates the ion Larmor radius and poloidal gyroradius spatial scales, responsible for the classical and neoclassical phenomena respectively, thereby conveniently allowing investigations of these two groups of effects in a systematic manner.

When formulated in such a form, gyrokinetics gives important pedestal results in leading order in the poloidal gyroradius expansion parameter. In particular, it suggests that in H Mode the profile of the background ion temperature cannot have a radial scale as short as the poloidal ion gyroradius scale of the plasma density, and so can only vary slowly across the pedestal. By going to the next order, we are able to find the equation that describes zonal flow and neoclassical collisional transport with both the finite Larmor radius (FLR) and finite drift orbit (neoclassical) effects retained. Putting aside the classical FLR effects, we can then concentrate on novel features that these drift phenomena acquire in the pedestal as compared to their well known core counterparts.

Zonal flow is a very common mechanism limiting the turbulence in dynamical systems. It was revealed by drift wave turbulence simulations [4, 11-13] that in the core of a tokamak the zonal flow drastically reduces anomalous transport near marginality by shearing the so-called "turbulent eddies", thereby improving plasma confinement. Soon

after, a proper analytical treatment was performed by Rosenbluth and Hinton [14, 15]. In particular, they found that the plasma shields or reduces the zonal flow by means of neoclassical polarization, but that some fraction of it, the residual, survives.

In the pedestal, neoclassical orbits are modified due to the strong electric field inherent to this region of a tokamak. Therefore, in this thesis we are led to substantially extend the Rosenbluth and Hinton [14] calculation. By studying tokamak particle trajectories in the presence of a strong external electric field and implementing the results in our gyrokinetic formalism we find the pedestal zonal flow is qualitatively different from that in the core. In particular, we demonstrate that for a steep enough density profile the residual is enhanced. This feature in turn allows us to suggest a mechanism for the L-H transition.

Once we realize that ion orbits in the pedestal are different from those in the core due to the electric field, we have to revisit the conventional calculation of neoclassical transport in the banana regime. To carry out this pedestal calculation in the most efficient way we adopt the general framework used by Kovrizhnikh [16], Rosenbluth [17] and others [16-20], along with our formalism that naturally accounts for the presence of background electric field. Then, by introducing a special treatment of the collision operator, we obtain an explicit expression for the neoclassical ion heat flux and parallel flow. Remarkably, we find that in the pedestal the electric field is likely to change the direction of the latter as compared to its core counterpart. This result elucidates the discrepancy between the conventional banana regime predictions and recent experimental measurements of the impurity flow performed at Alcator C-Mod [21].

In the three chapters to follow, each prefaced by a detailed introduction, we consecutively discuss the preceding issues. Accordingly, in the next chapter we derive our special version of gyrokinetics and demonstrate its first applications by clarifying the allowed behavior of the background ion temperature profile in the pedestal. This chapter culminates in deriving the equation for the perturbation of the distribution function that contains both the neoclassical and zonal flow drives. In chapter 3 we proceed by using this equation to see how the pedestal zonal flow is modified as compared to the conventional core case. This result then allows us to suggest a model of pedestal formation based on the turbulent transport picture. Finally, in chapter 4 we employ the same equation to calculate the neoclassical banana regime ion flow and heat flux in the pedestal. We then discuss the impact of the electric field modified ion flow on the impurity measurements in C-Mod. Chapter 5 summarizes our findings and draws an overall conclusion for the thesis.

2 Gyrokinetics and arbitrary poloidal gyroradius effects in a tokamak pedestal

2.1 Introduction

Understanding tokamak pedestal physics [22-24] is one of the more crucial challenges currently facing magnetic fusion science. A self-consistent, predictive description of this region is necessary to understand the reason for improved confinement or H mode operation [1] and to gain insight into the Greenwald density limit [25]. As the barrier between the core and scrape-of-layer, the pedestal also helps control particle and heat fluxes [26] to the first wall and divertor [27]. One of the many reasons that the pedestal appears complicated is that the well known kinetic approaches [9, 20, 28-30] fail in the presence of the strong plasma gradients associated with the pedestal [30, 31] as well as internal transport barriers (ITB) [32, 33]. In these regions, as well as near the magnetic axis [34, 35], finite ion orbit [29, 30], orbit squeezing [36], and even neutral [37-39] effects on the pedestal may need to be addressed. To deal with the geometrical complications associated with large drift departures from flux surfaces [40], a variation of standard gyrokinetics [9, 41, 42] using the canonical angular momentum as the radial variable is developed and applied. This alternate description is constructed to exactly preserve conservation of canonical angular momentum and energy and is thereby able to provide key insights into the behavior of the ions in regions with step gradients.

Canonical angular momentum has been employed as a variable in drift kinetic quasilinear descriptions [43, 44], but we are not aware of it being used in gyrokinetic descriptions.

Gyrokinetics is a well established formalism capable of handling phenomena with high perpendicular wavenumbers that is being successfully used for studies of turbulence in tokamak core plasmas [2-8]. However, its application to steep gradient regions becomes more transparent if an alternative analytical treatment involving canonical angular momentum is employed. We focus on the development and insights provided by such an electrostatic gyrokinetic formulation that explicitly makes use of the axisymmetric magnetic field of a tokamak while allowing strong radial variation of the background ion profiles so that barrier widths comparable to the poloidal ion gyroradius may be treated in fully turbulent plasmas.

The technique we employ is a generalization of a standard linear gyrokinetic procedure [45, 46] and its nonlinear counterpart that is used to consider the shortcomings of gyrokinetic quasineutrality at long wavelengths [47]. By modifying these procedures we construct nonlinear gyrokinetic variables to higher order than is typically done while retaining finite poloidal ion gyroradius effects. The resulting fully nonlinear gyrokinetic equation is not only valid for $k_\perp \rho \sim 1$, as any gyrokinetic approach would be, but also due to our choice of canonical angular momentum as one of the variables, it is naturally separable into departures from flux surfaces caused by neoclassical drifts and classical finite Larmor radius (ρ) effects. This feature is what makes the analysis of the leading

order solution for the ion distribution function in a tokamak pedestal and an ITB (and near the magnetic axis) intuitively easy to understand since it precisely retains the isothermal limit [48]. In particular, it allows us to conclude that in the pedestal and an ITB (and near the magnetic axis) the lowest order ion distribution function must be nearly isothermal in the banana regime. As a result, an ion temperature pedestal or internal ion heat transport barrier is not allowed in a tokamak operating in the banana regime.

Having this result, we go further to formulate the gyrokinetic equation for the next order corrections to the ion distribution function. The relevant gyrokinetic equation obtained consistently contains neoclassical effects [20, 28-30] and zonal flow phenomena [15, 49-51] in the pedestal or an ITB along with the terms responsible for orbit squeezing [52] and potato orbits [34, 35]. This gyrokinetic equation is also valid for zonal flow and neoclassical studies in core tokamak plasmas since our full nonlinear gyrokinetic equation with turbulence retained is constructed to smoothly connect to the core where it remains valid.

The remainder of the chapter is organized as follows. In sections 2.2 – 2.3 we outline the gyrokinetic procedure we use to derive the full nonlinear gyrokinetic equation and discuss how it differs from standard nonlinear gyrokinetics [47, 53-56] including a version developed especially for the edge [56]. The expressions for the gyrokinetic variables we employ and the orderings under which they are obtained are given in brief in sections 2.4 – 2.5 and in detail in appendices A - C. In section 2.6 the full nonlinear

gyrokinetic equation is derived and its main properties are discussed. An entropy production analysis is employed in section 2.7 (with some details relegated to appendix D) to obtain the most general form of the leading order solution for the ion distribution function. Section 2.8 provides further insight into the physics of a pedestal or an ITB with the help of pressure balance equations. The gyrokinetic equation for zonal flow and neoclassical phenomena is presented in section 2.9. We close with a brief discussion of the results in section 2.10.

2.2 Gyrokinetic procedure

An assumption that is a basis of the gyrokinetic procedure to be described is the slow spatial variation of the equilibrium magnetic field. In particular, the background magnetic field of interest is assumed to obey the ordering

$$\delta \equiv \frac{\rho_i}{L} \ll 1, \tag{2.1}$$

where $L \equiv |\nabla \ln(B)|^{-1}$ and $\rho_i \equiv v_i/\Omega_i$ with $v_i \equiv \sqrt{2T_i/M}$ the ion thermal speed and $\Omega_i \equiv ZeB/Mc$ the ion cyclotron frequency. For simplicity, the magnetic field will be also assumed constant in time so that electric field can be treated as electrostatic; however, the slowly evolving induced electric field in a tokamak can easily be retained.

Consider the Vlasov operator written in terms of $\{\vec{r}, \vec{v}, t\}$ variables:

$$\frac{d}{dt} \equiv \frac{\partial}{\partial t} + \vec{v} \cdot \nabla_r + \left(\Omega \vec{v} \times \hat{n} - \frac{Ze}{M} \nabla \phi \right) \cdot \nabla_v \ . \tag{2.2}$$

Then, the evolution of the distribution function is given by

$$\frac{df}{dt} = C\{f\}, \tag{2.3}$$

where C is the collision operator. Equation (2.3) includes the fast time scale associated with the gyromotion of particles in the external magnetic field. Generally, in order to remove this time scale an averaging over gyrophase (φ) is performed. This, in turn, requires switching to a new set of magnetic field aligned variables that includes the gyrophase and then gyrophase averaging (2.3) written in terms of these variables. If the new variables are denoted by $\{q_1, ...q_5, \varphi\}$, then (2.3) transforms into

$$\frac{\partial f}{\partial t} + \frac{\partial f}{\partial q_1}\frac{dq_1}{dt} + ... + \frac{\partial f}{\partial q_5}\frac{dq_5}{dt} + \frac{\partial f}{\partial \varphi}\frac{d\varphi}{dt} = C\{f\}. \tag{2.4}$$

The gyroaverage to be employed is defined as

$$\langle \cdot \rangle \equiv \frac{1}{2\pi} \oint d\varphi (\cdot), \tag{2.5}$$

where the integration is performed holding the q_j's fixed.

If the new variables are chosen so that $\left\{ \frac{dq_1}{dt}, ... \frac{dq_5}{dt}, \frac{d\varphi}{dt} \right\}$ do not depend on φ the averaging of the left side of (2.4) becomes particularly convenient. However, it is difficult to find variables that possess this property exactly. Fortunately, the existence of

the small parameter (2.1) allows us to construct variables whose total time derivatives are gyroindependent to the desired order in δ. The procedure follows.

We first choose a suitable set of initial variables $\{q_1^{(0)},...q_5^{(0)}\}$ and apply the $\frac{d}{dt}$ operator to them as well as to φ. Then, we extract the gyrodependent part of these total time derivatives and define the corrections $\{q_1^{(1)},...q_5^{(1)},\varphi^{(1)}\}$ such that $\frac{d}{dt}\left(q_j^{(0)}+q_j^{(1)}\right)$ is gyroindependent to next order, where $q_j^{(0)}+q_j^{(1)}$ is the improved variable. This procedure employs the lowest order result

$$\frac{d}{dt}q_j^{(1)} \approx -\Omega\frac{\partial}{\partial\varphi}q_j^{(1)}. \tag{2.6}$$

Thus, we can recover $q_j^{(1)}$ by performing an integration over φ as follows:

$$\Omega\frac{\partial}{\partial\varphi}q_j^{(1)} = \frac{d}{dt}q_j^{(0)} - \left\langle\frac{d}{dt}q_j^{(0)}\right\rangle. \tag{2.7}$$

This results in $q_j^{(1)} \sim \delta q_j^{(0)}$, thereby allowing us to determine the variables up to any given order by repeating the steps above. What this procedure yields is a particularly convenient set of *gyrokinetic variables*.

Note, that by this procedure we only find the gyrodependent part of $q_j^{(1)}$ that results in the gyroindependency of $\frac{d}{dt}\left(q_j^{(0)} + q_j^{(1)}\right)$. Thus, we can arbitrarily choose $\left\langle q_j^{(1)} \right\rangle \sim \delta q_j^{(0)}$ if it is convenient. Generally, we will set $\left\langle q_j^{(1)} \right\rangle = 0$, but sometimes a clever choice of $\left\langle q_j^{(1)} \right\rangle$ can further simplify (2.4). This freedom is what allows us to define a magnetic moment variable that will be an adiabatic invariant order by order, as will be demonstrated. Moreover, it is just the freedom needed to replace the regular radial gyrokinetic variable with the canonical angular momentum.

2.3 An alternative to regular gyrokinetics

Often, the initial set of variables is chosen as [9, 45, 46, 53-56]

$$\vec{r}\,;\ \frac{v^2}{2} + \frac{Ze}{M}\phi(\vec{r}) \text{ or } v_{\|};\ \mu_0 \equiv \frac{v_\perp^2}{2B};\ \varphi\,.$$

However, in the case of tokamaks it is convenient to make use of conservation of the toroidal component of the canonical angular momentum. To do so we employ

$$\psi_* \equiv \psi - \frac{Mc}{Ze} R\vec{v} \cdot \hat{\zeta} \tag{2.8}$$

as the radial variable. The other initial variables are chosen to be the poloidal angle θ, the toroidal angle ζ, the magnetic moment μ_0, and the kinetic energy $\frac{v^2}{2}$. The gyrophase is defined such that

$$\vec{v} = v_{\|}\hat{n} + v_{\perp}\left(\hat{e}_1 \cos\varphi + \hat{e}_2 \sin\varphi\right) \tag{2.9}$$

where $v_{\|} \equiv \vec{v} \cdot \hat{n} = \sqrt{v^2 - 2\mu_0 B}$, $\hat{n} \equiv \vec{B}/B$, and $B \equiv \left|\vec{B}\right|$. Also, $\hat{e}_1(\vec{r})$ and $\hat{e}_2(\vec{r})$ are orthogonal unit vectors in the plane perpendicular to $\vec{B}$ such that $\hat{e}_1 \times \hat{e}_2 = \hat{n}$.

2.4 Orderings

We desire to develop a formalism to handle both neoclassical (large spatial scale) and turbulent (small spatial scale) phenomena. For this purpose we adopt the ordering used in [34]. Basically, this ordering allows only weak variations along the magnetic field while rapid perpendicular gradients are allowed for small amplitude fluctuations of the potential. Mathematically, our orderings are expressed as

$$\hat{n} \cdot \nabla \sim \frac{1}{L} \tag{2.10}$$

and

$$\frac{e\left|\varphi_k\right|}{T} \sim \frac{1}{k_{\perp} L}, \tag{2.11}$$

where the subscript k denotes a Fourier component. Physically, (2.11) implies that the $E \times B$ drift can be only of order δv_{th} or smaller.

The distribution function f is ordered analogously to the potential by taking

$$\frac{f_k}{f_0} \sim \frac{1}{k_\perp L}, \tag{2.12}$$

where the equilibrium solution f_0 is assumed to have spatial scales of order L. These orderings allow perturbations of the potential, density, and temperature with sharp gradients, and are relevant to turbulence, zonal flow, and the pedestal, ITBs, and near the magnetic axis in tokamaks.

In addition to the preceding orderings, we assume the characteristic frequency of the turbulent behavior to be that of drift waves,

$$\omega_* \sim \frac{v_{th}}{L} k_\perp \rho, \tag{2.13}$$

and allow the species collision frequency ν to be of order of its transit frequency,

$$\nu \sim \frac{v_{th}}{L}, \tag{2.14}$$

where v_{th} is the species thermal speed and ρ is its Larmor radius.

2.5 Gyrokinetic variables for an axisymmetric magnetic field

We next briefly consider the explicit expressions for the gyrokinetic variables that result from the procedure of Sec. 2 along with the orderings of section 4. Gyrokinetic variables resulting from an initial variable $q^{(0)}$ will be denoted as q_* at each order. We perform the

calculation up to the second order in δ starting from the initial variables given in section 3. Here we summarize the results correct up to the first order, with the details of the derivation given in appendix A. Second order corrections and details of their derivation are given in appendix B.

2.5.1 Spatial variables

Applying the gyrokinetic procedure to $\theta_0 \equiv \theta$ and $\zeta_0 \equiv \zeta$ we find

$$\theta_* = \theta + \frac{\vec{v} \times \hat{n}}{\Omega} \cdot \nabla\theta \tag{2.15}$$

and

$$\zeta_* = \zeta + \frac{\vec{v} \times \hat{n}}{\Omega} \cdot \nabla\zeta \,. \tag{2.16}$$

No first order correction to the ψ_* of equation (2.8) is needed. Equations (2.15) and (2.16) give the usual θ and ζ coordinates of the gyrocenter, while ψ_* labels the so-called "drift surface" [20, 30]. The total time derivatives of the spatial variables to the requisite order are given by

$$\dot{\psi}_* \approx \left\langle \dot{\psi}_* \right\rangle = c\frac{\partial\overline{\phi}}{\partial\zeta_*}, \tag{2.17}$$

$$\dot{\theta}_* \approx \left\langle \dot{\theta}_* \right\rangle = (v_\parallel^* \hat{n}_* + \vec{v}_d) \cdot (\nabla\theta)_* + \frac{I v_\parallel}{\Omega} \frac{\partial\left(v_\parallel \hat{n} \cdot \nabla\theta\right)}{\partial\psi}, \tag{2.18}$$

$$\dot{\zeta}_* \approx \left\langle \dot{\zeta}_* \right\rangle = (v_\parallel^* \hat{n}_* + \vec{v}_d) \cdot (\nabla \zeta)_* + \frac{I v_\parallel}{\Omega} \frac{\partial \left(v_\parallel \hat{n} \cdot \nabla \zeta \right)}{\partial \psi} =$$

$$= \left(\frac{I v_\parallel}{B R^2} \right)_* + \vec{v}_d \cdot \nabla \zeta + \frac{I v_\parallel}{\Omega} \frac{\partial}{\partial \psi} \left(\frac{I v_\parallel}{B R^2} \right), \tag{2.19}$$

where

$$\vec{v}_d \equiv -\frac{c}{B} \nabla \bar{\phi} \times \hat{n} + \frac{v_\parallel^2}{\Omega} \hat{n} \times (\hat{n} \cdot \nabla \hat{n}) + \frac{\mu}{\Omega} \hat{n} \times \nabla B, \tag{2.20}$$

$$\bar{\phi} \equiv \langle \phi \rangle \equiv \frac{1}{2\pi} \oint \phi \left(\psi_*, \theta_*, \zeta_*, E_*, \mu_*, \varphi_* \right) d\varphi_*, \tag{2.21}$$

and $I = RB_t$, with B_t the toroidal magnetic field and R the tokamak major radius. The axisymmetric tokamak magnetic field is taken to be [30]

$$\vec{B} = I(\psi) \nabla \zeta + \nabla \zeta \times \nabla \psi, \tag{2.22}$$

so that ψ_* can be rewritten as

$$\psi_* = \psi + \frac{\vec{v} \times \hat{n}}{\Omega} \cdot \nabla \psi - \frac{I v_\parallel}{\Omega}. \tag{2.23}$$

Also, in the preceding formulas and throughout the paper we use the following notation. If a certain quantity is given in terms of initial variables by $Q = Q(\psi, \theta, \zeta, E, \mu, \varphi)$, then we define

$$Q_* \equiv Q\left(\psi_*, \theta_*, \zeta_*, E_*, \mu_*, \varphi_* \right). \tag{2.24}$$

For example,

$$v_{\|}^{*} = \sqrt{E_{*} - \mu_{*} B_{*}}\,. \tag{2.25}$$

The difference between Q and Q_{*} is of order δQ and sometimes is unimportant. For instance, in the last term in (2.18) we can replace $v_{\|}$ by $v_{\|}^{*}$ and still stay within the required precision. However, in the first term of the same equation we must distinguish between these two.

2.5.2 Energy

Applying the gyrokinetic procedure to $E_0 \equiv v^2/2$ we find

$$E_{*} = \frac{v^2}{2} + \frac{Ze}{M}\tilde{\phi}, \tag{2.26}$$

and to requisite order

$$\dot{E}_{*} \approx \left\langle \dot{E}_{*} \right\rangle = -\frac{Ze}{M}(\dot{\psi}_{*}\frac{\partial \bar{\phi}}{\partial \psi_{*}} + \dot{\theta}_{*}\frac{\partial \bar{\phi}}{\partial \theta_{*}} + \dot{\zeta}_{*}\frac{\partial \bar{\phi}}{\partial \zeta_{*}})\Big/\left(1 + \frac{Ze}{M}\frac{\partial \bar{\phi}}{\partial E_{*}}\right), \tag{2.27}$$

where

$$\tilde{\phi} \equiv \phi - \bar{\phi}\,. \tag{2.28}$$

In (2.27) the expressions for $\dot{\psi}_{*}$, $\dot{\theta}_{*}$, and $\dot{\zeta}_{*}$ are given by (2.17) – (2.19), and the small $\partial\bar{\phi}/\partial E_{*}$ term is given by (B.21) and must be retained to ensure that total energy remains an exact constant of the motion in the steady state.

2.5.3 Magnetic moment

The gyrokinetic procedure applied to $\mu_0 \equiv v_\perp^2/2B$ gives

$$\mu_1 = -\frac{\vec{v}\cdot\vec{v}_M}{B} - \frac{v_\parallel}{4B\Omega}[\vec{v}_\perp(\vec{v}\times\hat{n}) + (\vec{v}\times\hat{n})\vec{v}_\perp] : \nabla\hat{n} + \frac{Ze}{MB}\tilde{\phi} + \langle\mu_1\rangle, \quad (2.29)$$

where

$$\vec{v}_M \equiv \frac{v_\parallel^2}{\Omega}\hat{n}\times(\hat{n}\cdot\nabla\hat{n}) + \frac{\mu_0}{\Omega}\hat{n}\times\nabla B\,. \quad (2.30)$$

As mentioned at the end of section 2, $\langle\mu_1\rangle$ can be chosen arbitrarily as long as $\langle\mu_1\rangle \sim \delta\mu_0$. For all the other variables we set the gyroindependent part of the correction equal to zero (notice that ψ_* automatically retains a gyroindependent term). However, as the magnetic moment is an adiabatic invariant [57], we show we can define $\langle\mu_1\rangle$ such that $\langle\dot{\mu}_*\rangle = 0$ order by order. This feature is checked in the appendix C by choosing

$$\langle\mu_1\rangle = -\frac{v_\perp^2 v_\parallel}{2B\Omega}\hat{n}\cdot\nabla\times\hat{n} \quad (2.31)$$

to find

$$\langle\dot{\mu} + \dot{\mu}_1\rangle/\mu_0 \sim \delta^3\Omega\,. \quad (2.32)$$

This choice allows us to neglect the $\partial f/\partial \mu$ term in the gyrokinetic equation even with $k_\perp \rho \sim 1$ potential fluctuations retained.

2.5.4 Gyrophase

For the ordering we employ, $\partial f/\partial \varphi = 0$ to lowest order. As a result, for our purposes it is adequate to use $\varphi_* = \varphi$ as defined by (2.9). Then, we find

$$\dot{\varphi}_* \approx \left\langle \dot{\varphi}_* \right\rangle = -\Omega_* - \frac{v_\parallel}{2}\hat{n}\cdot\nabla\times\hat{n} + v_\parallel \hat{n}\cdot\nabla\hat{e}_2\cdot\hat{e}_1 - \frac{Z^2e^2}{M^2c}\frac{\partial\bar{\phi}}{\partial\mu} - \frac{ZeI}{Mv_\parallel}\frac{\partial\bar{\phi}}{\partial\psi_*} - Iv_\parallel\frac{\partial \ln B}{\partial\psi_*} \equiv$$

$$-\bar{\Omega}. \tag{2.33}$$

The first order correction to the gyrophase is given in appendix A for completeness.

2.6 Electrostatic gyrokinetic equation

Having defined the gyrokinetic variables we can now insert them into (2.4) and gyroaverage to find our full nonlinear gyrokinetic equation

$$\frac{\partial\bar{f}}{\partial t} + \dot{\psi}_*\frac{\partial\bar{f}}{\partial\psi_*} + \dot{\theta}_*\frac{\partial\bar{f}}{\partial\theta_*} + \dot{\zeta}_*\frac{\partial\bar{f}}{\partial\zeta_*} + \dot{E}_*\frac{\partial\bar{f}}{\partial E_*} = \langle C\{f\}\rangle, \tag{2.34}$$

where $\overline{f} \equiv \langle f \rangle$ and expressions (2.17) - (2.19) and (2.27) give $\dot{\psi}_*$, $\dot{\theta}_*$, $\dot{\zeta}_*$, and $\dot{E}_*$. Note that for $\dot{E}_*$ defined by (2.27) the total energy $\varepsilon \equiv E_* + \frac{Ze}{M}\overline{\phi}$ is exactly conserved by the gyrokinetic Vlasov operator. Consequently, we can construct an exact solution to (2.34) in the isothermal case in the same way as Catto and Hazeltine in [48].

To do so we observe that for a stationary and axisymmetric plasma any function of ε and ψ_* makes the left side of the equation exactly vanish. On the other hand, to make the right side vanish $\overline{f}$ has to be Maxwellian as ion-ion collisions dominate over those between ions and electrons. Combining these two statements we find an exact solution for arbitrary collisionality to be the rigidly toroidally rotating Maxwellian

$$f_* = n\left(\frac{M}{2\pi T}\right)^{3/2} \exp\left(-\frac{M\left(\vec{v} - \omega R\hat{\zeta}\right)^2}{2T}\right), \tag{2.35}$$

with the density given by

$$n = \eta \exp\left(-\frac{Ze\phi}{T} + \frac{M\omega^2 R^2}{2T} - \frac{Ze}{cT}\omega\psi\right), \tag{2.36}$$

where T, ω, and η are constants. In terms of the gyrokinetic variables this solution is only a function of the constants of motion ε and ψ_* since

$$f_* = \eta\left(\frac{M}{2\pi T}\right)^{3/2} e^{-\frac{M\varepsilon}{T} - \frac{Ze}{cT}\omega\psi_*}. \tag{2.37}$$

2.7 Entropy production

Now we analyze the case with spatially varying T still assuming $\partial/\partial\zeta = 0$. Physically, this assumption implies that non-axisymmetry can be only due to the fluctuations of the distribution function and potential in our axisymmetric magnetic field. It is convenient to switch to θ_* and ε variables so that our gyrokinetic equation becomes

$$\left.\frac{\partial \overline{f}}{\partial t}\right|_{\varepsilon} + \dot{\theta}_* \left.\frac{\partial \overline{f}}{\partial \theta_*}\right|_{\varepsilon} = \langle C\{f\}\rangle - \frac{Ze}{M}\frac{\partial \overline{\phi}}{\partial t}\frac{\partial \overline{f}}{\partial \varepsilon}. \tag{2.38}$$

Using orderings (2.12) and (2.13) the first term on the left side of (2.38) can be estimated as follows

$$\left.\frac{\partial f}{\partial t}\right|_{\varepsilon} \sim \frac{v_{th}}{L} k_\perp \rho f_0 \sim \frac{v_{th}}{L}\frac{\rho}{L} f_0, \tag{2.39}$$

where f_0 stands for the leading order distribution function. In the similar way it can be shown that the last term on the right side of (2.38) is of the same order. At the same time,

$$\dot{\theta}_* \left.\frac{\partial \overline{f}}{\partial \theta_*}\right|_{\varepsilon} \sim \frac{v_{th}}{L} f_0, \tag{2.40}$$

where (2.18) was used to estimate $\dot{\theta}_*$. Thus, the equation for the leading order distribution function f_0 is found to be

$$\dot{\theta}_* \left.\frac{\partial f_0}{\partial \theta_*}\right|_{\varepsilon} = \langle C\{f_0\}\rangle. \tag{2.41}$$

Transit averaging (2.41) we obtain the solubility constraint

$$\overline{\langle C\{f_0\}\rangle} = 0, \tag{2.42}$$

where the transit average is defined by

$$\bar{Q} \equiv \frac{\oint Q\, d\theta_* / \dot{\theta}_*}{\oint d\theta_* / \dot{\theta}_*}. \tag{2.43}$$

The full nonlinear constraint (2.42) must be satisfied for any physically acceptable stationary solution $f_0 = f_0(\psi_*, \theta_*, \varepsilon, \mu_*)$, and the transit average is performed holding ψ_*, ε and μ_* fixed by integrating over a complete bounce for trapped particles and a full poloidal circuit for the passing. Next, we use the preceding to determine the lowest order ion distribution function f_0 in a tokamak pedestal and internal transport barrier (ITB).

We define the radial scale w of the distribution function as

$$\left| \nabla\psi \frac{\partial \ln f}{\partial \psi} \right| \equiv \frac{1}{w}. \tag{2.44}$$

In a pedestal or in an internal barrier region we assume strong spatial gradients by allowing

$$w \sim \rho_{pol} \ll L, \tag{2.45}$$

where ρ_{pol} is the poloidal ion gyroradius. Gradients along the flux surface will be allowed to be strong as well

$$\left|\nabla\theta\frac{\partial \ln f}{\partial\theta}\right| \lesssim \frac{1}{\rho_{pol}}, \tag{2.46}$$

although we will demonstrate that only weak derivatives over θ are physically possible in the banana regime. The electrostatic potential ϕ is assumed to scale analogously to f. With these assumptions, we demonstrate that in the pedestal or an ITB the leading order solution to (2.42) remains Maxwellian (from now on we refer to the pedestal case only as proof for an ITB is exactly the same). Before doing so we remark that the original orderings (2.11) – (2.12) we used to derive the axisymmetric gyrokinetic equation imply that the characteristic scale of the leading order axisymmetric distribution function and potential is the size of tokamak L. However, all our results remain valid provided $\rho \ll \rho_{pol} \lesssim w$. Indeed, in all the estimates required for the derivation of the gyrokinetic variables we can then replace L by ρ_{pol} so that the outcome of the gyrokinetic procedure stays unchanged. As a result, (2.41) is still a valid equation for f_0 . However, the comparison among different terms in the gyrokinetic formulas can be affected. In particular, in (2.18) for $\dot{\theta}_*$ the contribution of the $\vec{E}\times\vec{B}$ term in $\vec{v}_d$ becomes comparable to that due to the $v_{\|}$ if the potential gradient is of order $1/\rho_{pol}$ so that orbit squeezing effects enter [36].

We begin our demonstration by multiplying (2.41) by $\ln f_0$, transit averaging, and integrating it over ε and μ_* to obtain the steady state result

$$0 = \iint d\varepsilon d\mu_* \oint \frac{d\theta_*}{\dot{\theta}_*} \oint d\varphi_* \ln f_0 C_{ii}\{f_0\}\,, \tag{2.47}$$

where we employ

$$\ln f_0 \frac{\partial f_0}{\partial \theta_*} = \frac{\partial}{\partial \theta_*}\left(f_0 \ln f_0 - f_0\right) \tag{2.48}$$

to annihilate the left side. Notice that all the integrals in equation (2.48) are performed holding ψ_* fixed. Next, we recall (2.18) and ordering (2.46) to find the leading order result

$$\dot{\theta}_* \approx v_{\|}\hat{n}\cdot\nabla\theta + \vec{v}_E\cdot\nabla\theta \approx \left(v_{\|} + \frac{cI}{B}\frac{\partial\phi}{\partial\psi}\right)\hat{n}\cdot\nabla\theta\,, \tag{2.49}$$

where we must retain the $\vec{E}\times\vec{B}$ term as noted at the end of the previous paragraph. Contributions of the other terms from (2.18) are always one order smaller in ρ/w. Rewriting we obtain

$$-\oint \frac{d\theta}{\vec{B}\cdot\nabla\theta}\iiint_{\psi_*} \frac{d\varepsilon d\mu_* d\varphi_*}{\left[v_{\|}/B + \left(cI/B^2\right)\partial\phi/\partial\psi\right]} \ln f_0 C_{ii}\{f_0\} = 0\,, \tag{2.50}$$

where the inner integrations are performed holding ψ_* fixed.

To clarify the novel features of a pedestal plasma, we first review the analysis of (2.47) in the weak gradient limit ($w \sim L$) relevant to the core (see [30] for example). In this

simpler case we can hold ψ fixed instead of ψ_* without an error to leading order. Then, neglecting the $\partial\phi/\partial\psi$ term in the denominator, equation (2.47) becomes

$$-\oint \frac{d\theta}{\vec{B}\cdot\nabla\theta}\iiint d\varepsilon d\mu_* d\varphi_* \frac{B}{v_{\|}} \ln f_0 C_{ii}\{f_0\} = 0\,. \tag{2.51}$$

Finally, employing

$$\frac{d\varepsilon d\mu_* d\varphi_*}{d^3v} \approx \frac{dE_0 d\mu_0 d\varphi_0}{d^3v} = \frac{v_{\|}}{B} \tag{2.52}$$

we see that the left side of (2.51) is the flux-surface averaged entropy production on a given flux surface. Thus, we can employ the Boltzmann H-theorem to determine that f_0 is Maxwellian.

In the pedestal $\left(\psi_* - \psi\right)\left(\partial f/\partial\psi\right) \sim \left(\rho_{pol}/w\right) f \sim f$ and integrating holding ψ_* fixed rather than ψ becomes important. To adjust the logic to the pedestal we need to integrate (2.50) with respect to ψ_* over the entire pedestal region. Then, we can use

$$\frac{d\psi_* d\theta_* d\zeta_* d\varepsilon d\mu_* d\varphi_*}{d^3r d^3v} \approx (\hat{n}\cdot\nabla\theta)\left(v_{\|} + \frac{cI}{B}\frac{\partial\phi}{\partial\psi}\right) \tag{2.53}$$

(see appendix D for the derivation) to transform (2.50) into

$$\int\limits_{V_{ped}} d^3r \int d^3v \ln f_0 C_{ii}\{f_0\} = 0\,, \tag{2.54}$$

where V_{ped} denotes the pedestal volume. As a result, we conclude from the H-theorem that $f_0 = f_0\left(\psi_*, \theta_*, \varepsilon, \mu_*\right)$ must be Maxwellian in the pedestal as well.

It is interesting to notice, that the proof for the core plasma only requires integration over a given flux surface, while for the pedestal plasma we have to integrate over the entire pedestal region (the presence of a separatrix complicates the pedestal case as discussed at the end of this section and in section 10; however for the ITB case this proof is robust). This feature suggests that in the absence of sharp gradients each flux surface equilibrates by itself, while within the pedestal all flux surfaces are coupled. Physically, this coupling is due to the order ρ_{pol} departures of ions from a flux surface. This effect is not important in the core plasma, where spatial variation is weak on the ρ_{pol} scale and therefore we can consider any given flux surface a closed system. However, when the radial gradient scale is as large as $1/\rho_{pol}$ these flux surface departures affect the equilibrating of the neighboring flux surfaces and therefore it is the entire pedestal region that is a closed system rather than its individual flux surfaces.

As a result of the preceding observations, the leading order ion distribution function must be Maxwellian, thereby satisfying constraint (2.42) and making $\langle C\{f_0\}\rangle = 0$ as well. Therefore, in the banana regime (2.41) results in $\partial f_0/\partial\theta_* = 0$ so that f_0 can only depend on ε, ψ_*, and μ_*, and allowing strong poloidal gradients [recall (2.46)] was

unnecessary. The only Maxwellian that satisfies these conditions must be independent of μ_* and given by the relations (2.35) - (2.37), in which T, ω, and η are now allowed to be slowly varying compared to ρ_{pol}:

$$\rho_{pol}\nabla \ln T_i \ll 1 \tag{2.55}$$

and

$$\rho_{pol}\nabla \ln \omega \ll 1,\ \rho_{pol}\nabla \ln \eta \ll 1. \tag{2.56}$$

Thus, for the ions we have proven that the solution to (2.41) in a pedestal or an ITB is an isothermal Maxwellian to lowest order in ρ / ρ_{pol}, no other solution is possible. Non-isothermal modifications enter in next order as indicated by (2.55) and (2.56). As a result, in the banana regime a pedestal in the background ion temperature is unlikely to exist in a tokamak. In the Pfirsh – Schlüter regime ion departures from a flux surface are much smaller and an ion temperature pedestal cannot be ruled out. The plateau regime is a transitional case.

In addition, an ion temperature pedestal in the near scrape-of-layer (SOL) (or at the separatrix) is unlikely since our kinetic equation (2.41) remains valid there and is satisfied by the very same nearly isothermal Maxwellian ion distribution function we find inside the separatrix. As a result, no entropy production or entropy flow occurs to lowest

order in the near SOL and no ion temperature pedestal is anticipated there as long as the near SOL remains in the banana regime.

2.8 Pressure balance in pedestal or ITB

In the previous section we studied pedestal and internal transport barrier plasmas given that the ion distribution function radial gradient is of order $1/\rho_{pol}$. This gradient can only be associated with the density (and potential) as the ion temperature is proven to be slowly varying. In this section we comment on how such large density gradients can be sustained.

We start by noting that from the ion pressure balance equation and (2.55) we find to lowest order that

$$\omega_i = -c\frac{d\phi}{d\psi} - \frac{cT_i}{Zen}\frac{dn}{d\psi}\,, \tag{2.57}$$

where $dn/d\psi$ obeys ordering (2.45). Then we estimate that

$$\omega_i \Big/ \frac{cT_i}{en}\frac{dn}{d\psi} \sim \frac{\omega_i R}{v_i} \tag{2.58}$$

with $\omega_i R$ the net ion flow. Thus, unless ions are sonic the left side of (2.57) must be smaller to lowest order than each of the terms on the right. Consequently, plasma density and potential must be connected through the lowest order radial Boltzmann relation

$$\frac{d\phi}{d\psi} \approx -\frac{T_i}{Zen}\frac{dn}{d\psi} \,. \tag{2.59}$$

Also, $dn/d\psi < 0$ and therefore (2.59) yields $d\phi/d\psi < 0$, so the *electric field in the pedestal is inward*, as indeed observed for pedestals in the presence of subsonic ion flow [58, 59].

Next, we consider electron flows in the pedestal by writing the net electron velocity as

$$\vec{V}_e = \omega_e R\hat{\zeta} + \vec{B}\, K_e(\psi)/n \,, \tag{2.60}$$

with K_e a flux function so that $\nabla \cdot \left(n\vec{V}_e\right) = 0$ to lowest order. Then, total pressure balance, $\vec{J} \times \vec{B} = c\nabla(p_e + p_i)$, reduces to the lowest order electron pressure balance result

$$\omega_e = -c\frac{d\phi}{d\psi} + \frac{c}{en}\frac{dp_e}{d\psi} \,, \tag{2.61}$$

when (2.59) is employed. But here the terms on the right side have the same sign and therefore cannot cancel as in the ion equation. Estimating, $\omega_e \sim \left|c\,\partial\phi/\partial\psi\right| \sim \left(c/en\right)\left|\partial p_e/\partial\psi\right|$ we find a large electron flow,

$$\omega_e R \sim v_i \,. \tag{2.62}$$

Thus, the electrostatic potential associated with the density gradient in the pedestal or an ITB can only be sustained by a large electron flow. As a result, *it is the electron dynamics*

that underlies pedestal or ITB physics, and we can say that ions are electrostatically confined by the electrons. Although it is not clear what establishes the pedestal, it is clear that subsonic ion flow implies the pedestal is maintained by a large electron current with the ions electrostatically confined. Any small small departure of the ions from a radial Maxwell - Boltzmann relation must be due to weak ion temperature variation.

2.9 Zonal flows and neoclassical transport

Now that we have the leading order solution to (2.38) we can seek higher order corrections to it. We proceed by writing

$$\overline{f} = f_*(\psi_*, \varepsilon) + g(\psi_*, \theta_*, \mu_*, \varepsilon, t), \tag{2.63}$$

with $g \ll f_*$ and f_* given by (2.35) - (2.37) but with T, η, and ω allowed to be slowly varying functions of ψ_*. Then, equation (2.38) becomes

$$\left.\frac{\partial g}{\partial t}\right|_{\varepsilon} + \langle \dot{\theta}_* \rangle \left.\frac{\partial g}{\partial \theta_*}\right|_{\varepsilon} - \langle C_{ii}\{f_* + g\}\rangle = -\frac{Ze}{M}\frac{\partial \overline{\phi}}{\partial t}\frac{\partial f_*}{\partial \varepsilon}. \tag{2.64}$$

Notice that due to (2.59) there is a significant equilibrium potential in the pedestal that will be denoted by ϕ_0. Accordingly, we can write $\phi = \phi_0 + \delta\phi$, with $\delta\phi$ standing for the zonal flow perturbation of the potential that is time dependent and driven by the turbulence. Thus, on the right side of (2.64) we can replace $\partial\overline{\phi}/\partial t$ with $\partial\overline{\delta\phi}/\partial t$ since $\partial\overline{\phi}_0/\partial t$ is negligibly small.

To evaluate the collision operator term in (2.64) we expand the slowly varying terms of f_* around ψ to obtain

$$f_* = \eta(\psi_*)\left(\frac{M}{2\pi T(\psi_*)}\right)^{3/2} e^{-\frac{M\varepsilon}{T(\psi_*)}-\frac{Ze\omega(\psi_*)}{cT(\psi_*)}\psi_*} \approx \eta(\psi)\left(\frac{M}{2\pi T(\psi)}\right)^{3/2} e^{-\frac{M\varepsilon}{T(\psi)}-\frac{Ze\omega(\psi)}{cT(\psi)}\psi_*}[1 +$$

$$(\psi_* - \psi)\left(\frac{M\varepsilon}{T^2}\frac{\partial T}{\partial \psi} + \frac{Ze\omega\psi_*}{cT^2}\frac{\partial T}{\partial \psi} - \frac{Ze\psi_*}{cT}\frac{\partial \omega}{\partial \psi} + \frac{1}{\eta}\frac{\partial \eta}{\partial \psi} - \frac{3}{2T}\frac{\partial T}{\partial \psi}\right)+\dots\,]. \qquad (2.65)$$

The expression preceding the square parentheses is a toroidally rotating Maxwellian at any given point in space

$$\eta(\psi)\left(\frac{M}{2\pi T(\psi)}\right)^{3/2} e^{-\frac{M\varepsilon}{T(\psi)}-\frac{Ze\omega(\psi)}{cT(\psi)}\psi_*} = n\left(\frac{M}{2\pi T(\psi)}\right)^{3/2} \exp\left(-\frac{M\left(\vec{v} - \omega(\psi)R\hat{\zeta}\right)^2 + Ze\phi}{2T(\psi)}\right)$$

$$\equiv f_M, \qquad (2.66)$$

where $n = n(\vec{r})$ is given by (2.36). We use

$$C_{ii}\{f_M\} = 0 \qquad (2.67)$$

and employ the linearized ion-ion collision operator C_{ii}^l along with momentum conservation to note that

$$C_{ii}^l\{\vec{v}f_M\} = 0. \qquad (2.68)$$

Recalling that $\psi_* - \psi = -\left(Mc/Ze\right)R\vec{v}\cdot\hat{\zeta}$ and using properties (2.67) - (2.68) we find

$$C_{ii}\{f_*\} \approx$$

$$C_{ii}^l\left\{-f_M\left(\frac{M^2cR}{Ze}\frac{v^2\vec{v}\cdot\hat{\zeta}}{2T^2}\frac{\partial T}{\partial\psi}+\frac{Ze\omega}{cT^2}\frac{\partial T}{\partial\psi}\left(\frac{McR}{Ze}\vec{v}\cdot\hat{\zeta}\right)^2-\frac{Ze}{cT}\frac{\partial\omega}{\partial\psi}\left(\frac{McR}{Ze}\vec{v}\cdot\hat{\zeta}\right)^2\right)\right\}. \quad (2.69)$$

Finally, we can neglect the last two terms in the collision operator for subsonic flows because of (2.55) - (2.56) to obtain the simple result

$$\left\langle C_{ii}\{f_*\}\right\rangle \approx C_{ii}^l\left\{-\frac{Iv_\parallel}{\Omega}f_M\frac{Mv^2}{2T^2}\frac{\partial T}{\partial\psi}\right\}. \quad (2.70)$$

Next, we evaluate the $\overline{\delta\phi}$ term on the right side of (2.64) assuming $\delta\phi = \delta\phi\left(\psi,t\right)$ to the requisite order [15, 49-51], and using an eikonal form

$$\delta\phi = \hat{\phi}e^{iS(\psi)}, \quad (2.71)$$

with $\vec{k}_\perp \equiv \nabla S(\psi)$. Then, expanding $S(\psi)$ around ψ_* and gyroaveraging ϕ holding ψ_* fixed yields

$$\overline{\phi}_1 \approx \left\langle \hat{\phi}e^{i\left[S(\psi_*)+(\psi-\psi_*)\frac{\partial S}{\partial\psi_*}+\ldots\right]}\right\rangle \approx \left\langle \hat{\phi}e^{i\left[S(\psi_*)-\frac{\vec{v}\times\hat{n}}{\Omega}\cdot\nabla S+\frac{Iv_\parallel}{\Omega}S'+\ldots\right]}\right\rangle = \phi_* J_0\left(\frac{k_\perp v_\perp}{\Omega}\right)e^{iQ}, \quad (2.72)$$

where $\phi_* \equiv \hat{\phi}e^{iS(\psi_*)}$ and $Q \equiv \left(Iv_\parallel/\Omega\right)S'$, with $S' \equiv \partial S/\partial\psi$ and S assumed slowly varying.

Now we insert (2.70) and (2.72) into (2.64) and use $\partial f_*/\partial\varepsilon \approx \left(-M/T\right) f_M$ to obtain the equation for g to be

$$\frac{\partial g}{\partial t} + \left\langle \dot{\theta}_* \right\rangle \frac{\partial g}{\partial \theta_*} - C_{ii}^l \left\{ g - \frac{I v_\parallel}{\Omega} f_M \frac{M v^2}{2T^2} \frac{\partial T}{\partial \psi} \right\} = \frac{Ze}{T} \frac{\partial \phi_*}{\partial t} f_M J_0 \left(\frac{k_\perp v_\perp}{\Omega} \right) e^{iQ}. \quad (2.73)$$

Finally, we consider the banana regime in which $\partial g/\partial\theta_* = 0$ to lowest order, so that transit averaging (2.73) gives

$$\frac{\partial g}{\partial t} - \overline{C_{ii}^l \left\{ g - \frac{I v_\parallel}{\Omega} f_M \frac{M v^2}{2T^2} \frac{\partial T}{\partial \psi} \right\}} = \frac{Ze}{T} \frac{\partial \phi_*}{\partial t} f_M \overline{J_0 \left(\frac{k_\perp v_\perp}{\Omega} \right) e^{iQ}} \quad (2.74)$$

with transit average defined as in (2.43). The distinctions between f_M, Q, $v_\parallel$, J_0 and f_*, Q_*, $v_\parallel^*$, J_0^* respectively are unimportant in (2.73) and (2.74). Equation (2.74) contains both neoclassical and zonal flow drives in an uncoupled manner. The neoclassical drive enters in the collision operator and for it the time derivatives in (2.74) are negligible. The zonal flow drive is due to the $\partial\phi_*/\partial t$ term that requires keeping $\partial g/\partial t$, but for which the neoclassical drive does not matter. This gyrokinetic equation is capable of retaining finite Larmor radius effects on these phenomena, as well as finite poloidal gyroradius and orbit squeezing effects since it is derived using ψ_* as the radial variable.

2.10 Discussion

An electrostatic gyrokinetic formalism for tokamaks is developed and its first applications are performed. Based on an entropy production argument that retains orbit

squeezing as well as $\vec{E} \times \vec{B}$ shear effects, the most important prediction is that in the banana regime the background ion temperature is not allowed to have a pedestal similar to the ones observed for plasma density, electrostatic potential, and electron temperature since inequality (2.55) must be satisfied. Although this prediction may seem to disagree with some widely cited experimental observations it is important to keep in mind that currently there are almost no direct measurements of the background ion temperature in a tokamak pedestal. The majority of existing ion temperature measurements are for impurities which have a smaller ion gyroradius and are more collisional than the background ions. Moreover, it must be noticed that in the pedestal temperature equilibration between impurities and background ions is no longer local (flux surface by flux surface) because finite orbit effects, and impurity radial heat transport and equilibration can compete. Indeed, the only direct measurements of the background ion temperature in the pedestal that we are aware of were performed in helium plasmas at the DIII-D tokamak and fully supports our conclusion [60].

Of course, the entropy production proof that the background ions do not have a temperature pedestal has some limitations. First, we can only apply it when the collision operator does not dominate over the streaming term in the kinetic equation. Therefore, our proof is valid in the banana regime, but not in the collisional Pfirsch-Schluter regime (with any plateau regime behavior expected to be transitional). Only in the banana regime does the distribution function being Maxwellian result in it being independent of θ_* and therefore μ_*, which in turn leads to slow radial temperature variation.

Another issue is the implicit assumption of the absence of any significant entropy flow from the pedestal into divertor plates that is needed to obtain (2.54). This assumption requires the pedestal region to be within the tokamak separatrix in such a way that all the flux surfaces carrying a significant amount of plasma are closed. If the separatrix were to fall part way up the pedestal our proof would no longer be mathematically robust. However, our almost isothermal Maxwellian solution remains valid in the near SOL so entropy flow into the divertor is negligible. Therefore, we expect that in the banana regime, it will be difficult to sustain strong background ion temperature variation comparable to that of the plasma density in ITER [61] unless the pedestal scale length is many poloidal gyroradii.

Other limitations of our proof are associated with the neglect of charge exchange and ionization, and direct orbit loss to physical structures outside the SOL, which may or may not be playing a role in establishing the pedestal [61]. Orbit loss results in non-Maxwellian features that cause the entropy production to be finite so we anticipate that ion orbit loss will have to remain a weak effect in a well defined pedestal in local equilibrium. Moreover, in the short neutral mean free path limit the velocity dependence of the neutral distribution function will become the same as that of the ions causing charge exchange collisions of the ions with the neutrals to produce no entropy. For longer neutral mean free paths we expect little entropy production due to the presence of the

neutrals based on a self-similar treatment of the neutrals which finds results roughly in agreement with short mean free path results [62].

Interestingly, we can apply our nonlocal entropy production proof to the case of the so-called "potato regime" near the magnetic axis [34, 35] that is the potato analog of the regular banana regime. In this region of a tokamak ρ_{pol} becomes large so that (2.55) requires an almost constant ion temperature in the vicinity of the magnetic axis meaning that there is no transport in a conventional sense. This analysis is in agreement with the point made in [35] that near the magnetic axis we should speak about a global solution in the entire region rather than about a local diffusive process. This point is in turn similar to the point about the non-local equilibration of the pedestal that we make in section 7.

Finally, we remark that a favorable consequence of the lack of a background ion temperature pedestal in the banana regime is the probable enhancement of the bootstrap current in the pedestal. To see this effect we employ the usual Z = 1, large aspect ratio expression

$$j_{BS} = -f_t n T_e R\left[1.66\left(1+\frac{T_i}{ZT_e}\right)\frac{d\ln n}{d\psi} + 0.47\frac{d\ln T_e}{d\psi} - \frac{0.29}{ZT_e}\frac{d\ln T_i}{d\psi}\right], \qquad (2.75)$$

where f_t is a trapped particles fraction (e.g. see [30]). We use (2.75) only as an estimate because neoclassical transport in the pedestal can be slightly different from this result in the large aspect ratio form due to strong shaping effects in the pedestal. Experiments

show that T_e and n profiles are very similar with strong electron temperature variation being allowed by the small poloidal gyroradius of the electrons. We recall that (2.55) prevents T_i from having a gradient comparable to that of n and T_e, so the ion temperature gradient term is expected to be negligible in the pedestal, but more importantly (2.55) leads us to expect $T_i/T_e \gg 1$ to hold in the coefficient of the ion density gradient term. Thus, the first term in square parentheses in (2.75) is expected to be greater in pedestal than in the core resulting in a larger bootstrap current closer to plasma edge.

In summary, the modified gyrokinetic approach we employ promises to be a useful tool for studies of plasma turbulence and transport in tokamaks. The choice of ψ_* as the gyrokinetic radial variable results in a convenient treatment of arbitrary poloidal gyroradius effects in the pedestal, in ITBs, and about the magnetic axis, while still allowing neoclassical collisional effects and zonal flow to enter naturally along with finite Larmor radius phenomena including orbit squeezing. As a result, our formalism is capable of handling such problems as collisional zonal flow damping with $k_\perp \rho_{pol} \sim 1$, zonal flow in a pedestal, and neoclassical transport in a pedestal, as well as turbulent phenomena.

3 Zonal flow in a tokamak pedestal

3.1 Introduction

Zonal flow is observed in nearly all the systems with turbulent behavior [63]. In tokamaks, zonal flow is a poloidally and toroidally symmetric sheared flow produced by drift wave turbulence on a time scale greater than the cyclotron period. By suppressing this turbulence, it limits anomalous transport and in turn improves plasma confinement. This mechanism seems to be rather universal and works for turbulence caused by ion [11, 12, 64] and electron [13] temperature gradient modes. Moreover, experimental observations of the zonal flow in the tokamak pedestal [65, 66] suggest that this phenomenon may be responsible for the transition between the high and low confinement modes. In this connection, the question of what limits zonal flow itself takes on special significance.

The pioneering work by Rosenbluth and Hinton [14] demonstrated that in the absence of collisions the zonal flow amplitude is controlled by neoclassical polarization, with a significant portion of it, the residual, surviving in the turbulent steady state. In their calculation, the assumptions of circular flux surfaces and large radial wavelengths were used. In subsequent work the effects of collisions on zonal flow were analyzed [50, 67] as well as those of the flux surfaces shape [68, 69] and shorter wavelengths [70, 71]. However, all of the preceding analyses involved an essentially homogeneous equilibrium

solution since the wavelength of the zonal flow perturbation was assumed to be much less than all background radial scale lengths. While plausible in the tokamak core, such an assumption is inappropriate in a pedestal whose background scale is comparable to the ion poloidal gyroradius $\rho_{pol} \equiv v_i Mc / ZeB_{pol}$, where $v_i \equiv \left(2T_i / M\right)^{1/2}$ is the ion thermal velocity and B_{pol} is the poloidal magnetic field. The purpose of the present calculation is to generalize the zonal flow calculation to the pedestal case.

A better understanding of the pedestal region is a key to modeling high confinement or H Mode operation [1, 23] for controlled fusion power production. In the first chapter of this thesis, we theoretically found some basic features inherent to a pedestal. The formalism developed there allows the radial pedestal width to be of the order of ion poloidal gyroradius while assuming $\rho \ll \rho_{pol}$, where ρ is the ion gyroradius. This assumption decouples the neoclassical phenomena from classical finite Larmor radius (FLR) effects and allows the development of a version of gyrokinetics that is particularly convenient for pedestal studies. With the help of this formalism we proved that in the banana regime the background ion temperature in the pedestal is not allowed to vary significantly on the poloidal gyroradius scale even if plasma density does. This result was recently confirmed by direct measurements in He plasmas in DIII-D [60]. Moreover, it allows the shape of the pedestal electric field to be deduced for subsonic ion flow since the $\vec{E} \times \vec{B}$ drift and diamagnetic flow must cancel to lowest order in ρ / ρ_{pol}.

When the pedestal width is of order ρ_{pol} it is important to recall that ion departures from a flux surface also scale with ρ_{pol} and therefore finite drift orbit effects on the zonal flow are significant. For the problem of ion transport these effects were considered by Shaing and Hazeltine [52], who presented the derivation of ion orbits in the presence of a strongly sheared radial electric field. They focused their studies on orbit squeezing [36] by assuming large electric field shear and expanding the potential around the flux surface where the radial electric field vanished. However, the electric field is large for most flux surfaces in the pedestal and we are led to solve for the particle motion in a tokamak retaining the electric field. A preliminary numerical investigation of this issue along with some analytical estimates is given in [72]. Here we present a fully self-consistent derivation of particle trajectories in a pedestal.

To carry out the pedestal zonal flow calculation we employ the Kagan and Catto [73] version of gyrokinetics derived in the previous section that readily provides the relation between the density and the potential perturbations. The explicit evaluation of the potential involves trajectory integrals and this is where the finite orbit effects enter. We find that for strong enough electric field the trapped particle fraction becomes exponentially small so that the neoclassical shielding disappears. This means that turbulent transport can be lower in the pedestal than in the core for the same turbulent drive, and may impact for how a sharp density gradient is established on the transport time scale.

The remainder of this chapter is organized as follows. In section 3.2 we derive the integral relation between the density and potential perturbations and give the expression for the zonal flow residual. Section 3.3 investigates ion motion in a tokamak pedestal and the results of this study are applied in section 3.4 to obtain explicit expressions for the neoclassical polarization and the zonal flow residual in the pedestal. Finally, in section 3.5 we summarize our findings and discuss their implications.

3.2 Neoclassical polarization in the presence of strong background electric field

Rosenbluth and Hinton demonstrated that neoclassical polarization is the key factor affecting the zonal flow dynamics in a tokamak [14, 67]. Thus, to see how zonal flow is modified as we move from the tokamak core to the pedestal, we have to evaluate neoclassical polarization in the presence of a sharp density gradient.

It may seem that as polarization density is due to modifying single particle orbits by the perturbation of the electric field, the density gradient should not have a strong impact on it. However, while a density gradient cannot affect single particle motion directly, it necessarily builds up a strong electric field to sustain pressure balance according to equation (2.59). Moreover, equation (2.49) yields that in a subsonic pedestal with a density gradient as large as $1/\rho_{pol}$, the resulting $\vec{E}\times\vec{B}$ drift ($\vec{v}_E$) contributes to the poloidal angular velocity $\dot{\theta}$ of the ions in leading order so that

$$\dot{\theta} = v_{\|}\hat{n}\cdot\nabla\theta + \vec{v}_E\cdot\nabla\theta = \left[v_{\|} + cI\phi'(\psi)/B\right]\hat{n}\cdot\nabla\theta, \qquad (3.1)$$

where the two terms on the right side are comparable (unlike the core where $v_{\|}$ dominates). Therefore, the distinctive pedestal feature that is crucial for the zonal flow dynamics is the existence of the strong background radial electric field as it directly affects equilibrium particle orbits. Accordingly, in this section we discuss the role of the equilibrium electric field on the neoclassical plasma polarization.

Plasma polarization ε^{pol} relates density and potential perturbations δn and $\delta\phi$ through

$$\varepsilon^{pol}k_{\perp}^2\delta\phi = -4\pi Ze\delta n. \qquad (3.2)$$

Therefore, what one technically has to do to evaluate ε^{pol} is to assume that a small density perturbation is introduced into the pedestal and find the potential response to this perturbation. To this end, it is convenient to start from the equation (2.64) derived in the previous chapter

$$\frac{\partial g}{\partial t} + \dot{\theta}_*\frac{\partial g}{\partial\theta_*} - \left\langle C_{ii}^l\left\{g - \frac{Iv_{\|}}{\Omega}f_M\frac{Mv^2}{2T^2}\frac{\partial T}{\partial\psi}\right\}\right\rangle = -\frac{Ze}{M}\frac{\partial\langle\phi\rangle}{\partial t}\frac{\partial f_M}{\partial E}. \qquad (3.3)$$

The distinction between $\dot{\theta}_*$, poloidal angular velocity of the ion gyrocenters given by (2.18), and the poloidal ion angular velocity $\dot{\theta}$ as given by (3.1) will turn out to be unimportant in this chapter.

Here, to apply (3.3) to the problem of the neoclassical polarization we evaluate $\langle\phi\rangle$ in a slightly different manner as compared to the procedure outlined in Sec. 2.9. To do so we still notice that there is a significant equilibrium potential in the pedestal and therefore ϕ consists of the unperturbed piece ϕ_0, whose gradient balances the diamagnetic drift to keep the ion flow subsonic $\left[\partial\phi_0 / \partial\psi \approx -\left(T_i / en\right)\partial n / \partial\psi\right]$, and the perturbation $\delta\phi$ such that $\partial\langle\phi\rangle / \partial t = \partial\langle\delta\phi\rangle / \partial t$. Assuming an eikonal form for $\delta\phi$ we write

$$\delta\phi = \hat{\phi}e^{iG(\psi)} \approx \hat{\phi}e^{iG\left(\psi_* + Iv_{||}/\Omega - \vec{v}\times\hat{n}\cdot\nabla\psi/\Omega\right)}. \tag{3.4}$$

In Sec. 2.9 we expanded G around ψ_* to obtain

$$G(\psi) \approx G\left(\psi_*\right) + \left(Iv_{||}/\Omega - \vec{v}\times\hat{n}\cdot\nabla\psi/\Omega\right)G' \tag{3.5}$$

and gyroaveraged this result to find

$$\langle\delta\phi\rangle \approx \phi_* J_0\left(k_\perp v_\perp / \Omega\right)e^{iQ}, \tag{3.6}$$

where $\phi_* \equiv \hat{\phi}e^{iG(\psi_*)}$, $Q \equiv \left(Iv_{||} / \Omega\right)G'$ and $\vec{k}_\perp \equiv \nabla G$. However, the underlying assumption made to perform expansion (3.5) is that, for the particles of interest, $v_{||}$ is small. In the conventional case this is justified because neoclassical response is mainly due to the trapped and barely passing particles whose $v_{||}$ is indeed small in the large aspect ratio limit. Now that we allow a strong electric field, the poloidal motion described by (3.1) suggests that the trapped-passing boundary is shifted to $v_{||} \approx -cI\phi'(\psi)/B$. In the pedestal, $cI\phi'/B$ is of order v_i while the wavelengths of interest are of order ρ_{pol} or less. Thus, the particles contributing the most to the neoclassical polarization, have

$(Iv_\parallel/\Omega)G' \sim G(\psi)$, making (3.5) inappropriate. To address this issue we expand G around $\psi_* - Iu/\Omega$ rather than around ψ_* itself, where u accounts for the effect of $\vec{E}\times\vec{B}$ drift and is approximately equal to $-cI\phi'/B$. The explicit definition of u in terms of constants of the motion will be provided in the next section where single particle orbits are analyzed. Now, anticipating that trapped and barely passing particles still lie within a narrow vicinity of the trapped-passing boundary, we replace (3.5) with

$$G(\psi) \approx G\left(\psi_* - Iu/\Omega\right) + \left[I\left(v_\parallel + u\right)/\Omega - \vec{v}\times\hat{n}\cdot\nabla\psi/\Omega\right]G', \tag{3.7}$$

so that we can directly adopt (3.6) by redefining Q as

$$Q \equiv \left[I\left(v_\parallel + u\right)/\Omega\right]G' \tag{3.8}$$

and ϕ_* as $\hat{\phi}e^{iG\left(\psi_* - Iu/\Omega\right)}$.

Next, we transit average (3.3), using $\partial g/\partial\theta_* = 0$ to leading order in the banana regime, to find

$$\frac{\partial g}{\partial t} - \overline{C_{ii}^l\left\{g - \frac{Iv_\parallel}{\Omega}f_M\frac{Mv^2}{2T^2}\frac{\partial T}{\partial\psi}\right\}} = \frac{Ze}{T}\frac{\partial\phi_*}{\partial t}f_M\overline{J_0\left(\frac{k_\perp v_\perp}{\Omega}\right)e^{iQ}}, \tag{3.9}$$

where the transit average of a quantity A is defined over a full bounce (for trapped) or a complete poloidal circuit (for passing) by

$$\bar{A} \equiv \frac{\oint A\,d\theta_*/\dot{\theta}_*}{\oint d\theta_*/\dot{\theta}_*}. \tag{3.10}$$

We consider the collisionless limit, use $J_0\left(k_\perp v_\perp / \Omega\right) \approx 1 - k_\perp^2 v_\perp^2 / 2\Omega^2$ since we assume $B \gg B_{pol}$, and extract the $k_\perp^2 v_\perp^2 / 2\Omega^2$ piece as the classical polarization that will be added back later to give the overall plasma response. With these assumptions (3.9) yields

$$g = \frac{Ze}{T}\phi_* f_M \overline{e^{iQ}}. \tag{3.11}$$

To relate g and δf, the perturbation of the distribution function from its equilibrium value, we write

$$\delta f \equiv f - f_0 = f_M\left(\psi_*, E\right) + g - f_0 \approx -\frac{Ze\delta\phi}{T} f_M + g + \left[f_M\left(\psi_*, E_0\right) - f_M\left(\psi, E_0\right)\right], \tag{3.12}$$

where we used that $f_0 = f_M\left(\phi = \phi_0\right)$ and Taylor expanded f_M for small $\delta\phi$. We do not explicitly perform the ψ_* expansion in the square brackets because the resulting terms are linear in $\vec{v}$ and therefore do not contribute to density perturbation. Then, we obtain the linearized neoclassical relation between the density and potential response on a flux surface in a form similar to the one found in [70]:

$$\delta n = \frac{Ze}{T}\delta\phi\left\langle \int d^3v f_0 \left(e^{-iQ}\overline{e^{iQ}} - 1\right)\right\rangle_\theta, \tag{3.13}$$

where $\left\langle ... \right\rangle_\theta$ stands for the flux surface average. Again using that parallel velocities of the particles of interest are localized around $-u$, we expand the right side of (3.13) up to the second order in Q to obtain

$$\delta n = \frac{Ze}{T}\delta\phi\left\langle \int d^3v f_0 \left(i\bar{Q} - iQ - \frac{Q^2 - 2Q\bar{Q} + \overline{Q^2}}{2} \right) \right\rangle_\theta . \qquad (3.14)$$

In the Rosenbluth-Hinton case [14], the terms of the first order in Q do not contribute to the density perturbation. Indeed, in the absence of the electric field $\overline{v}_{||}$ and $\bar{Q}$ are odd functions of $v_{||}$ while f_0 is even in it. That is, for each particle passing clockwise there is a particle with the same absolute value of $\overline{v}_{||}$ passing counterclockwise so that their cumulative response is canceled. Also, for any trapped particle $\overline{v}_{||} = 0 = \bar{Q}$. Thus, in the Rosenbluth-Hinton limit, it is the terms quadratic in Q that give the leading order response.

In our case, there is a preferred direction of rotation in the poloidal plane due to the $\vec{E} \times \vec{B}$ drift. Therefore, $\bar{Q}$ is no longer an odd function of $v_{||}$. Neither have we $\overline{v}_{||} = 0$ for trapped particles. Thus, the terms linear in Q are expected to contribute to the neoclassical polarization. Interestingly, these terms have a preceding factor of i making the plasma susceptibility complex. Consequently, in contrast to the Rosenbluth-Hinton case there is now a spatial phase shift between the density and potential perturbations.

Once we explicitly relate δn and $\delta\phi$ with the help of (3.14) we are able to predict the long-term behavior of the zonal flow using the Rosenbluth-Hinton framework. Namely,

we will assume that at times greater than the cyclotron period, but less than the bounce period, the potential response to the zonal flow density is solely provided by the classical polarization ε_{cl}^{pol}, whereas at the times much greater than the bounce period neoclassical shielding enters as well so that $\varepsilon^{pol}\left(t \to \infty\right) = \varepsilon_{nc}^{pol} + \varepsilon_{cl}^{pol}$. Thus, solving for the potential response to a constant density step, $\delta n\left(t\right) = \delta n\left(t = 0\right)$, we obtain

$$\frac{\delta\phi\left(t \to \infty\right)}{\delta\phi\left(t = 0\right)} = \frac{\varepsilon_{cl}^{pol}}{\varepsilon_{nc}^{pol} + \varepsilon_{cl}^{pol}} \tag{3.15}$$

with $\varepsilon_{cl}^{pol} = \omega_{pi}^2 / \omega_{ci}^2$, where ω_{pi} and ω_{ci} are the plasma and ion cyclotron frequencies respectively. Notice, that in our case ε_{nc}^{pol} is complex and therefore the zonal flow residual is phase shifted with respect to the initial perturbation of the potential. In the following section, finite $\vec{E} \times \vec{B}$ drift departures from flux surfaces will be shown to substantially modify the Rosenbluth-Hinton [10] result further.

3.3 Particle orbits in a tokamak pedestal

In this section we analyze single ion motion in a tokamak in the presence of a strong electrostatic field. Namely, we investigate how accounting for the $\vec{E} \times \vec{B}$ drift on the right side of (3.1) modifies poloidal dynamics of an ion. It is necessary to emphasize that the $\vec{E} \times \vec{B}$ drift itself need not be comparable to $v_{||}$ in order to have significant effect. In fact, due to geometrical factors even v_E of order $\left(\rho / \rho_{pol}\right) v_i \ll v_{||}$ causes qualitative

changes. Indeed, for $\rho / \rho_{pol} \ll 1$, $\vec{v}_{||}$ is nearly perpendicular to the poloidal plane, while $\vec{v}_E$ is almost parallel to it as shown in Fig 3.2. Consequently, if $|Ze\nabla\phi / T| \sim 1/\rho_{pol}$ these two streaming contributions in (3.1) compete in the poloidal cross-section of a tokamak.

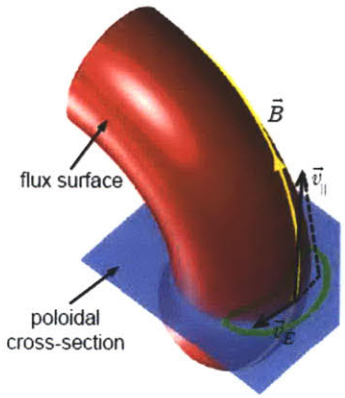

FIG 3.2. Gyrocenter motion on a torus with poloidal orbit projection plotted (in green). Even though $v_{||}$ is much greater than v_E, their contributions to the poloidal motion are comparable due to geometrical effects.

The evaluation of particle orbits to follow assumes a quadratic electric potential well. In such a case we can expand $\phi_0(\psi)$ about ψ_*

$$\phi_0(\psi) = \phi_0(\psi_*) + (\psi - \psi_*)\phi_0'(\psi_*) + \frac{1}{2}(\psi - \psi_*)^2 \phi_0''(\psi_*). \quad (3.16)$$

Because of the preceding expansion, results of this section can strictly be applied only in the pedestal with a perfectly quadratic electric potential. However, providing that the radial extent of particle orbits is much less than ρ_{pol}, we can Taylor expand the realistic equilibrium electric potential around a point on the trajectory to extend our solution to the general case.

We assume further that the radial variation of B is weak so that $B(\psi,\theta) \approx B(\psi_* - \Delta,\theta) \approx B(\psi_*,\theta)$. Then, denoting

$$\phi_* \equiv \phi_0(\psi_*), \phi_*' \equiv \phi_0'(\psi_*), \phi_*'' \equiv \phi_0''(\psi_*) \tag{3.17}$$

we can rewrite (3.1) as

$$qR_0\dot{\theta} = \left(1 + \frac{cI^2\phi_*''}{B\Omega}\right)v_{\|} + \frac{cI\phi_*'}{B}, \tag{3.18}$$

where R_0 stands for the major radius and finite orbit effects are retained. Defining

$$u_* \equiv cI\phi_*'/SB \tag{3.19}$$

(3.18) becomes

$$qR_0\dot{\theta} = S(v_{\|} + u_*), \tag{3.20}$$

where $S \equiv 1 + cI^2\phi_*''/B\Omega$ is the orbit squeezing factor [33]. Next, we use an aspect ratio expansion to write

$$B = B_0(1+\varepsilon)/(1+\varepsilon\cos\theta) \approx B_0\left(1 + 2\varepsilon\sin^2\frac{\theta}{2}\right) \tag{3.21}$$

with $B_0 \equiv B(\theta = 0)$ and $\theta = 0$ at the outer equatorial plane. We also define $v_{\|0} \equiv v_{\|}(\theta = 0)$, $u_{*0} \equiv u_*(\theta = 0) = cI\phi_*'/S_0B_0$ and $S_0 \equiv 1 + cI^2\phi_*''/B_0\Omega_0$ so that $qR_0\dot{\theta}\big|_{\theta=0} = S_0(u_0 + v_{\|0})$.

Next, we employ energy conservation

$$E \equiv \frac{v_{\|}^2}{2} + \mu B + \frac{Ze}{M}\phi(\psi) = const. \tag{3.22}$$

Using ψ_* conservation this becomes

$$\frac{S\left(v_{\|} + u_*\right)^2}{2} + \mu B - \frac{Su_*^2}{2} = const.. \tag{3.23}$$

As a result, we can describe the particle motion solely in terms of θ and $\dot{\theta}$:

$$\frac{\left(qR_0\dot{\theta}\right)^2}{2S} + \mu B - \frac{Su_*^2}{2} = \frac{\left(qR_0\dot{\theta}_0\right)^2}{2S_0} + \mu B_0 - \frac{S_0u_{*0}^2}{2}. \tag{3.24}$$

In the Eq. (3.24), for $S < 0$ the $\left(\dot{\theta}\right)^2$ term is negative and therefore trapped particles reside on the inside of the tokamak. For what follows we assume $S > 0$ so that banana particles are localized on the outside of the tokamak as in the conventional case. Evaluating the θ dependence of u and S with the help of (3.21) and solving (3.24) for $\dot{\theta}$ we obtain

$$\dot{\theta}qR_0 = \pm\dot{\theta}_0qR_0\sqrt{1 - \kappa^2\sin^2\left(\theta/2\right)}, \tag{3.25}$$

where we assume $4\varepsilon\left(S_0 - 1\right)/S_0 \ll 1$ and define

$$\kappa^2 \equiv 4\varepsilon S_0\frac{u_{*0}^2 + \mu B_0}{\left(\dot{\theta}_0qR\right)^2} = \frac{4\varepsilon}{S_0}\frac{u_{*0}^2 + \mu B_0}{\left(u_{*0} + v_{\|0}\right)^2} \tag{3.26}$$

with the trapped particles corresponding to $\kappa > 1$ and the passing to $0 < \kappa < 1$, and where $\mu B_0 \equiv v_{\perp 0}^2 / 2$. For $4\varepsilon / S_0 \ll 1$ the particles of interest are indeed localized around the trapped-passing boundary justifying our initial assumption.

Notice, that u_{*0} is defined through the electric field evaluated at ψ_* that is ρ_{pol} far from the particle orbit for $u_{*0} \sim v_i$. On the other hand, for some applications it is convenient to operate with quantities evaluated on a given orbit. To address this issue we introduce

$$u \equiv cI\phi'(\psi)/B \tag{3.27}$$

and

$$u_0 \equiv cI\phi'(\psi_0)/B_0, \tag{3.28}$$

where ψ_0 is the outermost point on the particle orbit. To relate u_0 and u_{*0} we write

$$\phi_0'(\psi_*) = \phi_0'(\psi) + \phi_0''(\psi)(\psi_* - \psi), \tag{3.29}$$

where $\psi_* - \psi = -Iv_\parallel/\Omega$. Then, recalling (3.19) and (3.28) we find

$$v_\parallel + u = S(v_\parallel + u_*) \tag{3.30}$$

and

$$S(v_{\parallel 0} + u_{*0}) = v_{\parallel 0} + u_0. \tag{3.31}$$

Inserting (3.31) in (3.26) then gives

$$\kappa^2 \approx 4\varepsilon S_0 \frac{u_0^2 + \mu B_0}{\left(u_0 + v_{||0}\right)^2}, \tag{3.32}$$

where we drop terms small by $\sqrt{\varepsilon}$. Also, upon using that $S \approx S_0$ near the trapped-passing boundary equation of motion (3.25) becomes

$$v_{||} + u = \left(v_{||0} + u_0\right)\sqrt{1 - \kappa^2 \sin^2\left(\theta/2\right)}. \tag{3.33}$$

Equations (3.32) - (3.33) will be used in the next chapter to find the neoclassical ion heat flux and poloidal flow in the pedestal.

It is instructive to plot the trapped-passing boundary on the $\left(v_{\perp 0}, v_{||0}\right)$ plane as shown in Fig 3.3. Compared to the conventional case there are two novelties worth mentioning. First, due to the effective poloidal potential well, particles with no magnetic moment can be trapped. Second, as anticipated, the trapped particle region is no longer centered at $v_{||0} = 0$, which is the Maxwellian distribution axis of symmetry. Consequently, the terms linear in Q on the right side of (3.14) no longer vanish. Furthermore, for $4\varepsilon / S_0 < 1$, as u_{*0} grows the overlap between the trapped region and the distribution

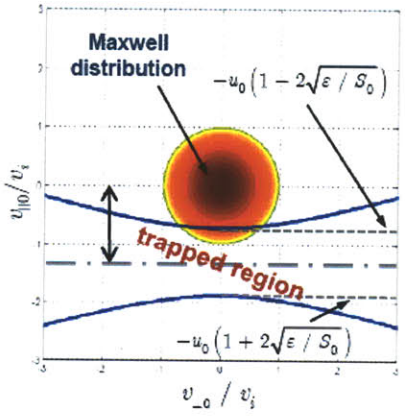

FIG 3.3. The trapped particle region is shifted by a factor of u_{*0}, while its width scales like $(\varepsilon/S_0)^{1/2}$. For $4\varepsilon/S_0<1$, as u_{*0} grows, the trapped particle fraction decays exponentially.

function decreases exponentially. Thus, we expect neoclassical phenomena to disappear for a strong enough electric field!

The important qualitative change in the $(v_{\perp 0}, v_{\|0})$ plane is due to the large electric field, rather than its shear. Indeed, for $u_{*0} = 0$ and $S_0 \gg 1$ the trapped particle region is still a cone centered at the origin [52] and therefore electric field shear alone can only modify the Rosenbluth-Hinton result algebraically. Therefore, even though S_0 is expected to contribute to neoclassical polarization, the key features in the pedestal zonal flow behavior are governed by the parameter u_{*0}.

We are now in a position to revisit our localization assumption which allowed us to replace a general electric potential with the quadratic one given by (3.16). To do so we recall (3.33) along with (3.31) to find that for a given particle

$$\psi - \psi_0 \approx \left(I / \Omega_0\right)\left(u_0 + v_{\|0}\right)\sqrt{1 - \kappa^2 \sin^2\left(\theta/2\right)} \lesssim \sqrt{2\varepsilon / S_0}\left(I v_{th} / \Omega_0\right), \qquad (3.34)$$

as required, while $\psi_* - \psi(\theta) \sim I v_{th} / \Omega_0$. Thus, provided ε / S_0 is small enough our results apply to a general pedestal potential with characteristic radial scale of order ρ_{pol}. In order the eikonal expansion of the previous section to be valid we also require $k_\perp \rho_{pol}\sqrt{2\varepsilon / S_0} \ll 1$, as well as $k_\perp \rho_{pol} \gtrsim 1$. The integrals in (3.14) are evaluated in the next section in the limit of no orbit squeezing ($S = 1$).

3.4 Evaluation of the neoclassical response

Now that we have solved for the particle trajectories we can obtain an explicit expression for the neoclassical polarization in the pedestal. To do so it is convenient to define

$$Y \equiv \frac{1}{n_0}\left\langle \int_{\psi} d^3v f_0 \left(i\bar{Q} - iQ - \frac{Q^2 - 2Q\bar{Q} + \overline{Q^2}}{2} \right) \right\rangle_{\theta} \tag{3.35}$$

so that the zonal flow residual is given by

$$\frac{\delta\phi\left(t \to \infty\right)}{\delta\phi\left(t = 0\right)} = \frac{k_{\perp}^2\rho_i^2}{k_{\perp}^2\rho_i^2 + Y}, \tag{3.36}$$

where (3.2), (3.14), and (3.15) are used along with $\varepsilon_{nc}^{pol} = Y\omega_{pi}^2 / \left(\omega_{ci}^2 k_{\perp}^2 \rho_i^2\right)$. To evaluate Y we first transit average Q and Q^2 based on the particle equations of motion, and then perform the integration over velocity space and the flux surface average on the right side of (3.35). In the calculation to follow we set $S = 1$ to focus on the qualitative changes that are due to the electric field itself rather than its shear.

3.4.1 Transit Averages

We start by noticing that to the requisite order $\overline{Q} = \left(G'I / \Omega\right)\overline{\left(v_{\|} + u\right)}$ as well as $\overline{Q^2} = \left(G'I / \Omega\right)^2 \overline{\left(v_{\|} + u\right)^2}$. Then, for passing particles ($0 < \kappa < 1$),

$$\overline{Q} = \left(G'I / \Omega\right)\frac{\pi\left(v_{\|0} + u_0\right)}{2K\left(\kappa\right)} \tag{3.37}$$

and

$$\overline{Q^2} = \left(G'I / \Omega\right)^2 \left(v_{\|0} + u_0\right)^2 \frac{E\left(\kappa\right)}{K\left(\kappa\right)}, \tag{3.38}$$

where (3.33) is used and K and E are the complete elliptic integrals of the first and second kinds respectively:

$$E\left(\kappa\right) \equiv \int_0^{\pi/2} d\xi \sqrt{1 - \kappa^2 \sin^2 \xi}\,, \tag{3.39}$$

$$K\left(\kappa\right) \equiv \int_0^{\pi/2} \frac{d\xi}{\sqrt{1 - \kappa^2 \sin^2 \xi}}. \tag{3.40}$$

For trapped particles ($\kappa > 1$),

$$\overline{Q} = 0 \tag{3.41}$$

and

$$\overline{Q^2} = \left(G'I / \Omega\right)^2 \left(v_{\|0} + u_0\right)^2 \left[\frac{\kappa^2 E\left(1/\kappa\right)}{K\left(1/\kappa\right)} + 1 - \kappa^2\right]. \qquad (3.42)$$

3.4.2 Velocity and Flux Surface Average Integrals

Equations (3.37) - (3.42) provide us with $\overline{Q}$ and $\overline{Q^2}$ in terms of $\left(v_{\|0} + u_0\right)$ and κ. Therefore, it is convenient to switch from integration over $\vec{v}$ to integration over $\left(v_{\|0} + u_0\right)$ and κ in (3.35). To account for the Jacobean of this transformation we use (3.33) to obtain

$$2\pi v_\perp dv_\perp dv_\| = \frac{\pi B\left(v_{\|0} + u_0\right)^2 d\kappa^2 d\left(v_{\|0} + u_0\right)}{2\varepsilon B_0 \sqrt{1 - \kappa^2 \sin^2\left(\theta / 2\right)}}. \qquad (3.43)$$

Then, upon performing the flux surface average we rewrite (3.35) as

$$Y = \frac{\pi Q_0^2}{\varepsilon}\left(\frac{M}{2\pi T}\right)^{3/2} e^{Mu_0^2/2T}\left(1 + \frac{iMu_0}{TQ_0}\right)\times$$

$$\int d\kappa^2 \int d\left(v_{\|0} + u_0\right)\left(v_{\|0} + u_0\right)^4 e^{-M\kappa^2\left(v_{\|0}+u_0\right)^2/4\varepsilon T} \times$$

$$\left\{\underset{0<\kappa<1}{\left[\frac{2}{\pi}E\left(\kappa\right) - \frac{\pi/2}{K\left(\kappa\right)}\right]} + \frac{2}{\pi\kappa}\underset{\kappa>1}{\left[\left(1-\kappa^2\right)K\left(1/\kappa\right) + \kappa^2 E\left(1/\kappa\right)\right]}\right\}, \qquad (3.44)$$

where $Q_0 \equiv IG'/\Omega_0$. In equation (3.44), the first term in the curly brackets is employed for the evaluation of the passing particle response by integrating over $0 < \kappa < 1$ after

performing the $v_{\|0}+u_0$ integration from $|u_0|(2/\kappa)\sqrt{\varepsilon}$ to $+\infty$ and from $-\infty$ to $-|u_0|(2/\kappa)\sqrt{\varepsilon}$ (see Fig 3.3). The second term is used for the integration over the trapped particle region $\kappa>1$ and again between $\pm|u_0|(2/\kappa)\sqrt{\varepsilon}$ and $\pm\infty$. Letting $y=M\kappa^2\left(v_{\|0}+u_0\right)^2/4\varepsilon T-Mu_0^2/T$ and replacing κ with $1/\kappa$ in the $1<\kappa$ range, the trapped particle response on the right side of (3.44) can be evaluated explicitly to obtain

$$Y=\frac{4}{\sqrt{\pi}}\left(\frac{q}{\varepsilon}\right)^2 k_\perp^2\rho_i^2\left(2\varepsilon\right)^{3/2}e^{-Mu_0^2/2T}\left(1+\frac{iMu_0}{TQ_0}\right)$$

$$\times\left\{\frac{4}{9\pi}+\int_0^1\frac{d\kappa}{\kappa^4}\left[\frac{2E(\kappa)}{\pi}-\frac{\pi}{2K(\kappa)}\right]\right\}\int_0^\infty dye^{-y}\left(y+\frac{Mu_0^2}{T}\right)^{3/2}, \quad (3.45)$$

where numerical evaluation of the expression in the curly brackets gives an approximate value of 0.193. Absent the electric field, $u_0=0$ and $S_0=1$ so that the last integral in (3.45) is equal to $3\sqrt{\pi}/4$ and (3.45) recovers the Rosenbluth-Hinton result [10]

$$Y_{RH}\approx 1.6k_\perp^2\rho_i^2\left(\frac{q}{\varepsilon}\right)^2\varepsilon^{3/2}. \quad (3.46)$$

Therefore, normalizing (3.45) to Y_{RH} we obtain the final answer in a more compact form

$$\frac{Y}{Y_{RH}}=\left(1+2i\frac{u_0/v_i}{k_\perp\rho_{pol}}\right)\frac{4e^{-\left(u_0/v_i\right)^2}}{3\sqrt{\pi}}\int_0^\infty dye^{-y}\left[y+2\left(u_0/v_i\right)^2\right]^{3/2}. \quad (3.47)$$

Expression (3.47) possesses the features qualitatively expected. In particular, it captures a spatial phase shift between density and potential perturbations as well as exponential decay in the large electric field limit. Notice, that for the wavelengths of order pedestal size the imaginary part of the residual is comparable to its real part and therefore simulations should reveal a non-trivial phase shift between the initial and resulting zonal flow potentials.

To see in greater detail how neoclassical polarization depends on the electric field we plot

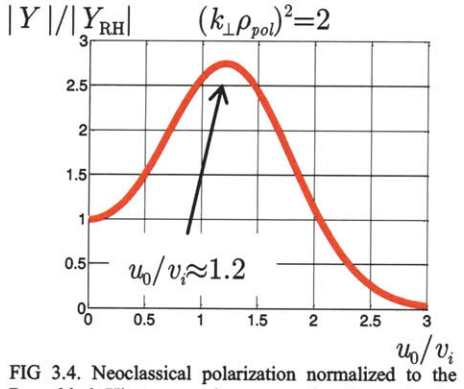

FIG 3.4. Neoclassical polarization normalized to the Rosenbluth-Hinton result as a function of the equilibrium electric field.

$\left|\varepsilon_{nc}^{pol}\right| / \varepsilon_{nc}^{pol}\Big|_{RH} = |Y| / Y_{RH}$ for $k_\perp\rho_{pol} = 1$ in Fig 3.4, where $\varepsilon_{nc}^{pol}\Big|_{RH} \approx 1.6\left(\omega_{pi}^2 q^2\right)/\left(\omega_{ci}^2\sqrt{\varepsilon}\right)$ is the neoclassical polarization in the tokamak core [14]. Notice that $\varepsilon_{nc}^{pol}\left(u_0\right)$ has a maximum at $u_0 \approx 1.2v_i$. To the right of this maximum, an increase in the equilibrium electric field leads to an increase of the zonal flow residual according to (3.36). Recalling that in a subsonic pedestal pressure balance yields the radial Boltzmann relation between the equilibrium potential and plasma density (2.59), we find that, for a steep enough density profile, its further sharpening leads to the enhancement of the zonal flow residual. This feature has an important consequence as noted in the next section.

3.5 Discussion

In the preceding section we present an explicit evaluation of the collisionless neoclassical polarization and zonal flow residual in the pedestal. It importantly generalizes the classic Rosenbluth-Hinton result [14] because it allows for the strong electric field that is an intrinsic feature of a subsonic pedestal in a banana regime. The mechanism by which strong radial electric field modifies the zonal flow in the banana regime can be schematically explained in the following way. In a pedestal of width ρ_{pol}, the electrostatic potential satisfies $|Ze\nabla\phi/T| \sim 1/\rho_{pol}$ to sustain pressure balance. A simple estimate then gives that the $\vec{E}\times\vec{B}$ drift significantly contributes to the poloidal motion of an ion, thereby qualitatively changing ion orbits compared to those in the core. Consequently, the neoclassical response to a density perturbation provided by these changed orbits modifies the Rosenbluth-Hinton zonal flow dynamics and the residual.

As it can be seen from (3.47), even in the absence of orbit squeezing the zonal flow the electric field makes the neoclassical polarization complex, resulting in a zonal flow residual that is phase shifted with respect to the initial perturbation. Moreover, for $u_0/v_i > 1$ the neoclassical polarization decays exponentially as the square of the electric field so that the zonal flow is no longer neoclassically shielded! In this limit, the zonal flow residual approaches unity so once it is generated it can continue to act strongly in regulating the turbulent transport. For a device such as C-Mod or DIII-D tokamaks, the

electric field corresponding to $u_0/v_i \sim 1$ is approximately equal to 200 V/cm. Such a magnitude of the field is indeed observed in experiments [59], thereby making the theory presented in this chapter physically relevant.

If we now imagine that zonal flow is the dominant factor limiting turbulent transport in the tokamak edge, the preceding results suggest that a strong background electric field reduces transport. This in turn suggests a feedback mechanism that could play a role in pedestal formation. Indeed, consider a tokamak with a shallow density profile and initial zonal flow. Assume that a perturbation causes a sharp density gradient. We might expect this gradient to be eliminated by transport processes. However, when the flow is subsonic, creating such a density step at the same time increases the radial electric field to sustain pressure balance (2.59). When this field becomes large enough for u_0 to go beyond the maximum of the curve in Fig 3.4 it enhances the zonal flow residual in that region making the turbulent transport level lower and sharpening the density profile further. Thus, this feedback phenomenon may allow creation of a steep density profile before it can be relaxed by anomalous transport and therefore it could be involved in establishing, as well as maintaining, a tokamak pedestal. Importantly, it is the strength of the electric field, rather than its shear, that is expected to play the key role since it enters exponentially.

4 Neoclassical radial ion heat flux and poloidal flow in a tokamak pedestal

4.1 Introduction

The neoclassical theory of plasma transport considers transport processes that are due to the non-uniformity of the confining magnetic field. In the original work by Galeev and Sagdeev in 1968 [19] it was pointed out that such non-uniformity results in more complicated particle trajectories as compared to simple Larmor orbits in straight magnetic field line geometry. More specifically, they observed that in toroidal magnetic fields the gyrocenters of these orbits perform cyclic motion that allow them to depart noticeably from their reference magnetic field surface. In a tokamak, particles can be classified as either trapped or passing based on the character of their gyrocenter trajectory. In particular, the poloidal projection is banana like for the former and an off-center circle with respect to the reference flux surface for the latter. These orbits of particle gyrocenters are often referred to as drift surfaces.

For ions, the characteristic size of the drift surface departure from its flux surface scales with poloidal ion gyroradius, $\rho_{pol} \equiv v_i Mc/ZeB_{pol}$, where $v_i \equiv \sqrt{2T/M}$ is the ion thermal speed and B_{pol} is the poloidal magnetic field. Accordingly, in the so-called "banana regime", in which collisions are rare enough for an ion to circulate several times

over its neoclassical orbit before being scattered, it is ρ_{pol} that defines the elementary diffusive step in contrast to classical transport in a uniform magnetic field that is governed by a step in the Larmor radius $\rho \equiv v_i Mc/ZeB$. For most tokamaks, the poloidal component of the magnetic field is much less than toroidal, making $\rho \ll \rho_{pol}$. Therefore, neoclassical transport normally dominates over classical.

Neoclassical radial transport in the core of a tokamak has been investigated in great detail [16-20, 28, 30]. Extensions to the potato orbits near the magnetic axis have also been considered [34, 35]. However, all these works rely on the Galeev and Sagdeev equations of particle motion, making their results inapplicable to the pedestal case. The reason for this limitation is the strong electric field, present in a subsonic pedestal. It is needed to sustain ion pressure balance, making the ions nearly electrostatically confined as it is pointed out in the first chapter of this thesis. The strong electric field substantially modifies ion orbits, thereby requiring reconsideration of the conventional neoclassical results. The effect of strongly sheared but weak electric field on the neoclassical ion transport in the banana regime, usually referred to as orbit squeezing [36], was considered in [52]. However, this model can realistically apply only to a narrow tokamak region, because over a reasonably long distance large field shear results in a large field. Moreover, the calculation of the neoclassical polarization in a pedestal, carried out in chapter 3, demonstrates that the shear free electric field introduces qualitatively novel features resulting in crucial kinetic implications. Therefore, we are led to investigate the

full effect of strong radial electric field on the banana regime neoclassical ion heat flux and poloidal flow to gain insight into transport properties of the tokamak pedestal.

The evaluation of the neoclassical ion heat flux in the tokamak core has been done in a number of ways [16-18, 20, 30]. Our calculation of its pedestal counterpart extends the logic outlined in [30] to the retention of a strong radial electric field. To do so, in the second section of this chapter we utilize the linearized Rosenbluth form of the full like particle collision operator [74] to derive a model collision operator that is particularly convenient for describing processes near the $\vec{E} \times \vec{B}$ modified trapped-passing boundary. In the next section we employ the model to solve the kinetic equation with only the neoclassical drive term retained. This solution provides us with the first order correction to the distribution function so that we can continue to section 4.4 where we explicitly evaluate the neoclassical ion heat flux with the help of the moment approach. The insight developed to calculate the ion heat flux is then employed to determine the parallel ion flow in section 4.5. Finally, in the last section we discuss implications of these newly obtained results.

4.2 Model collision operator in the pedestal

We start by deriving a model of the like particle collision operator that conveniently describes the collisional transitions across the trapped-passing boundary in the pedestal. In the core of a tokamak, this boundary is a cone centered at the origin of the $\left(v_{\perp}, v_{\parallel}\right)$

plane and therefore to retain neoclassical transport processes in the large aspect ratio limit it is sufficient to use a momentum conserving pitch-angle scattering operator. In a subsonic pedestal with a width comparable to ρ_{pol}, the dramatic density drop gives rise to a strong radial electric field to compensate the ion pressure gradient. The resulting $\vec{E} \times \vec{B}$ drift enters poloidal ion motion in leading order, thereby modifying particle orbits. Consequently, as shown on Fig 4.5, the trapped-passing boundary is curved and shifted so that the energy scattering component of the collision operator contributes to neoclassical transport as well.

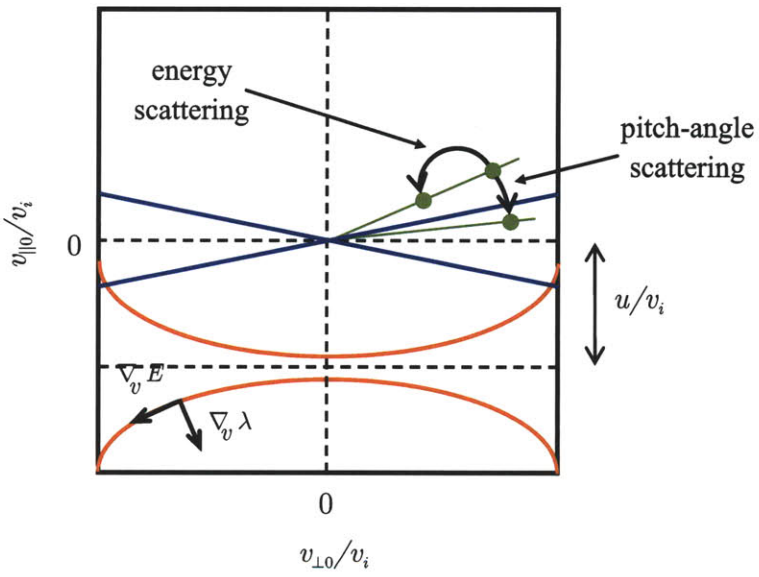

FIG 4.5. The trapped-passing boundary in the core (upper curves) and pedestal (lower curves) cases. In the pedestal, energy scattering can take an ion across the trapped passing boundary, whereas in the core this transition is solely due to pitch-angle scattering. Therefore, we employ a new set of variables, W and λ, such that the gradient of the former is parallel to the trapped-passing boundary in the pedestal and gradient of the latter is perpendicular to it. As a result, our model collision operator (4.21)-(4.22) involves the $\partial/\partial\lambda$ terms only. Notice that in the pedestal, the trapped region axis of symmetry is shifted by u/v_i from its core counterpart. As the equilibrium Maxwellian is still centered at v_i=0, we therefore expect neoclassical ion heat flux to decay exponentially for u/v_i>1.

To find a model collision operator more relevant to our problem, we use the fully consistent calculation of the tokamak particle trajectories in the presence of a strong radial electric field performed in section 3.3. There, conservation of the total energy $E = v^2/2 + Ze\phi(\psi)/M$ and canonical angular momentum $\psi_* \approx \psi - Iv_{||}/\Omega$, as well as the adiabatic invariant $\mu = v_\perp^2/2B$, allowed us to write the pedestal trapping condition in terms of the parameter κ

$$\kappa^2 \equiv 4\varepsilon S_0 \frac{u_0^2 + \mu B_0}{\left(u_0 + v_{||0}\right)^2}, \tag{4.1}$$

such that

$$v_{||} + u = \left(v_{||0} + u_0\right)\sqrt{1 - \kappa^2 \sin^2\left(\theta/2\right)}, \tag{4.2}$$

where $u(\psi) \equiv \left(cI/B\right)\phi'(\psi)$, $S \equiv 1 + cI^2\phi''/B\Omega$, $\phi(\psi)$ stands for the electrostatic potential, $\Omega \equiv ZeB/Mc$ and $I \equiv RB_{tor}$ with B_{tor} the toroidal magnetic field. Here, θ denotes the poloidal angle and the subscript "0" refers to quantities evaluated in the equatorial mid-plane ($\theta = 0$) on a given particle orbit. In the kinetic calculation to follow the distinction between S_0 and S is unimportant. Consequently, we replace S_0 with S hereafter.

To obtain equations (4.1) and (4.2) the potential $\phi(\psi)$ must be expanded about $\psi_* - Iu/\Omega$ to second order to retain orbit squeezing as well as the finite u effects. Finally, equation (4.2) is derived in the large aspect ratio limit so that

$$B/B_0 \approx 1 + 2\varepsilon \sin^2(\theta/2), \tag{4.3}$$

where $\varepsilon \ll 1$ is the inverse aspect ratio and we assume $4\varepsilon S \ll 1$. Notice that the range $0 < \kappa^2 < 1$ corresponds to passing particles and $\kappa^2 > 1$ to trapped so that near the trapped-passing boundary $(v_{\|0} + u_0) \sim v_i\sqrt{\varepsilon}$ for $S \sim 1$. These ions are the ones of most concern since we will need to carefully evaluate the portion of the ion distribution function localized to this region.

To capture collisional processes near the trapped-passing boundary in a simple manner it is convenient to employ some function of κ^2 as an independent variable in the model collision operator. Also, it is convenient to choose variables that reduce to the conventional ones, $2\mu B_0/v^2$ and $v^2/2$, in the limit of no electric field to make it easier to keep track of the changes associated with the pedestal case. Finally, to simplify solving the kinetic equation it is desirable to have these variables conserved along a single particle orbit.

To this end, it is useful to employ the variables

$$W \equiv \frac{\left(v_{\|0} + u_0\right)^2}{2S_0} + \left(\mu B_0 + u_0^2\right) \text{ and } \lambda \equiv \frac{\mu B_0 + u_0^2}{W}. \tag{4.4}$$

As long as particle dynamics is described by equation (4.2), W and λ are useful constants of the motion through order $\sqrt{\varepsilon S}$. Also observe that (4.1) and (4.4) give

$$\kappa^2 = \frac{2\varepsilon\lambda}{1-\lambda} \tag{4.5}$$

and therefore

$$\lambda = \frac{\kappa^2}{\kappa^2 + 2\varepsilon}. \tag{4.6}$$

That is, λ can be defined solely in terms of κ^2 and therefore $\nabla_v \lambda$ is orthogonal to the trapped passing boundary.

For many purposes it is convenient to rewrite (4.4) so that $v_{\|} + u$ is expressed in terms of W and λ similarly to how $v_{\|}$ is expressed in terms of $v^2/2$ and $2\mu B_0/v^2$ in the conventional calculation. The desired form is derived with the help of (4.1) - (4.3) to obtain

$$\left(v_{\|} + u\right)^2 / 2S = W\left(1 - \lambda B/B_0\right). \tag{4.7}$$

In the following sections this form will be found helpful for evaluating integrals over λ. Here, we employ it to check orthogonality of the variables by evaluating

$$\nabla_v W = \hat{n}\left(v_{\|} + u\right)/S + \vec{v}_{\perp} \tag{4.8}$$

and

$$\left(B/B_0\right)W\nabla_v\lambda = \left(1-\lambda B/B_0\right)\nabla_v W - \left[\left(v_{\|}+u\right)/S\right]\hat{n} \tag{4.9}$$

to find

$$\left(B/B_0\right)W\nabla_v\lambda\cdot\nabla_v E = \mu B\left(v_{\|}+u\right)^2/SW - \left(\lambda B/S^2B_0\right)\left(v_{\|}+u\right)^2. \tag{4.10}$$

In the vicinity of the trapped-passing boundary $\left(v_{\|}+u\right)\sim v_i\sqrt{\varepsilon}$ for $S\sim 1$, making W and λ nearly orthogonal. Thus, we may anticipate that once the collision operator is written in terms of these variables, the main contribution to neoclassical transport will come from the $\partial/\partial\lambda$ terms. We proceed by finding an explicit expression for such an operator.

To do so we first recall the Rosenbluth form of the collision operator [74]

$$C_R\left\{\delta f\right\} = \nabla_v\cdot\vec{\Gamma}\left\{\delta f\right\}, \tag{4.11}$$

where

$$\vec{\Gamma}\left\{\delta f\right\} \equiv \gamma f_0\nabla_v\nabla_v G_M\cdot\nabla_v\left(\delta f/f_M\right) \tag{4.12}$$

with f_M a stationary Maxwellian and

$$\gamma\nabla_v\nabla_v G_M = \frac{\nu_{\perp}}{4}\left(v^2\vec{\vec{I}} - \vec{v}\vec{v}\right) + \frac{\nu_{\|}}{2}\vec{v}\vec{v}\,. \tag{4.13}$$

The collision frequencies $\nu_{\perp}$ and $\nu_{\|}$ are functions of v^2 only and defined by

$$\nu_{\perp} \equiv \frac{3\sqrt{2\pi}}{2x^3}\left[\operatorname{erf}(x) - \Psi(x)\right]\nu_B \text{ and } \nu_{\parallel} \equiv \frac{3\sqrt{2\pi}}{2x^3}\Psi(x)\nu_B, \quad (4.14)$$

where $\nu_B = 4\pi^{1/2}Z^4e^4n_i \ln\Lambda / 3M^{1/2}T^{3/2}$ is the Braginskii ion-ion collision frequency,

$$\Psi(x) \equiv \frac{\operatorname{erf}(x) - x\operatorname{erf}'(x)}{2x^2} \text{ and } \operatorname{erf}(x) \equiv \frac{2}{\sqrt{\pi}}\int_0^x e^{-t^2}dt, \quad (4.15)$$

with $x \equiv v\sqrt{M/2T} = v/v_i$.

Switching to W, λ and gyrophase φ variables and writing (4.11) in conservative form we obtain

$$C\{\delta f\} = \frac{1}{J}\frac{\partial}{\partial\lambda}\left(J\vec{\Gamma}\cdot\nabla_v\lambda\right) + \frac{1}{J}\frac{\partial}{\partial W}\left(J\vec{\Gamma}\cdot\nabla_v W\right) + \frac{1}{J}\frac{\partial}{\partial\varphi}\left(J\vec{\Gamma}\cdot\nabla_v\varphi\right), \quad (4.16)$$

where the $\partial/\partial\varphi$ term is set equal to zero since classical effects are ignored. Upon accounting for both signs of $\left(v_{\parallel} + u\right)$, equation (4.9) gives the Jacobian of the transformation to be

$$J = \frac{d^3v}{d\varphi dW d\lambda} = \frac{2BWS}{B_0\left(v_{\parallel} + u\right)}. \quad (4.17)$$

The model collision operator to be constructed will eventually be applied to $g - h_{\sigma}$, where h_{σ} denotes the neoclassical collisional drive term in the kinetic equation, whose explicit momentum conserving form convenient for our purpose we provide in the next

section, while g is the neoclassical response to h_σ. In the absence of the electric field, $g - h_\sigma$ is localized around the trapped-passing boundary, so that $\partial\left[\left(g - h_\sigma\right)/f_M\right]/\partial\lambda \sim O\left(\varepsilon^{-1}\right)$, while $\partial\left[\left(g - h_\sigma\right)/f_M\right]/\partial W = O(1)$ [17, 30]. Assuming that these estimates remain appropriate in the pedestal, equations (4.8), (4.9) and (4.13) give

$$\vec{\Gamma}\left\{g - h_\sigma\right\} \cdot \nabla_v \lambda \approx f_M \nabla_v \lambda \cdot \left[\frac{\nu_\perp}{4}\left(v^2 \vec{\vec{I}} - \vec{v}\vec{v}\right) + \frac{\nu_\parallel}{2}\vec{v}\vec{v}\right] \cdot \nabla_v \lambda \frac{\partial}{\partial \lambda}\left(\frac{g - h_\sigma}{f_M}\right), \tag{4.18}$$

where due to our orderings we may drop the $\partial/\partial W$ term. The same reasoning allows us to drop the $\partial/\partial W$ term on the right side of (4.16) as well.

To simplify (4.18) further we use that for the calculation to follow it is sufficient to account only for particles lying in the close proximity of the trapped-passing boundary and therefore we can consider $\lambda \approx B_0/B \approx 1$ to obtain

$$W^2\left(\nabla_v \lambda\right)^2 \approx \left(v_\parallel + u\right)^2 / S^2 \tag{4.19}$$

and

$$W^2\left(\vec{v} \cdot \nabla_v \lambda\right)^2 \approx u^2\left(v_\parallel + u\right)^2 / S^2 . \tag{4.20}$$

Thus, we rewrite equation (4.18) as

$$\vec{\Gamma}\left\{g - h_\sigma\right\} \cdot \nabla_v \lambda \approx f_M \frac{\left(v_\parallel + u\right)^2}{S^2 W^2}\left[\frac{\nu_\perp}{4} v^2 + \left(\frac{\nu_\parallel}{2} - \frac{\nu_\perp}{4}\right) u^2\right] \frac{\partial}{\partial \lambda}\left(\frac{g - h_\sigma}{f_M}\right) \tag{4.21}$$

to obtain our pedestal collision operator to lowest order to be

$$C\{g-h_\sigma\}=\frac{B_0\left(v_\parallel+u\right)}{B}\frac{\partial}{\partial\lambda}\left[\frac{B}{B_0\left(v_\parallel+u\right)}\vec{\Gamma}\cdot\nabla_v\lambda\right]. \tag{4.22}$$

The model operator defined by equations (4.21) - (4.22) must manifestly conserve momentum. To explicitly display this property, intrinsic to the full like particle collision operator, we introduce a free parameter σ to redefine $\vec{\Gamma}\cdot\nabla_v\lambda$ by

$$\vec{\Gamma}\{g-h_\sigma\}\cdot\nabla_v\lambda=$$

$$f_M\frac{\left(v_\parallel+u\right)^2}{S^2W^2}\left[\frac{\nu_\perp}{4}v^2+\left(\frac{\nu_\parallel}{2}-\frac{\nu_\perp}{4}\right)u^2\right]\frac{\partial}{\partial\lambda}\left[\frac{g-h}{f_M}-\frac{\sigma I\left(v_\parallel+u\right)}{\Omega T}\frac{\partial T}{\partial\psi}\right], \tag{4.23}$$

where

$$h_\sigma\equiv h+f_M\frac{\sigma I\left(v_\parallel+u\right)}{\Omega T}\frac{\partial T}{\partial\psi}, \tag{4.24}$$

with the drive term h defined in the next section. Then, after solving for the first order correction to the distribution function we determine σ such that the operator given by (4.22) - (4.23) conserves momentum.

4.3 Passing constraint

Now that we have a convenient model of the collision operator we can solve for the first order distribution function that is responsible for the neoclassical transport. A form of

kinetic equation appropriate in the pedestal is obtained section 2.9 whose expression (11) readily provides the equation for the perturbation of the equilibrium Maxwellian f_M. Setting aside zonal flow phenomenon by omitting the $\partial/\partial t$ terms and transit averaging, we obtain the neoclassical constraint on the distribution function in the pedestal to be

$$\overline{C\{g-h\}}=0, \tag{4.25}$$

where the bar on top of the full linearized like particle collision operator denotes transit averaging, g stands for the non-diamagnetic perturbation of the leading order Maxwellian and the neoclassical collisional drive h is defined by

$$h \equiv f_M \frac{Iv_{\|}}{\Omega}\frac{Mv^2}{2T^2}\frac{\partial T}{\partial \psi}. \tag{4.26}$$

Written in this form our passing constraint looks identical to the conventional one [30]. Notice, however, that in contrast to the core case transit averaging in the pedestal must keep the distinction between the flux function ψ and canonical angular momentum $\psi_* \approx \psi - Iv_{\|}/\Omega$ and account for the effect of the $\vec{E}\times\vec{B}$ drift in leading order of the poloidal ion velocity. That is, transit averaging of a quantity Q is now defined by

$$\overline{Q} \equiv \oint_* \frac{d\theta Q}{v_{\|}+u} \Big/ \oint_* \frac{d\theta}{v_{\|}+u}, \tag{4.27}$$

where the integration on the right side must be performed holding ψ_*, μ and total energy fixed as indicated by the $*$ subscript on the integral. In the core of a tokamak u is negligible compared to $v_{\|}$ and ψ is approximately constant along the ion trajectory. In

such a case, equations (4.25) - (4.27) reduce to the conventional ones by dropping the u terms and $*$ subscript on the trajectory integrals.

To proceed with solving for g we use the number, momentum, and energy conservation properties of the linearized like particle collision operator to replace the drive term h by

$$h \equiv f_M \frac{I\left(v_{\|}+u\right)}{\Omega} \frac{M\left(v^2+u^2\right)}{2T^2} \frac{\partial T}{\partial \psi}. \tag{4.28}$$

For $\lambda \approx 1$ equation (4.4) gives

$$\frac{v^2+u^2}{2} \approx W \tag{4.29}$$

so that (4.28) becomes

$$h \approx f_M \frac{I\left(v_{\|}+u\right)}{\Omega} \frac{MW}{T^2} \frac{\partial T}{\partial \psi}. \tag{4.30}$$

Analogously to the conventional case, for the trapped particles $g = 0$ since the drive term vanishes upon transit averaging over a complete bounce. The goal of this section is therefore to solve (4.25) for g in the passing region of the $\left(W,\lambda\right)$ space.

Employing our collision operator (4.22) - (4.23) along with the fact that λ and W are constants of the motion we obtain

$$\oint_* d\theta \left(v_{\|}+u\right) \frac{\partial}{\partial \lambda}\left[\frac{g}{f_M} - \frac{I\left(v_{\|}+u\right)}{\Omega} \frac{M\left(W - T\sigma/M\right)}{T^2} \frac{\partial T}{\partial \psi}\right] = 0. \tag{4.31}$$

In the banana regime g/f_M is independent of θ to leading order giving

$$\frac{\partial}{\partial\lambda}\left(\frac{g}{f_M}\right)\oint_* d\theta\left(v_\parallel+u\right)=\oint_* d\theta\left(v_\parallel+u\right)\frac{\partial}{\partial\lambda}\left[\frac{IM\left(v_\parallel+u\right)\left(W-T\sigma/M\right)}{\Omega T^2}\frac{\partial T}{\partial\psi}\right]. \quad (4.32)$$

We observe that due to (4.7)

$$\left(v_\parallel+u\right)\frac{\partial\left(v_\parallel+u\right)}{\partial\lambda}=-SW\frac{B}{B_0}. \quad (4.33)$$

Thus, setting $B/B_0\approx 1$ we obtain

$$\frac{\partial}{\partial\lambda}\left(\frac{g}{f_M}\right)\Big|_p\approx-\frac{SIMW\left(W-T\sigma/M\right)}{\left\langle v_\parallel+u\right\rangle\Omega_0T^2}\frac{\partial T}{\partial\psi}, \quad (4.34)$$

where angle brackets denote the flux surface average such that

$$\left\langle v_\parallel+u\right\rangle\equiv\frac{1}{2\pi}\oint_* d\theta\left(v_\parallel+u\right). \quad (4.35)$$

Now we can verify the localization assumption made to derive our model collision operator. To do so we form

$$\frac{\partial}{\partial\lambda}\left(\frac{g-h_\sigma}{f_M}\right)=\frac{SIMW\left(W-\sigma T/M\right)}{\Omega_0T^2}\frac{\partial T}{\partial\psi}\left(\frac{1}{v_\parallel+u}-\frac{1}{\left\langle v_\parallel+u\right\rangle}\right). \quad (4.36)$$

To estimate the expression on the right side of (4.36) we flux surface average it and notice that

$$\left\langle \frac{1}{v_{\|}+u} \right\rangle - \frac{1}{\left\langle v_{\|}+u \right\rangle} \propto \left\langle \frac{1}{\sqrt{1-\kappa^2 \sin^2 \theta/2}} \right\rangle - \frac{1}{\left\langle \sqrt{1-\kappa^2 \sin^2 \theta/2} \right\rangle}. \tag{4.37}$$

We also observe from (4.5) that at the trapped-passing boundary $\lambda = 1/(1+2\varepsilon)$ when $\kappa^2 = 1$. However, once λ leaves the ε vicinity of the trapped-passing boundary, κ^2 becomes small and we can Taylor expand the expression on the right side of (4.37) to find

$$\left\langle \frac{1}{\sqrt{1-\kappa^2 \sin^2 \theta/2}} \right\rangle - \frac{1}{\left\langle \sqrt{1-\kappa^2 \sin^2 \theta/2} \right\rangle} \sim O\left(\kappa^4\right) \ll 1. \tag{4.38}$$

Thus, for the particles of interest, the λ derivative of the function inside the collision operator in (4.25) indeed goes like $O\left(\varepsilon^{-1}\right)$, justifying our dropping of the $\partial/\partial W$ terms in the equations (4.16) and (4.18).

It is necessary to emphasize that because of approximations made, solution (4.34) is only valid for $\lambda \approx 1$ and should not be applied in the freely passing particle region. Fortunately, the integral for the ion heat flux calculated in section 4.4 involves the expression (4.36) rather than $\partial g/\partial \lambda$ alone, thereby making the freely passing particles unimportant for the final result. Evaluation of the neoclassical parallel ion flow does not have the same advantage and therefore requires the alternate treatment presented in section 4.5.

Next, we have to ensure momentum conservation by choosing an appropriate value of σ. That is, we have to find σ such that

$$\left\langle \int \frac{d^3v}{B} v_{\|} C\{g-h\} \right\rangle = \left\langle \int \frac{d^3v}{B} (v_{\|}+u) C\{g-h\} \right\rangle = 0, \quad (4.39)$$

where the number conservation property of the full like particle collision operator is employed. To evaluate the right side of (4.39) we approximate $C\{g-h\}$ by (4.22) and use (4.23) along with (4.36) to write

$$\vec{\Gamma}\left\{\frac{g-h_\sigma}{f_M}\right\}\cdot\nabla_v\lambda = f_M \frac{(u+v_{\|})^2}{S^2W^2}\times$$

$$\left[\frac{\nu_\perp}{4}v^2 + \left(\frac{\nu_{\|}}{2}-\frac{\nu_\perp}{4}\right)u^2\right]\frac{SIMW(W-T\sigma/M)}{\Omega_0 T^2}\frac{\partial T}{\partial\psi}\left(\frac{1}{v_{\|}+u}-\frac{1}{\langle v_{\|}+u\rangle}\right). \quad (4.40)$$

Then, we recall (4.17) and (4.22) and integrate (4.39) by parts over λ to obtain

$$\int dW d\lambda f_M W(W-T\sigma/M)\left(\frac{1}{\langle v_{\|}+u\rangle}-\left\langle\frac{1}{v_{\|}+u}\right\rangle\right)\left[\frac{\nu_\perp}{4}v^2+\left(\frac{\nu_{\|}}{2}-\frac{\nu_\perp}{4}\right)u^2\right]=0, \quad (4.41)$$

where (4.33) is used to find $\partial(v_{\|}+u)/\partial\lambda$. Using (4.7) we now complete the integration over λ in (4.48) by employing [17]

$$\int d\lambda\left(\frac{1}{\sqrt{1-\lambda B/B_0}}-\frac{1}{\left\langle\sqrt{1-\lambda B/B_0}\right\rangle}\right)=$$

$$\int_0^{B_0/B}\frac{d\lambda}{\sqrt{1-\lambda B/B_0}}-\int_p\frac{d\lambda}{\left\langle\sqrt{1-\lambda B/B_0}\right\rangle}\approx 1.38\sqrt{2\varepsilon}, \quad (4.42)$$

where the p subscript on the second integral denotes that only the passing region is integrated over. Then, (4.41) reduces to

$$\int dW W^{1/2}\left(W-\sigma T/M\right)\left[\nu_{\perp}v^2+\left(2\nu_{\parallel}-\nu_{\perp}\right)u^2\right]f_M=0. \quad (4.43)$$

Finally, we introduce a new variable of integration $y\equiv M\left(v^2-u^2\right)/2T=M\left(W-u^2\right)/T$ in (4.43) and solve for σ to obtain

$$\sigma=\frac{\int_0^{\infty}dye^{-y}\left(y+Mu^2/T\right)^{3/2}\left[\nu_{\perp}y+\nu_{\parallel}\left(Mu^2/T\right)\right]}{\int_0^{\infty}dye^{-y}\left(y+Mu^2/T\right)^{1/2}\left[\nu_{\perp}y+\nu_{\parallel}\left(Mu^2/T\right)\right]}, \quad (4.44)$$

where frequencies $\nu_{\perp}$ and $\nu_{\parallel}$ are defined in terms of $x=\sqrt{y+Mu^2/2T}$ by (4.14).

In the absence of the background electric field $u=0$ and $x^2=y$ so that

$$\sigma=\frac{\int_0^{\infty}dxe^{-x^2}x^3\left[\mathrm{erf}\left(x\right)-\Psi\left(x\right)\right]}{\int_0^{\infty}dxe^{-x^2}x\left[\mathrm{erf}\left(x\right)-\Psi\left(x\right)\right]}=\frac{\sqrt{2}}{2\left[\sqrt{2}-\ln\left(1+\sqrt{2}\right)\right]}\approx 1.33 \quad (4.45)$$

which agrees with the conventional result [17, 20, 30].

4.4 Neoclassical ion heat flux in the pedestal

Here we proceed by calculating the neoclassical radial ion heat flux in the pedestal using the moment approach [30] so we need only evaluate

$$\left\langle \vec{q}\cdot\nabla\psi\right\rangle = -\frac{McIT}{Ze}\left\langle \int \frac{d^3v}{B}\left(\frac{Mv^2}{2T}-\frac{5}{2}\right)v_{\|}C\left\{g-h\right\}\right\rangle. \qquad (4.46)$$

To evaluate the integral on the right side of (4.46) we first employ the number, momentum and energy conservation properties of the linearized collision operator to rewrite it as

$$\left\langle \vec{q}\cdot\nabla\psi\right\rangle = -\frac{McIT}{Ze}\left\langle \int \frac{d^3v}{B}\frac{M\left(v^2+u^2\right)\left(v_{\|}+u\right)}{2T}f_M C\left\{g-h\right\}\right\rangle. \qquad (4.47)$$

Now we can continue in a manner similar to the one used in the previous section to find σ. That is, we again replace $C\left\{g-h\right\}$ with (4.22), then use (4.40) inside the collision operator and integrate the result by parts using (4.33) and (4.29). Then, (4.47) transforms into

$$\left\langle \vec{q}\cdot\nabla\psi\right\rangle = -\frac{4\pi M^2I^2S}{\Omega_0^2T^2}\frac{\partial T}{\partial\psi}\int dWd\lambda f_M W^2\left(W-T\sigma/M\right)\left(\frac{1}{\left\langle v_{\|}+u\right\rangle}-\left\langle\frac{1}{v_{\|}+u}\right\rangle\right)\times$$

$$\left[\frac{\nu_{\perp}}{4}v^2+\left(\frac{\nu_{\|}}{2}-\frac{\nu_{\perp}}{4}\right)u^2\right] \qquad (4.48)$$

and we can carry out the λ integration with the help of (4.42) to obtain

$$\left\langle \vec{q}\cdot\nabla\psi\right\rangle = -1.38\frac{\pi M^2I^2}{\Omega_0^2T^2}\frac{\partial T}{\partial\psi}\sqrt{\varepsilon S}\int dWW^{3/2}\left(W-T\sigma/M\right)\times$$

$$\left[\nu_{\perp}v^2 + \left(2\nu_{\parallel} - \nu_{\perp}\right)u^2\right]f_M . \tag{4.49}$$

Finally, we again substitute y for W to find

$$\left\langle \vec{q}\cdot\nabla\psi \right\rangle = -1.38\frac{n_i TI^2 e^{-Mu^2/2T}}{\sqrt{2\pi}\Omega_0^2 M}\frac{\partial T}{\partial\psi}\sqrt{\varepsilon S}\int_0^{\infty} dy e^{-y}\left(y + Mu^2/T\right)^{3/2}\times$$

$$\left(y + Mu^2/T - \sigma\right)\left[\nu_{\perp}y + \nu_{\parallel}\left(Mu^2/T\right)\right], \tag{4.50}$$

where n_i stands for the ion density and the parameter σ is provided by equation (4.44).

To proceed with the analysis we insert expression (4.14) for the collision frequencies into (4.50) to obtain

$$\left\langle \vec{q}\cdot\nabla\psi \right\rangle = -4.14e^{-\left(u/v_i\right)^2}\frac{n_i\nu_B TI^2}{\Omega_0^2 M}\frac{\partial T}{\partial\psi}\sqrt{\varepsilon S}\int_0^{\infty} dy e^{-y}\left[y + 2\left(u/v_i\right)^2\right]^{3/2}\times$$

$$\left[y + 2\left(u/v_i\right)^2 - \sigma\right]\left[y + \left(u/v_i\right)^2\right]^{-3/2}\left\{y\left[\mathrm{erf}\left(x\right) - \Psi\left(x\right)\right] + 2\left(u/v_i\right)^2\Psi\left(x\right)\right\}. \tag{4.51}$$

First, we consider the conventional limit in which $u = 0$ and $S = 1$. In this case, σ is given by (4.45) and $y = x^2$ so that (4.51) becomes

$$\left\langle \vec{q}\cdot\nabla\psi \right\rangle \approx -4.14n_i\frac{\nu_B TI^2\sqrt{\varepsilon}}{\Omega_0^2 M}\frac{\partial T}{\partial\psi}\int_0^{\infty} dx e^{-x^2}x^3\left(x^2 - 1.33\right)\left[\mathrm{erf}\left(x\right) - \Psi\left(x\right)\right] \approx$$

$$-1.35n_i\nu_B\frac{TI^2\sqrt{\varepsilon}}{\Omega_0^2 M}\frac{\partial T}{\partial\psi} \tag{4.52}$$

in agreement with the usual neoclassical result [17, 20, 30]. Now we can write the full result (4.51) in a normalized form as

$$\left\langle \vec{q}\cdot\nabla\psi\right\rangle = -1.35 n_i \nu_B \frac{TI^2\sqrt{\varepsilon}}{\Omega_0^2 M}\frac{\partial T}{\partial\psi} G\left(u\right)\sqrt{S_0}\,, \tag{4.53}$$

where $G\left(u\right)$ is given by

$$G\left(u\right) = 1.53 e^{-\left(u/v_i\right)^2}\int_0^\infty dy e^{-y}\left[y+2\left(u/v_i\right)^2\right]^{3/2}\left[y+2\left(u/v_i\right)^2-\sigma\right]\times$$

$$\left[y+\left(u/v_i\right)^2\right]^{-3/2}\left\{y\left[\mathrm{erf}\left(x\right)-\Psi\left(x\right)\right]+2\left(u/v_i\right)^2\Psi\left(x\right)\right\} \tag{4.54}$$

so that $G\left(0\right)=1$. The dependence of the normalized neoclassical heat flux on u is plotted in Fig 4.6. Notice, that as u goes beyond unity $G\left(u\right)$ decays exponentially with the electric field. As in the problem of the zonal flow in the pedestal discussed in the previous chapter, this decay is due to the trapped-passing boundary shifting towards the tail of the ion distribution function, thereby making the number of particles contributing to neoclassical heat flux negligible once the electric field is large enough as sketched in Fig 4.5.

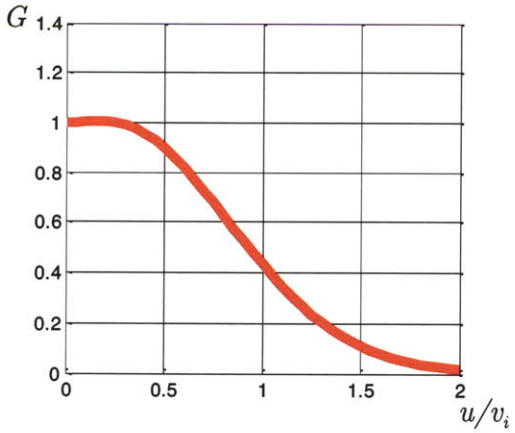

FIG 4.6. Normalized banana regime ion heat flux as a function of the equilibrium electric field.

4.5 Poloidal ion flow in the pedestal

Based on the technique of the previous sections it is also possible to evaluate the parallel ion flow in the pedestal. The ion velocity $\vec{V}_i$ is defined by

$$n_i \vec{V}_i \equiv \int d^3v \vec{v} f \tag{4.55}$$

giving

$$n_i \vec{V}_i = -\frac{cR}{Ze}\left(\frac{\partial p}{\partial \psi} + Zen_i \frac{\partial \phi}{\partial \psi}\right)\hat{\zeta} + \hat{n}\int d^3v v_{\|} g \tag{4.56}$$

where the two toroidally directed terms on the right side are diamagnetic and $\vec{E} \times \vec{B}$ while the parallel term is neoclassical, with $\hat{\zeta}$ the toroidal unit vector. To proceed it is convenient to rewrite (4.56) further as

$$\vec{V}_i = \omega R \hat{\zeta} - \hat{n}\frac{u}{n_i}\int d^3v g + \frac{\hat{n}}{n_i}\int d^3v \left(v_{\|} + u\right) g, \tag{4.57}$$

where $\omega \equiv -c\left(\partial\phi/\partial\psi\right) - \left(c/Zen_i\right)\left(\partial p/\partial\psi\right)$ with $p = n_i T$.

It is shown in Appendix E that to leading order in $\sqrt{\varepsilon S}$

$$\int d^3v g = 0. \tag{4.58}$$

Therefore, we only have to evaluate the last integral on the right side of (4.57). At this point, the previously mentioned difference between the treatment of the neoclassical ion heat flux and poloidal flow enters. The former is carried by the trapped and barely passing particles, which is mathematically manifested by the integrand in (4.46) being localized at $\lambda \approx 1$. This feature is what justifies our procedure of evaluating the ion heat flux because our model collision operator, as well as the resulting solution for the distribution function (4.34), is derived under the same localization assumption.

However, the integral for the neoclassical ion flow does not have this property. As in the conventional case, freely passing particles are expected to contribute to give the final answer to zeroth order in the $\sqrt{\varepsilon S}$ expansion. To ensure validity of the calculation we rewrite the last integral on the right side of (4.57) as follows

$$\int d^3v\left(v_{\|}+u\right)g = \int d^3v\left(v_{\|}+u\right)\left(g-h_\sigma\right)+\int d^3v\left(v_{\|}+u\right)h_\sigma \approx$$

$$-4\pi\int dWd\lambda W\lambda\frac{\partial\left(g-h_\sigma\right)}{\partial\lambda}+\int d^3v\left(v_{\|}+u\right)h_\sigma\,, \qquad (4.59)$$

where the integration by parts over λ is completed upon employing the Jacobian (4.17) with B/B_0 set equal unity. The first integral on the right side of (4.59) involves the function $\partial\left(g-h_\sigma\right)/\partial\lambda$ that satisfies our localization assumption as discussed after equation (4.36), thereby making appropriate our solution (4.34) for $\partial g/\partial\lambda$. The second integral on the right side of (4.59) only involves h_σ defined by equations (4.24), (4.28), and (4.44) that are valid for the freely passing particles as well as for the trapped and

barely passing. Thus, equation (4.59) is appropriate for evaluating the neoclassical ion flow in a self-consistent manner.

To proceed with finding an explicit expression for the ion flow we notice that the first integral on the right side of (4.59) can be evaluated in the same way as the neoclassical ion heat flux in section 4.4 to give a non-zero answer at first order in $\sqrt{\varepsilon S}$. Based on the conventional calculation we anticipate that the overall result for the neoclassical flow is of the zeroth order in this expansion parameter and therefore it is the second integral on the right side of (4.59) that contributes to the leading order flow, whereas the first one is negligible and of the same order as $\int d^3vg$ already ignored.

Having made the preceding comments, the calculation becomes straightforward. We use (4.24) and (4.28) to write

$$\int d^3v\left(v_{\|}+u\right)h_{\sigma}=\frac{I}{\Omega T}\frac{\partial T}{\partial\psi}\int d^3v\left(v_{\|}+u\right)^2\left[\frac{M\left(v^2+u^2\right)}{2T}-\sigma\right]f_M, \qquad (4.60)$$

that is easily evaluated to obtain

$$\int d^3v\left(v_{\|}+u\right)h_{\sigma}=\frac{n_iI}{M\Omega_0}\frac{\partial T}{\partial\psi}\left[\left(5/2-\sigma\right)+2\left(1-\sigma\right)\left(u/v_i\right)^2+2\left(u/v_i\right)^4\right]. \qquad (4.61)$$

To recover the conventional result, we insert (4.45) for σ to obtain

$$\frac{1}{n_i}\int d^3v\left(v_{\|}+u\right)h=\frac{7I}{6\Omega_0 M}\frac{\partial T}{\partial\psi}\approx 1.17\frac{I}{\Omega_0 M}\frac{\partial T}{\partial\psi}, \tag{4.62}$$

matching the answer given in [30]. To write (4.62) in a normalized form we introduce

$$J\left(u\right)\equiv\frac{6}{7}\left[\left(5/2-\sigma\right)+2\left(1-\sigma\right)\left(u/v_i\right)^2+2\left(u/v_i\right)^4\right] \tag{4.63}$$

such that

$$\frac{1}{n_i}\int d^3v\left(v_{\|}+u\right)g=\frac{7I}{6\Omega_0 M}\frac{\partial T}{\partial\psi}J\left(u\right) \tag{4.64}$$

with $J\left(0\right)=1$. Thus, recalling equation (4.57) we find the poloidal ion flow in the pedestal to be

$$V_i^{pol}=\frac{7IB_{pol}}{6\Omega_0 MB}\frac{\partial T}{\partial\psi}J\left(u\right)\approx\frac{7J\left(u\right)}{6\Omega_0 M}\frac{\partial T}{\partial r}, \tag{4.65}$$

where r stands for the minor radius of a given flux surface.

As shown on Fig 4.7, this normalized neoclassical flow does not decay exponentially with u/v_i in contrast to the behavior of the neoclassical heat flux found in the previous section and neoclassical polarization discussed in chapter 3. This aspect can be understood by observing that, unlike neoclassical ion heat flux and polarization, the leading order neoclassical ion flow is provided by the freely passing particles, making this flow persist even if the trapped and barely passing particle populations are diminished by a strong electric field. The replacement of (4.26) by (4.28) in (4.24) is due

to the electric field modified trapped-passing boundary along with the need to conserve momentum during ion-ion collisions which changes σ from its usual value. We discuss this result further in the next section.

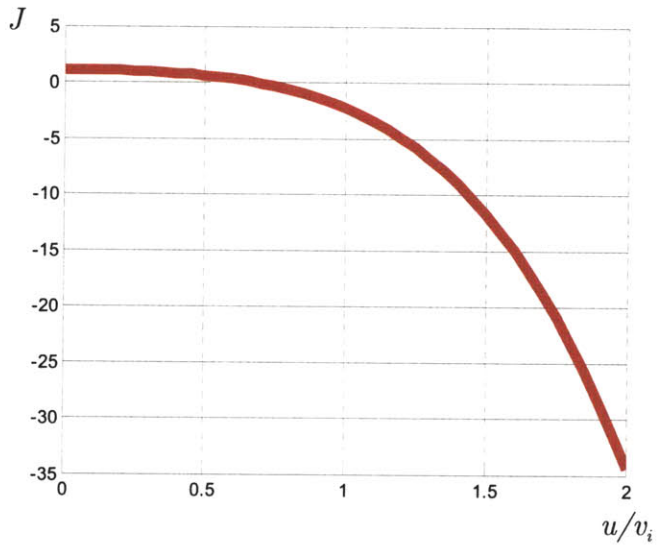

FIG 4.7. Neoclassical current as a function of the equilibrium electric field.

4.6 Discussion

In the preceding sections, we introduce the technique for evaluating the neoclassical ion behavior in the presence of a strong background electric field and use it to explicitly calculate the neoclassical ion heat flux and poloidal flow in the pedestal. A key step is the construction of the model collision operator (4.22) - (4.23) to replace the pitch angle scattering operator employed in the conventional calculation. The need for choosing a different model to describe collisions in the pedestal is due to the electric field modifying

the trapped-passing boundary in velocity space, thereby making the conventional operator inadequate for the particles that contribute the most to neoclassical ion heat flux.

Importantly, the effects of the electric field modified trapped-passing boundary impact the freely passing particles along with the need to conserve momentum in the like particle collisions. As a result, the neoclassical poloidal ion flow, carried by these particles, is rather sensitive to the electric field (though independent of orbit squeezing). Due to this sensitivity the ion flow can change direction within the pedestal as indicated by the sign change of $J\left(u\right)$ for $u > 0.6v_i$ as plotted in Fig 4.7. This new feature may explain the results of the experiments performed in the Alcator C-Mod by Kenneth Marr and coauthors [21] in which the absolute values of the observed banana regime ion flows are much bigger than those predicted by conventional formulas. Of course, their measurements focus on the impurity ion velocities, whereas the theory presented here applies to the background ions. However, for the purposes of an estimate we can neglect the effect of the electric field on the more collisional impurity orbits. In such a case, the net velocity of impurity ions can be evaluated given that of the background ions with the help of the following formula [28, 75-77]

$$V_z^{pol} = V_i^{pol} - \frac{cIB_{pol}}{eB^2}\left(\frac{1}{n_i}\frac{\partial p_i}{\partial \psi} - \frac{1}{Zn_z}\frac{\partial p_z}{\partial \psi}\right), \tag{4.66}$$

where we have dropped all terms small in $\sqrt{\varepsilon}$. Employing the conventional banana regime formula for the poloidal ion flow in (4.66) gives that V_i^{pol} and the sum of the diamagnetic terms have opposite signs, thereby resulting in a relatively low prediction for

the impurity flow. However, for a more realistic pedestal case of $u/v_i > 0.6$ the newly obtained expression (4.65) gives the terms on the right side of (4.66) adding to make V_z^{pol} larger. Thus, accounting for the effect of the electric field on the background ion orbits is expected to lead to better agreement between the theoretical and experimental results for the impurity ion flow. Also, because the neoclassical *electron* current depends on the net ion velocity [30], the bootstrap current will be increased in the pedestal.

Our new result for the banana regime ion heat flux possesses the same qualitative feature as the neoclassical polarization discussed in [78]. Namely, the neoclassical ion heat flux given by (4.53) decays exponentially in u. Obviously, this behavior is again explained by the fact that the trapped particle region is shifted to the tail of the Maxwellian distribution once electric field is large enough. We observe that the qualitative modifications of the pedestal case as compared to the conventional one are due to the parameter u, while the orbit squeezing parameter S only enters algebraically. In other words, it is the magnitude of the radial electric field rather than its shear that is the central quantity governing neoclassical phenomena in the pedestal.

The case of substantial electric field shear in the absence of a significant electric field itself was considered by Shaing and Hazeltine in [52]. It is important to emphasize that their problem formulation is not appropriate for most of flux surfaces in the pedestal, with the only possible exceptions being the very top or very bottom of this region, where the electric field can be considered small. Our calculation for the ion neoclassical heat

flux therefore captures the more important physics of the electric field, while still retaining orbit squeezing. Notice, that the heat conductivity given in [52] has the factor of $S^{3/2}$ in the denominator contradicting our equation (4.53) which involves $S^{1/2}$ instead. As far as we can follow the calculation carried out in [52] this contradiction is due to different approaches to modeling and treatment of the like particle collision operator. In particular, these differences result in our finding the effective ion-ion collision frequency to be $\sim \nu_B S/\varepsilon$, rather than the Shaing and Hazeltine estimate of $\sim \nu_B/\varepsilon S$. We provide the further comparison of our technique against that of [52] in Appendix F.

In brief, the banana regime ion heat conductivity we derive accounts for the presence of a strong radial electric field. As this electric field is inevitably present in tokamak regions such as a pedestal, it is this newly derived expression that has to be used there instead of the conventional formula. Moreover, as the parallel ion flow is altered by the electric field, we expect the bootstrap current to be enhanced in the pedestal.

5 Summary

This thesis encompasses several aspects of the physics of the pedestal, a tokamak region with a strong density gradient that is a defining feature of the High Confinement Mode of operation. Experiments find that the drastic density drop across the pedestal must be responsible for superior transport properties of H Mode plasmas as compared to those for L Mode, but the mechanism of this improvement is still poorly understood. In fact, it is this existence of short background scale, comparable to poloidal ion gyroradius, that greatly complicates the theoretical description of the H Mode regime. In this thesis we suggest an elegant resolution to this issue by developing a special version of the gyrokinetic formalism that allows both the larger background scale of the tokamak core and the shorter scale of the pedestal. This feature makes it a promising simulation tool capable of global H Mode modeling. Furthermore, this formalism allows us to determine analytical consequences about crucial pedestal features such as the allowed ion temperature profile; and neoclassical and turbulent transport coefficients.

The cornerstone of our version of gyrokinetics is employing the canonical angular momentum ψ_* as the radial variable. This choice accounts for classical Finite Larmor Radius effects and neoclassical Finite Drift Orbit effects in a systematic manner that is illustrated by equation (2.23), where the second and the third terms on the right side are of order $(\rho / L)\psi$ and $(\rho_{pol} / L)\psi$ respectively. Moreover, by omitting the $(\rho / L)\psi$

term we can investigate the effect of the pedestal size being as small as ρ_{pol} in a natural way. Applying this framework, we find that the leading order pedestal solution for ions in the banana regime must be a Maxwellian with temperature slowly varying over the ρ_{pol} scale of the plasma density. In other words, the background ion temperature profile cannot have as steep a pedestal region as the plasma density. This new insight is supported by recent direct measurements of helium ions temperature made at the DIII-D tokamak [60].

Our version of gyrokinetics culminates in the full nonlinear equation (2.74) for the first order correction to the distribution function which retains neoclassical collisional transport and the zonal flow drives. This equation has a general gyrokinetic feature of allowing small perpendicular wavelengths. It also includes the $\vec{E} \times \vec{B}$ drift in leading order in the streaming operator, a feature that is relevant specifically to the pedestal. Therefore, equation (2.74) is capable of describing turbulent phenomena in the pedestal that cannot be conveniently treated with currently prevailing approaches. Of course, a complete turbulent study requires implementing our equation in a code. However, we can get an idea of how plasma turbulence in the pedestal is different from that in the core by considering the zonal flow, which is done by solely analytical means in the second chapter of the thesis.

By revisiting the pioneering calculation of Rosenbluth and Hinton [11, 49] we find that in contrast to the core case there is a spatial phase shift between the zonal flow perturbations of the density and potential in the pedestal. This novelty is due to the strong electric field that is necessary to sustain the pedestal ion pressure balance. More importantly, we demonstrate that if this electric field goes beyond a certain critical value the zonal flow is effectively undamped since the residual starts approaching unity. Therefore, as zonal flow is the dominant mechanism limiting the turbulent transport and electric field is connected to density gradient by radial Boltzmann relation (2.59), we demonstrate for the first time that having a steep enough density profile improves confinement. That is, based on our analysis we suggest a first principles explanation for the advantage that H Mode operation has over L Mode as observed in experiments. Moreover, this logic also provides a new qualitative model of pedestal formation. Indeed, the preceding means that for a well developed zonal flow, once a steep enough density step is introduced over an L Mode type of density profile, turbulent transport is reduced, thereby causing this step to sharpen further.

Having said that anomalous transport in the pedestal is lowered by the background electric field we are led to consider neoclassical transport mechanisms. Accordingly, in chapter 3 we present the first fully self-consistent calculation of the neoclassical ion heat flux and poloidal flow in a banana-regime pedestal. Not surprisingly, we find that these quantities are also sensitive to the local electric field. In particular, the change in the parallel ion flow is consistent with recent C-mod observations [21] and will have a

significant impact on the tokamak stability and equilibrium because of the increased pedestal bootstrap current.

In summary, this thesis provides a multifaceted analytical description of the pedestal in tokamaks by focusing on the different physics issues underlying its formation and sustainment. It also presents a special version of gyrokinetics (a convenient tool that could be implemented in a code) that can successfully address the issue of finding an overall solution for the ion distribution function in H Mode in both the core and pedestal regions.

6 Bibliography

[1] F. Wagner, G. Becker, K. Behringer, D. Campbell, A. Eberhagen, W. Engelhardt, G. Fussmann, O. Gehre, J. Gernhardt, and G. Gierke, Phys. Rev. Lett. **49**, 1408 (1982).

[2] M. Kotschenreuther, G. Rewoldt, and W. Tang, Comput. Phys. Commun. **88**, 128 (1995).

[3] W. Dorland, F. Jenko, M. Kotschenreuther, and B. Rogers, Phys Plasmas **7**, 1904 (2000).

[4] A. Dimits, T. Williams, J. Byers, and B. Cohen, Phys. Rev. Lett. **77**, 71 (1996).

[5] Z. Lin, S. Ethier, T. Hahm, and W. Tang, Phys. Rev. Lett. **88**, 195004 (2002).

[6] J. Candy and R. Waltz, Journal of Computational Physics **186**, 545 (2003).

[7] J. Heikkinen, J. Janhunen, T. Kiviniemi, and P. Kaall, Contributions to Plasma Physics **44**, 13 (2004).

[8] J. Heikkinen, T. Kiviniemi, T. Kurki-Suonio, A. Peeters, and S. Sipilä, Journal of Computational Physics **173**, 527 (2001).

[9] P. Catto, Plasma Physics **20**, 719 (1978).

[10] G. G. Howes, S. C. Cowley, W. Dorland, G. W. Hammett, E. Quataert, and A. A. Schekochihin, Astrophys. J. **651**, 590 (2006).

[11] Z. Lin, T. Hahm, W. Lee, W. Tang, and R. White, Science **281**, 1835 (1998).

[12] J. Candy and R. Waltz, Phys. Rev. Lett. **91**, 45001 (2003).

[13] D. R. Ernst, P. T. Bonoli, P. J. Catto, W. Dorland, C. L. Fiore, R. S. Granetz, M. Greenwald, A. E. Hubbard, M. Porkolab, and M. H. Redi, Phys Plasmas **11**, 2637 (2004).

[14] M. N. Rosenbluth and F. L. Hinton, Phys. Rev. Lett. **80**, 724 (1998).

[15] F. Hinton and M. Rosenbluth, Plasma Phys. Controlled Fusion **41**, A653 (1999).

[16] L. M. Kovrizhnikh, Sov. Phys. -JETP **29**, 475 (1969).

[17] M. Rosenbluth, R. Hazeltine, and F. Hinton, Phys. Fluids **15**, 116 (1972).

[18] P. Rutherford, Phys. Fluids **13**, 482 (1970).

[19] Galeev, A. A. and Sagdeev R. Z., Sov. Phys. -JETP **26**, 233 (1968).

[20] F. Hinton and R. Hazeltine, Reviews of Modern Physics **48**, 239 (1976).

[21] Marr K, Lipschultz B , McDermott R, Catto P , Simakov A, Hutchinson I, Hughes J, Reinke M,
http://www.psfc.mit.edu/research/alcator/pubs/APS/APS2008/Marr_Poster_APS2008.pdf

[22] M. Tendler, Plasma Phys. Controlled Fusion **39**, B371 (1997).

[23] K. Burrell, Phys Plasmas **4**, 1499 (1997).

[24] J. Connor and H. Wilson, Plasma Phys.Control.Fusion **42**, R1 (2000).

[25] M. Greenwald, J. Terry, S. Wolfe, S. Ejima, M. Bell, S. Kaye, and G. Neilson, Nucl Fusion **28**, 2199 (1988).

[26] J. Taylor, J. Connor, and P. Helander, Phys Plasmas 5, 3065 (1998).

[27] S. Krasheninnikov and T. Soboleva, Phys Plasmas **13**, 094502 (2006).

[28] S. Hirshman and D. Sigmar, Nucl Fusion **21**, 1079 (1981).

[29] Hazeltine R D and Meiss J D, (Redwood City, CA: Addison-Wesley) (1991).

[30] Helander P and Sigmar D J, Collisional Transport in Magnetized Plasmas (Cambridge: Cambridge University Press) (2002).

[31] P. Helander, Phys Plasmas 5, 3999 (1998).

[32] F. M. Levinton, M. C. Zarnstorff, S. H. Batha, *et al*, Phys. Rev. Lett. **75**, 4417 (1995).

[33] E. J. Strait, L. L. Lao, M. E. Mauel, *et al*, Phys. Rev. Lett. **75**, 4421 (1995).

[34] P. Helander, Phys Plasmas 7, 2878 (2000).

[35] P. Helander, Phys Plasmas 9, 734 (2002).

[36] R. Hazeltine, Physics of Fluids B: Plasma Physics 1, 2031 (1989).

[37] T. Fulop, P. Helander, and P. J. Catto, Phys. Rev. Lett. **89**, 225003 (2002).

[38] A. N. Simakov and P. J. Catto, Phys Plasmas **10**, 398 (2003).

[39] T. Fülöp, P. J. Catto, and P. Helander, Phys Plasmas 8, 5214 (2001).

[40] J. Egedal, Nucl Fusion **40**, 1597 (2000).

[41] D. Hitchcock and R. Hazeltine, Plasma Physics **20**, 1241 (1978).

[42] P. Catto, W. Tang, and D. Baldwin, Plasma Physics **23**, 639 (1981).

[43] A. N. Kaufman, Phys.Fluids **15**, 1063 (1972).

[44] R. Hazeltine, S. Mahajan, and D. Hitchcock, Phys. Fluids **24**, 1164 (1981).

[45] X. Lee, J. Myra, and P. Catto, Phys. Fluids **26**, 223 (1983).

[46] I. B. Bernstein and P. J. Catto, Phys. Fluids **28**, 1342 (1985).

[47] F. I. Parra and P. J. Catto, Plasma Phys. Controlled Fusion **50**, 65014 (2008).

[48] P. J. Catto and R. Hazeltine, Phys Plasmas **13**, 122508 (2006).

[49] M. Rosenbluth and F. Hinton, Phys. Rev. Lett. **80**, 724 (1998).

[50] Y. Xiao, P. J. Catto, and K. Molvig, Phys Plasmas **14**, 032302 (2007).

[51] Y. Xiao, P. J. Catto, and W. Dorland, Phys Plasmas **14**, 055910 (2007).

[52] K. Shaing and R. Hazeltine, Physics of Fluids B: Plasma Physics **4**, 2547 (1992).

[53] D. H. E. Dubin, J. A. Krommes, C. Oberman, and W. Lee, Phys. Fluids **26**, 3524 (1983).

[54] T. Hahm, W. Lee, and A. Brizard, Phys. Fluids **31**, 1940 (1988).

[55] Brizard A, J. Plasma Physics **41**, 541 (1989).

[56] H. Qin, R. Cohen, W. Nevins, and X. Xu, Phys Plasmas **14**, 056110 (2007).

[57] Kruskal M D, J. Math. Phys. 3, 806 (1962).

[58] K. Ida, Plasma Phys. Controlled Fusion **40**, 1429 (1998).

[59] R. McDermott, B. Lipschultz, J. Hughes, P. Catto, A. Hubbard, I. Hutchinson, R. Granetz, M. Greenwald, B. LaBombard, and K. Marr, Phys Plasmas **16**, 056103 (2009).

[60] J. deGrassie, Private Communication (2008).

[61] E. Doyle, W. Houlberg, Y. Kamada, V. Mukhovatov, T. Osborne, A. Polevoi, G. Bateman, J. Connor, J. Cordey, and T. Fujita, Nucl Fusion **47**, S18 (2007).

[62] T. Fülöp and P. Helander, Phys Plasmas 8, 3305 (2001).

[63] P. Diamond, S. Itoh, K. Itoh, and T. Hahm, Plasma Phys.Control.Fusion **47**, 35–161 (2005).

[64] W. Dorland and G. Hammett, PHYSICS OF FLUIDS B PLASMA PHYSICS 5, 812 (1993).

[65] S. Coda, M. Porkolab, and K. Burrell, Physics Letters **A 273**, 125 (2000).

[66] S. Coda, M. Porkolab, and K. Burrell, Phys. Rev. Lett. **86**, 4835 (2001).

[67] F. L. Hinton and M. N. Rosenbluth, (1999).

[68] Y. Xiao and P. J. Catto, Phys Plasmas **13**, 082307 (2006).

[69] Belli E., (Ph.D. dissertation, Princeton University, 2006).

[70] Y. Xiao and P. J. Catto, Phys Plasmas **13**, 102311 (2006).

[71] F. Jenko, W. Dorland, M. Kotschenreuther, and B. Rogers, Phys Plasmas 7, 1904 (2000).

[72] H. Baek, S. Ku, and C. Chang, Phys Plasmas 13, 012503 (2006).

[73] G. Kagan and P. J. Catto, Plasma Phys. Controlled Fusion 50, 085010 (2008).

[74] M. N. Rosenbluth, W. M. MacDonald, and D. L. Judd, Physical Review 107, 1 (1957).

[75] Y. Kim, P. Diamond, and R. Groebner, Physics of Fluids B: Plasma Physics 3, 2050 (1991).

[76] P. Helander, Phys Plasmas 8, 4700 (2001).

[77] P. J. Catto and A. N. Simakov, Phys Plasmas 13, 052507 (2006).

[78] G. Kagan and P. J. Catto, Phys Plasmas 16, 056105 (2009).

7 Appendices

A First order corrections to gyrokinetic variables

We show in this appendix how the gyrokinetic procedure we describe in section 2 is implemented to obtain our gyrokinetic variables correct up to first order in δ.

Spatial variables. Following the steps outlined in section 2 we first apply the Vlasov operator to $\theta_0 \equiv \theta$ to obtain

$$\frac{d\theta_0}{dt} = \vec{v} \cdot \nabla\theta . \tag{A.67}$$

Next, we extract gyrodependent part of $d\theta_0/dt$ by writing

$$\frac{d\theta_0}{dt} - \left\langle \frac{d\theta_0}{dt} \right\rangle = \vec{v}_\perp \cdot \nabla\theta . \tag{A.68}$$

Then, we have to solve for θ_1 such that to lowest order

$$\frac{d}{dt}(\theta_0 + \theta_1) - \left\langle \frac{d}{dt}(\theta_0 + \theta_1) \right\rangle = 0 . \tag{A.69}$$

Using (A.68) and (2.6), (A.69) gives the equation

$$\Omega \frac{\partial\theta_1}{\partial\varphi} = \frac{d\theta_0}{dt} - \left\langle \frac{d\theta_0}{dt} \right\rangle = \vec{v}_\perp \cdot \nabla\theta . \tag{A.70}$$

To perform the integration over φ we use $\int \vec{v}_{\perp} d\varphi = \vec{v} \times \hat{n}$. Thus, setting $\langle \theta_1 \rangle = 0$ gives $\theta_1 = \Omega^{-1} \vec{v} \times \hat{n} \cdot \nabla \theta$, reproducing the relation (2.15) given in Sec 2.5.

We get the first order correction to ζ by similar procedure to find $\zeta_1 = \Omega^{-1} \vec{v} \times \hat{n} \cdot \nabla \zeta$ and (2.16).

As has already been mentioned, the ψ_* variable does not require a first order correction. However, if we were to simply take ψ as the initial variable and then proceed analogously to θ and ζ, we find

$$\tilde{\psi}_1 = \frac{\vec{v} \times \hat{n}}{\Omega} \cdot \nabla \psi. \tag{A.71}$$

If we define

$$\psi_1 \equiv \psi_* - \psi = -\frac{Mc}{Ze} R \vec{v} \cdot \hat{\zeta}, \tag{A.72}$$

then we see the gyrodependent part of ψ_1 is equal to $\tilde{\psi}_1$. This can be verified by using (2.22) for the magnetic field in tokamaks to rewrite ψ_1 as $\psi_1 = \Omega^{-1} \vec{v} \times \hat{n} \cdot \nabla \psi - I v_{\|} / \Omega$, as in (2.23).

Magnetic moment. Here we will only show the derivation of the gyrodependent part of μ_1 denoted as $\tilde{\mu}_1$. The gyroindependent term $\langle \mu_1 \rangle$ will be considered in the appendix C. As usual, we first evaluate

$$\frac{d\mu_0}{dt} = \frac{d}{dt}\left(\frac{v_\perp^2}{2B}\right) = -\mu_0 v_\parallel \hat{n}\cdot\nabla \ln B - \mu_0 v_\parallel \nabla\cdot\hat{n} - \mu_0 \vec{v}_\perp\cdot\nabla\ln B - \frac{v_\parallel^2}{B}\hat{n}\cdot\nabla\hat{n}\cdot\vec{v}_\perp$$

$$-\frac{v_\parallel}{2B}[\vec{v}_\perp\vec{v}_\perp - (\vec{v}\times\hat{n})(\vec{v}\times\hat{n})] : \nabla\hat{n} - \frac{Ze}{MB}\vec{v}_\perp\cdot\nabla\phi\,. \qquad \text{(A.73)}$$

We notice that

$$\left\langle \frac{d\mu_0}{dt}\right\rangle = -\mu_0 v_\parallel(\hat{n}\cdot\nabla\ln B - \nabla\cdot\hat{n}) = -\mu_0 v_\parallel \nabla\cdot B = 0, \qquad \text{(A.74)}$$

giving $d\mu_0/dt$ as purely gyrodependent. Then, we write

$$\Omega\frac{\partial\tilde{\mu}_1}{\partial\varphi} = \frac{d\mu_0}{dt} - \left\langle\frac{d\mu_0}{dt}\right\rangle = -\frac{v_\perp^2}{2B}\vec{v}_\perp\cdot\nabla\ln B - \frac{v_\parallel^2}{B}\hat{n}\cdot\nabla\hat{n}\cdot\vec{v}$$

$$-\frac{v_\parallel}{2B}[\vec{v}_\perp\vec{v}_\perp - (\vec{v}\times\hat{n})(\vec{v}\times\hat{n})] : \nabla\hat{n} - \frac{Ze}{MB}\vec{v}_\perp\cdot\nabla\phi\,. \qquad \text{(A.75)}$$

Our ordering allows large gradients for the electric potential and therefore the last term in (A.75) must be analyzed carefully. To do so, notice that

$$\left(\frac{\partial\phi}{\partial\varphi}\right)_{\psi_*,\theta_*,\zeta_*} \approx \frac{\partial\phi(\psi_* - \psi_1, \theta_* - \theta_1, \zeta_* - \zeta_1)}{\partial\varphi} = -\frac{\partial\phi}{\partial\psi}\frac{\partial\psi_1}{\partial\varphi} - \frac{\partial\phi}{\partial\theta}\frac{\partial\theta_1}{\partial\varphi} - \frac{\partial\phi}{\partial\zeta}\frac{\partial\zeta_1}{\partial\varphi}. \qquad \text{(A.76)}$$

Using the relations for θ_1, ζ_1, and ψ_1 we obtain

$$\left(\frac{\partial\phi}{\partial\varphi}\right)_{\psi_*,\theta_*,\zeta_*} \approx -\frac{\partial\phi}{\partial\psi}\frac{\vec{v}_\perp\cdot\nabla\psi}{\Omega} - \frac{\partial\phi}{\partial\theta}\frac{\vec{v}_\perp\cdot\nabla\theta}{\Omega} - \frac{\partial\phi}{\partial\zeta}\frac{\vec{v}_\perp\cdot\nabla\zeta}{\Omega} = -\frac{\vec{v}_\perp\cdot\nabla\phi}{\Omega}. \quad \text{(A.77)}$$

This form is conveniently integrated over φ to find (2.29).

Energy. Once again, we begin by applying the Vlasov operator to the initial variable to find

$$\frac{dE_0}{dt} \equiv \frac{d}{dt}\left(\frac{v^2}{2}\right) = -\frac{Ze}{M}\vec{v}\cdot\nabla\phi = -\frac{Ze}{M}\vec{v}_\perp\cdot\nabla\phi - \frac{Ze}{M}v_\parallel\hat{n}\cdot\nabla\phi. \quad \text{(A.78)}$$

Next, with the help of (A.77) we extract the gyrodependent part of the total time derivative to find

$$\frac{dE_0}{dt} - \left\langle\frac{dE_0}{dt}\right\rangle \approx -\frac{Ze}{M}v_\parallel\hat{n}\cdot\nabla\tilde{\phi} + \frac{Ze}{M}\Omega\frac{\partial\tilde{\phi}}{\partial\varphi}. \quad \text{(A.79)}$$

Our orderings allow us to neglect the first term on the right side of (A.79) and therefore the equation for E_1 can be written as

$$\Omega\frac{\partial E_1}{\partial\varphi} = \frac{dE_0}{dt} - \left\langle\frac{dE_0}{dt}\right\rangle = \frac{Ze}{M}\Omega\frac{\partial\tilde{\phi}}{\partial\varphi}. \quad \text{(A.80)}$$

Integrating setting $\langle E_1\rangle = 0$ gives

$$E_1 = \frac{Ze}{M}\tilde{\phi}. \quad \text{(A.81)}$$

A useful expression. Before deriving the first order correction to the gyrophase we obtain a useful relation that will also be helpful during the calculation of the second order corrections. Suppose we have a physical quantity given in terms of original spatial variables $Q = Q(\psi,\theta,\zeta)$. Then, according to (2.24) we define $Q_* \equiv Q(\psi_*,\theta_*,\zeta_*)$. As it has been already mentioned there is a first order difference between Q and Q_*. For a slowly varying function we have upon Taylor expanding

$$Q \approx Q(\psi_* - \psi_1, \theta_* - \theta_1, \zeta_* - \zeta_1,) \approx Q_* - \psi_1 \frac{\partial Q}{\partial \psi} - \theta_1 \frac{\partial Q}{\partial \theta} - \zeta_1 \frac{\partial Q}{\partial \zeta}.$$

Note that this expansion is not normally valid for such quantities as electric potential and distribution function because they contain strong spatial gradients. Inserting the relations for θ_1, ζ_1, and ψ_1 we find

$$Q \approx Q_* - \frac{\partial f}{\partial \theta}\frac{\vec{v}\times\hat{n}}{\Omega}\cdot\nabla\theta - \frac{\partial f}{\partial \zeta}\frac{\vec{v}\times\hat{n}}{\Omega}\cdot\nabla\zeta - \frac{\partial f}{\partial \psi}\frac{\vec{v}\times\hat{n}}{\Omega}\cdot\nabla\psi + \frac{\partial f}{\partial \psi}\frac{Mc}{Ze}Rv_{\|}\hat{n}\cdot\hat{\zeta},$$

or defining I as in (2.22)

$$Q \approx Q_* - \frac{\vec{v}\times\hat{n}}{\Omega}\cdot\nabla Q + \frac{Iv_{\|}}{\Omega}\frac{\partial Q}{\partial \psi}. \qquad \text{(A.82)}$$

Gyrophase. Evaluating $d\varphi_0/dt$ gives

$$\frac{d\varphi_0}{dt} = \frac{v_{\|}}{v_{\perp}^2}\vec{v}\cdot\nabla\hat{n}\cdot(\vec{v}\times\hat{n}) + \vec{v}\cdot\nabla\hat{e}_2\cdot\hat{e}_1 + \frac{Ze}{Mv_{\perp}^2}(\vec{v}\times\hat{n})\cdot\nabla\phi - \Omega. \qquad \text{(A.83)}$$

To extract the gyrodependent part of $d\varphi_0/dt$ we have to take into account that Ω becomes slightly gyrodependent when expressed in terms of the starred variables. To do so we employ Eq. (A.82) to write

$$\Omega \approx \Omega_* - \frac{\vec{v}\times\hat{n}}{\Omega}\cdot\nabla\Omega + \frac{Iv_\parallel}{\Omega}\frac{\partial\Omega}{\partial\psi}. \tag{A.84}$$

In addition, we use the vector relation

$$\vec{v}\cdot\nabla\hat{n}\cdot\left(\vec{v}\times\hat{n}\right) = v_\parallel\vec{v}_\perp\cdot\hat{n}\times\vec{\kappa} - \frac{v_\perp^2}{2}\hat{n}\cdot\nabla\times\hat{n} +$$

$$\frac{1}{2}\left[\left(\vec{v}\times\hat{n}\right)\vec{v}_\perp + \vec{v}_\perp\left(\vec{v}\times\hat{n}\right)\right]:\nabla\hat{n}, \tag{A.85}$$

where $\vec{\kappa}\equiv\hat{n}\cdot\nabla\hat{n}$ and the double-dot notation is defined by $\vec{a}\vec{c}:\vec{\vec{T}}\equiv\vec{c}\cdot\vec{\vec{T}}\cdot\vec{a}$.

Finally, we rewrite the $(\vec{v}\times\hat{n})\cdot\nabla\phi$ term so that it can be integrated over φ. For this purpose we notice that

$$\left(\frac{\partial\phi}{\partial\mu}\right)_{\psi_*,\theta_*,\zeta_*} \approx \frac{\partial\phi\left(\psi_*-\psi_1,\theta_*-\theta_1,\zeta_*-\zeta_1\right)}{\partial\mu_*} = -\frac{\partial\phi}{\partial\psi}\frac{\partial\psi_1}{\partial\mu} - \frac{\partial\phi}{\partial\theta}\frac{\partial\theta_1}{\partial\mu} - \frac{\partial\phi}{\partial\zeta}\frac{\partial\zeta_1}{\partial\mu}. \tag{A.86}$$

Using the relations for θ_1, ζ_1, and ψ_1, we find that

$$\left(\frac{\partial\phi}{\partial\mu}\right)_{\psi_*,\theta_*,\zeta_*} \approx -\frac{B}{\Omega v_\perp^2}\vec{v}\times\hat{n}\cdot\nabla\phi - \frac{B}{v_\parallel}\frac{Mc}{Ze}I\frac{\partial\phi}{\partial\psi}. \tag{A.87}$$

or

$$\frac{\vec{v}\times\hat{n}\cdot\nabla\phi}{v_\perp^2}=-\frac{\Omega}{B}\left(\frac{\partial\phi}{\partial\mu}+\frac{B}{v_\parallel}\frac{Mc}{Ze}I\frac{\partial\phi}{\partial\psi}\right). \tag{A.88}$$

On the right side of the last formula the original variables can be replaced by the starred ones without an error to the order of interest. Thus, the only φ dependence in $(\vec{v}\times\hat{n})\cdot\nabla\phi$ enters through the electric potential.

Inserting (A.84), (A.85), and (A.88) into (A.83) and gyroaveraging we obtain $\left\langle d\varphi_0/dt\right\rangle=-\bar{\Omega}$ as given by (2.33). Extracting the gyrodependent part of $d\varphi_0/dt$ and using $\Omega\,\partial\varphi_1/\partial\varphi_0=d\varphi_0/dt-\left\langle d\varphi_0/dt\right\rangle$ yields

$$\varphi_1=-\frac{\vec{v}_\perp}{\Omega}\cdot\left(\frac{v_\parallel^2}{v_\perp^2}\vec{\kappa}-\hat{n}\times\nabla\hat{e}_2\cdot\hat{e}_1+\nabla\ln B\right)-\frac{v_\parallel^2}{4\Omega v_\perp^2}\left[\vec{v}_\perp\vec{v}_\perp-\left(\vec{v}\times\hat{n}\right)\left(\vec{v}\times\hat{n}\right)\right]:\nabla\hat{n}-$$

$$\frac{Ze}{MB}\left(\frac{\partial\tilde{\Phi}}{\partial\mu}+\frac{B}{v_\parallel}\frac{Mc}{Ze}I\frac{\partial\tilde{\Phi}}{\partial\psi_*}\right), \tag{A89}$$

where

$$\tilde{\Phi}\equiv\frac{1}{2\pi}\int^{\varphi}\phi\left(\psi_*,\theta_*,\zeta_*,E_*,\mu_*,\varphi_0'\right)d\varphi_0' \tag{A.90}$$

with $\left\langle\tilde{\Phi}\right\rangle=0$.

Expression for $\nabla_\perp \phi$. To complete appendix A we give an expression that will be used in appendix C to prove that the magnetic moment correction given by (2.29) and (2.31) makes μ a good adiabatic invariant. This expression is obtained by using the relations (A.77) and (A.88) to decompose the perpendicular component of electric field as

$$\nabla_\perp \phi = -\frac{\Omega}{v_\perp^2}\frac{\partial \phi}{\partial \varphi}\vec{v}_\perp - \frac{\Omega}{B}\left(\frac{\partial \phi}{\partial \mu} + \frac{BI}{\Omega v_\parallel}\frac{\partial \phi}{\partial \psi_*}\right)\vec{v}\times\hat{n}. \qquad \text{(A.91)}$$

B Second order corrections to gyrokinetic variables

In this appendix we perform a second iteration to evaluate the gyrokinetic variables to second order in δ. To carry out this calculation we apply the gyrokinetic procedure to the variables correct up the first order that were calculated in appendix A.

Spatial variables. We begin by evaluating

$$\frac{d}{dt}(\theta_0+\theta_1) = v_\parallel \hat{n}\cdot\nabla\theta + \frac{\vec{v}\times\hat{n}\vec{v}}{\Omega} : \nabla\nabla\theta - \vec{v}\cdot\nabla\left(\frac{\hat{n}}{\Omega}\right)\times\vec{v}\cdot\nabla\theta - \frac{c}{B}\nabla\phi\times\hat{n}\cdot\nabla\theta \,. \qquad \text{(B.1)}$$

Here, the first term is one order larger than the others and therefore it needs to be expressed in terms of the new variables up to order δ. To do so for $\hat{n}\cdot\nabla\theta$, we employ (A.82),

$$\hat{n}\cdot\nabla\theta = (\hat{n}\cdot\nabla\theta)_* - \frac{\vec{v}\times\hat{n}}{\Omega}\cdot\nabla(\hat{n}\cdot\nabla\theta) + \frac{McI}{Ze}v_\parallel\frac{\partial}{\partial\psi_*}(\hat{n}\cdot\nabla\theta). \qquad \text{(B.2)}$$

In addition, $v_{||}$ requires some special care. Writing

$$v_{||} = \sqrt{2\left(E_0 - \mu_0 B(\vec{r})\right)} \tag{B.3}$$

and using $v_{||}^*$ from (2.25) we expand to obtain

$$v_{||}^* - v_{||} = \frac{\left(\mu_0 - \mu_*\right)B_* + \left(B - B_*\right)\mu_* + \left(E_* - E_0\right)}{v_{||}}. \tag{B.4}$$

Using (2.29), (2.31), and (A.81) and applying (A.82) to B we find

$$v_{||}^* - v_{||} = \frac{\vec{v}\cdot\vec{v}_M}{v_{||}} - \mu_* \frac{\vec{v}\times\hat{n}}{\Omega v_{||}}\cdot\nabla B + \mu_* \frac{I}{\Omega}\frac{\partial B}{\partial \psi_*} + \frac{\vec{v}_\perp\vec{v}_\perp}{4\Omega} : \left(\hat{n}\times\nabla\hat{n} - \nabla\hat{n}\times\hat{n}\right) +$$

$$+ \frac{v_\perp^2}{2\Omega}\hat{n}\cdot\nabla\times\hat{n}. \tag{B.5}$$

Having (B.2) and (B.5), we can now gyroaverage $v_{||}\hat{n}\cdot\nabla\theta$ by writing

$$v_{||}\hat{n}\cdot\nabla\theta = v_{||}^*(\hat{n}\cdot\nabla\theta)_* + \left(v_{||} - v_{||}^*\right)(\hat{n}\cdot\nabla\theta)_* + \left[\hat{n}\cdot\nabla\theta - (\hat{n}\cdot\nabla\theta)_*\right]v_{||}^*, \tag{B.6}$$

and after some algebra find

$$\left\langle v_{||}\hat{n}\cdot\nabla\theta\right\rangle = v_{||}^*(\hat{n}\cdot\nabla\theta)_* + \frac{Iv_{||}}{\Omega}\frac{\partial\left(v_{||}\hat{n}\cdot\nabla\theta\right)}{\partial\psi} - \frac{v_\perp^2}{2\Omega}(\hat{n}\cdot\nabla\times\hat{n})(\hat{n}\cdot\nabla\theta). \tag{B.7}$$

Next, we need to gyroaverage the rest of the terms in (B.1). These calculations give

$$\left\langle \frac{\vec{v}\times\hat{n}\vec{v}}{\Omega} : \nabla\nabla\theta \right\rangle = \frac{\vec{\vec{I}}\times\hat{n}}{\Omega} : \nabla\nabla\theta = 0, \tag{B.8}$$

$$\left\langle \vec{v}\cdot\nabla\left(\frac{\hat{n}}{\Omega}\right)\times\vec{v}\cdot\nabla\theta\right\rangle = -\left[\hat{n}\times\left(\frac{v_{\|}^2}{\Omega}\vec{\kappa}+\frac{v_{\perp}^2}{2\Omega}\nabla\ln B\right)+\frac{v_{\perp}^2}{2\Omega}\hat{n}(\hat{n}\cdot\nabla\times\hat{n})\right]\cdot\nabla\theta, \quad \text{(B.9)}$$

and

$$\left\langle \frac{c}{B}\nabla\phi\times\hat{n}\cdot\nabla\theta\right\rangle = \frac{c}{B}\nabla\bar{\phi}\times\hat{n}\cdot\nabla\theta. \quad \text{(B.10)}$$

Collecting the terms we reproduce the relation (2.18) for $\left\langle d(\theta_0+\theta_1)/dt\right\rangle = \left\langle \dot{\theta}_*\right\rangle$.

Now, we can extract the gyrodependent part of (B.1) and, using

$$\Omega\frac{\partial\theta_2}{\partial\varphi_0} = \frac{d}{dt}(\theta_0+\theta_1)-\left\langle\frac{d}{dt}(\theta_0+\theta_1)\right\rangle,$$

integrate it over φ setting $\langle\theta_2\rangle = 0$ to obtain θ_2 as

$$\theta_2 = \frac{\vec{v}\times\hat{n}\vec{v}\times\hat{n}-\vec{v}_{\perp}\vec{v}_{\perp}}{4}:\frac{\nabla\nabla\theta}{\Omega^2}+\frac{1}{\Omega}\left[\left(\frac{\vec{v}_{\perp}}{4}+\vec{v}_{\|}\right)\vec{v}\times\hat{n}+\vec{v}\times\hat{n}\left(\frac{\vec{v}_{\perp}}{4}+\vec{v}_{\|}\right)\right]:\nabla\left(\frac{\hat{n}}{\Omega}\right)\times\nabla\theta+$$
$$\frac{\hat{n}\cdot\nabla\theta}{\Omega^2}\left[v_{\|}\vec{v}\cdot\vec{\kappa}+\frac{1}{8}\left(\vec{v}_{\perp}\vec{v}\times\hat{n}+\vec{v}\times\hat{n}\vec{v}_{\perp}\right):\nabla\hat{n}\right]+$$
$$\frac{v_{\|}}{\Omega^2}\vec{v}_{\perp}\cdot\nabla\hat{n}\cdot\nabla\theta-\frac{c}{B\Omega}\nabla\tilde{\Phi}\times\hat{n}\cdot\nabla\theta \quad \text{(B11)}$$

The calculation of ζ_2 involves exactly the same procedure as used for θ_2 giving (2.19) as well as

$$\zeta_2 = \frac{\vec{v}\times\hat{n}\vec{v}\times\hat{n}-\vec{v}_{\perp}\vec{v}_{\perp}}{4}:\frac{\nabla\nabla\zeta}{\Omega^2}+\frac{1}{\Omega}\left[\left(\frac{\vec{v}_{\perp}}{4}+\vec{v}_{\|}\right)\vec{v}\times\hat{n}+\vec{v}\times\hat{n}\left(\frac{\vec{v}_{\perp}}{4}+\vec{v}_{\|}\right)\right]:\nabla\left(\frac{\hat{n}}{\Omega}\right)\times\nabla\zeta+$$

$$\frac{\hat{n}\cdot\nabla\zeta}{\Omega^2}\left[v_{\|}\vec{v}\cdot\vec{\kappa}+\frac{1}{8}\left(\vec{v}_{\perp}\vec{v}\times\hat{n}+\vec{v}\times\hat{n}\vec{v}_{\perp}\right):\nabla\hat{n}\right]+\frac{v_{\|}}{\Omega^2}\vec{v}_{\perp}\cdot\nabla\hat{n}\cdot\nabla\zeta-\frac{c}{B\Omega}\nabla\tilde{\Phi}\times\hat{n}\cdot\nabla\zeta, \quad \text{(B.12)}$$

where $\nabla\zeta=\hat{\zeta}/R$ and $\nabla\nabla\zeta=-\left(\hat{\zeta}\hat{R}+\hat{R}\hat{\zeta}\right)/R^2$.

The total time derivative of ψ_* has been already given in the appendix A. Here we only have to extract the gyrodependent part of $\dot{\psi}_*$ in order to obtain $\left(\psi_*\right)_2$,

$$\dot{\psi}_*-\left\langle\dot{\psi}_*\right\rangle=c\frac{\partial\tilde{\phi}}{\partial\zeta}. \quad \text{(B.13)}$$

Integrating $\Omega\partial\left(\psi_*\right)_2/\partial\varphi_0=\dot{\psi}_*-\left\langle\dot{\psi}_*\right\rangle$ along with using $\left\langle\left(\psi_*\right)_2\right\rangle=0$ gives

$$\left(\psi_*\right)_2=\frac{c}{\Omega}\frac{\partial\tilde{\Phi}}{\partial\zeta_*}, \quad \text{(B.14)}$$

where to second order $\psi_*\rightarrow\psi-\left(Mc/Ze\right)R\vec{v}\cdot\hat{\zeta}+\left(\psi_*\right)_2$.

Energy. To evaluate the Vlasov operator with the required precision it is convenient to write

$$\frac{d\left(E_0+E_1\right)}{dt}=-\frac{Ze}{M}\vec{v}\cdot\nabla\phi+\frac{Ze}{M}\frac{d\tilde{\phi}}{dt}\equiv\frac{Ze}{M}(-\frac{d\phi}{dt}+\left(\frac{\partial\phi}{\partial t}\right)_{\vec{r}})+\frac{Ze}{M}\frac{d\tilde{\phi}}{dt}=$$

$$\frac{Ze}{M}(-\frac{d\bar{\phi}}{dt}+\left(\frac{\partial\phi}{\partial t}\right)_{\vec{r}}). \quad \text{(B.15)}$$

We can express the total time derivative in terms of the starred variables as

$$\frac{d\bar{\phi}}{dt} = \left(\frac{\partial\bar{\phi}}{\partial t}\right)_* + \frac{\partial\bar{\phi}}{\partial\zeta_*}\dot{\zeta}_* + \frac{\partial\bar{\phi}}{\partial\theta_*}\dot{\theta}_* + \frac{\partial\bar{\phi}}{\partial\psi_*}\dot{\psi}_* + \frac{\partial\bar{\phi}}{\partial E_*}\dot{E}_* + \frac{\partial\bar{\phi}}{\partial\mu_*}\dot{\mu}_*, \tag{B.16}$$

where the $\partial\bar{\phi}/\partial\mu_*$ term can be neglected since $\dot{\mu}_* = 0$ to the requisite order. Also, using

$$\left(\frac{\partial\bar{\phi}}{\partial t}\right)_{\vec{r}} - \left(\frac{\partial\bar{\phi}}{\partial t}\right)_* \sim \delta\left(\frac{\partial\bar{\phi}}{\partial t}\right)_{\vec{r}} \sim \delta^2\Omega k_\perp\rho\bar{\phi}$$

and inserting (B.16) into (B.15) we find

$$\frac{d(E_0 + E_1)}{dt} = \frac{Ze}{M}\frac{\partial\tilde{\phi}}{\partial t} - \frac{Ze}{M}\left(\frac{\partial\bar{\phi}}{\partial\zeta_*}\dot{\zeta}_* + \frac{\partial\bar{\phi}}{\partial\theta_*}\dot{\theta}_* + \frac{\partial\bar{\phi}}{\partial\psi_*}\dot{\psi}_* + \frac{\partial\bar{\phi}}{\partial E_*}\dot{E}_*\right). \tag{B.17}$$

Gyroaveraging and using $\left\langle\left(\dot{E}_0 + \dot{E}_1\right)\right\rangle \approx \dot{E}_*$, we solve for $\dot{E}_*$ to find (2.27).

Next, we extract the gyrodependent part of $d(E_0 + E_1)/dt$ to obtain the equation for E_2 to be

$$\Omega\frac{\partial E_2}{\partial\varphi} = \dot{E}_* - \left\langle\dot{E}_*\right\rangle = \frac{Ze}{M}\frac{\partial\tilde{\phi}}{\partial t}, \tag{B.18}$$

which upon integrating and setting $\langle E_2\rangle = 0$ yields

$$E_2 = \frac{c}{B}\frac{\partial\tilde{\Phi}}{\partial t}. \tag{B.19}$$

To finish this section we analyze the $\partial\bar{\phi}/\partial E_*$ term

$$\frac{\partial\bar{\phi}}{\partial E_*} \approx \frac{\partial\bar{\phi}\left(\psi_* - \frac{\vec{v}\times\hat{n}}{\Omega}\cdot\nabla\psi + \frac{Mc}{Ze}Rv_{\|}\hat{n}\cdot\hat{\zeta}, \theta_* - \frac{\vec{v}\times\hat{n}}{\Omega}\cdot\nabla\theta, \zeta_* - \frac{\vec{v}\times\hat{n}}{\Omega}\cdot\nabla\zeta\right)}{\partial E_*}. \quad \text{(B.20)}$$

Note, that in conventional gyrokinetics the first order corrections to the spatial variables involve only $v_\perp$ and therefore do not depend on E in leading order. Here, the correction to ψ_* involves $v_{\|}$ and therefore this term needs to be retained. From (B.20) we find

$$\frac{\partial\bar{\phi}}{\partial E_*} \approx \frac{Mc}{Ze}R\hat{n}\cdot\hat{\zeta}\frac{\partial\bar{\phi}}{\partial\psi_*}\frac{\partial v_{\|}}{\partial E} \approx \frac{I}{\Omega v_{\|}}\frac{\partial\bar{\phi}}{\partial\psi_*}. \quad \text{(B.21)}$$

This expression will be helpful for proving that the magnetic moment is a good invariant. Also, for numerical simulations the right side of the relation (B.21) may be more preferable to use than $\partial\phi/\partial E_*$. Indeed, the E_* dependence of $\bar{\phi}$ is weaker than the ψ_* dependence of $\bar{\phi}$ and therefore numerical evaluation of $\partial\phi/\partial E_*$ potentially contains a greater error than that of $\partial\bar{\phi}/\partial\psi_*$.

C Magnetic moment

This appendix verifies that the corrections to the magnetic moment we employ allow us to neglect $\partial f/\partial\mu$ term in the kinetic equation. To do so, we need to prove that

$\langle \dot{\mu}_* \rangle / \mu_0 \sim \delta^3 \Omega$. This has been already proven for the case without electric potential [39,47,57]. Here, we need only check that the first and second order terms of $\dot{\mu}$ explicitly involving the electric potential gyroaverage away. These terms are given by

$$(\dot{\mu})_\phi \equiv -\frac{Ze}{MB}\vec{v}_\perp \cdot \nabla\phi + \frac{d}{dt}\left(\frac{Ze}{MB}\tilde{\phi}\right) - \frac{Ze}{M}\nabla\phi \cdot \nabla_v\left(\mu_1|_{\vec{r},\vec{v}}\right), \quad \text{(C.1)}$$

where we define

$$\mu_1|_{\vec{r},\vec{v}} \equiv -\frac{\vec{v}\cdot\vec{v}_M}{B} - \frac{v_\parallel}{4B\Omega}[\vec{v}_\perp(\vec{v}\times\hat{n}) + (\vec{v}\times\hat{n})\vec{v}_\perp] : \nabla\hat{n} - \frac{\mu_0 v_\parallel}{\Omega}\hat{n}\cdot\nabla\times\hat{n}\,. \quad \text{(C.2)}$$

It is convenient to consider the first two terms on the right side of (C.1) together

$$-\frac{Ze}{MB}\vec{v}_\perp \cdot \nabla\phi + \frac{d}{dt}\left(\frac{Ze}{MB}\tilde{\phi}\right) = -\frac{Ze}{MB}\left(\frac{d\bar{\phi}}{dt} - \left(\frac{\partial\phi}{\partial t}\right)_r - v_\parallel\hat{n}\cdot\nabla\phi\right) + \tilde{\phi}\frac{d}{dt}\left(\frac{Ze}{MB}\right).$$

Using the preceding allows us to rewrite $(\dot{\mu})_\phi$ as

$$(\dot{\mu})_\phi \equiv -\frac{Ze}{MB}\left(\frac{d\bar{\phi}}{dt} - \left(\frac{\partial\phi}{\partial t}\right)_r - v_\parallel\hat{n}\cdot\nabla\phi\right) - \frac{Ze}{MB}\tilde{\phi}\vec{v}\cdot\nabla\ln B - \frac{Ze}{M}\nabla\phi\cdot\nabla_v\left(\mu_1|_{\vec{r},\vec{v}}\right). \quad \text{(C.3)}$$

In the following subsections we evaluate each term of (C.3) up to order $\delta^2\Omega\mu_0$ in terms of the starred variables and then gyroaverage.

Third term. Here, we express $v_\parallel\hat{n}\cdot\nabla\phi$ in terms of starred variables before considering the first three terms together. We start by writing

$$\nabla\phi = \frac{\partial\phi}{\partial\psi_*}\nabla\psi_* + \frac{\partial\phi}{\partial\theta_*}\nabla\theta_* + \frac{\partial\phi}{\partial\zeta_*}\nabla\zeta_* + \frac{\partial\phi}{\partial E_*}\nabla E_* + \frac{\partial\phi}{\partial\mu_*}\nabla\mu_* + \frac{\partial\phi}{\partial\varphi_*}\nabla\varphi_*. \qquad \text{(C.4)}$$

To evaluate the right side of (C.3) to the required order, relations (2.17), (2.15), (2.16), and (2.26) must be inserted for ψ_*, θ_*, ζ_*, and E_*, respectively. To the same order, for μ_* and φ_* we only need insert the zero order expressions in terms of δ. As a result, (C.4) becomes

$$\nabla\phi \approx \frac{\partial\phi}{\partial\zeta_*}\nabla\zeta + \frac{\partial\phi}{\partial\theta_*}\nabla\theta + \frac{\partial\phi}{\partial\psi_*}\nabla\psi + \frac{\partial\phi}{\partial\zeta_*}\left(-\nabla\left(\frac{\hat{n}}{\Omega}\right)\times\vec{v}\cdot\nabla\zeta + \frac{\vec{v}\times\hat{n}}{\Omega}\cdot\nabla\nabla\zeta\right)$$
$$+\frac{\partial\phi}{\partial\theta_*}\left(-\nabla\left(\frac{\hat{n}}{\Omega}\right)\times\vec{v}\cdot\nabla\theta + \frac{\vec{v}\times\hat{n}}{\Omega}\cdot\nabla\nabla\theta\right) - \frac{\partial\phi}{\partial\psi_*}\frac{Mc}{Ze}\nabla\left(R\hat{\zeta}\right)\cdot\vec{v} + \frac{\partial\phi}{\partial E_*}\frac{Ze}{M}\nabla\tilde{\phi}$$

$$-\frac{\partial\phi}{\partial\mu_*}\left(\mu_0\nabla\ln B + \frac{v_\parallel}{B}\nabla\hat{n}\cdot\vec{v}\right) + \frac{\partial\phi}{\partial\varphi_*}\left(\frac{v_\parallel}{v_\perp^2}\nabla\hat{n}\cdot(\vec{v}\times\hat{n}) + \nabla\hat{e}_2\cdot\hat{e}_1\right). \qquad \text{(C.5)}$$

The first three terms in the preceding equation are one order larger than the rest so the difference between $\nabla\zeta$, $\nabla\theta$, $\nabla\psi$ and $(\nabla\zeta)_*$, $(\nabla\theta)_*$, $(\nabla\psi)_*$ has to be taken into account. To do this we employ (2.23) and (A.82) so that Eq. (C.5) transforms into

$$\nabla\phi = \frac{\partial\phi}{\partial\psi_*}\left(\nabla\psi\right)_* + \frac{\partial\phi}{\partial\theta_*}\left(\nabla\theta\right)_* + \frac{\partial\phi}{\partial\zeta_*}\left(\nabla\zeta\right)_* + \frac{Iv_\parallel}{\Omega}\left(\frac{\partial\phi}{\partial\zeta_*}\frac{\partial\left(\nabla\zeta\right)}{\partial\psi} + \frac{\partial\phi}{\partial\theta_*}\frac{\partial\left(\nabla\theta\right)}{\partial\psi} + \frac{\partial\phi}{\partial\psi_*}\frac{\partial\left(\nabla\psi\right)}{\partial\psi}\right)$$

$$-\nabla\left(\frac{\hat{n}}{\Omega}\right)\times\vec{v}\cdot\left(\frac{\partial\phi}{\partial\zeta_*}\nabla\zeta + \frac{\partial\phi}{\partial\theta_*}\nabla\theta + \frac{\partial\phi}{\partial\psi_*}\nabla\psi\right) - \frac{\partial\phi}{\partial\psi_*}\frac{Mc}{Ze}\nabla\left(v_\parallel R\hat{\zeta}\cdot\hat{n}\right) + \frac{\partial\phi}{\partial E}\frac{Ze}{M}\nabla\tilde{\phi}$$

$$-\frac{\partial\phi}{\partial\mu_*}\left(\mu_*\nabla\ln B + \frac{v_\parallel}{B}\nabla\hat{n}\cdot\vec{v}\right) + \frac{\partial\phi}{\partial\varphi_*}\left(\frac{v_\parallel}{v_\perp^2}\nabla\hat{n}\cdot(\vec{v}\times\hat{n}) + \nabla\hat{e}_2\cdot\hat{e}_1\right). \qquad \text{(C.6)}$$

To the required order we can write

$$\nabla\left(\frac{\hat{n}}{\Omega}\right)\times\vec{v}\cdot\left(\frac{\partial\phi}{\partial\psi_*}\nabla\psi+\frac{\partial\phi}{\partial\theta_*}\nabla\theta+\frac{\partial\phi}{\partial\zeta_*}\nabla\zeta\right)\approx\nabla\left(\frac{\hat{n}}{\Omega}\right)\times\vec{v}\cdot\nabla\phi=$$

$$=\frac{\nabla\hat{n}\times\vec{v}\cdot\nabla\phi}{\Omega}+\frac{\nabla\ln B}{\Omega}\vec{v}\times\hat{n}\cdot\nabla\phi, \qquad \text{(C7)}$$

and with the help of relation (A.91) we get

$$\nabla\left(\frac{\hat{n}}{\Omega}\right)\times\vec{v}\cdot\nabla\phi=-\left(\frac{\partial\phi}{\partial\mu}+\frac{BI}{\Omega v_{\|}}\frac{\partial\phi}{\partial\psi_*}\right)\left(\frac{v_\perp^2}{B}\nabla\ln B+\frac{v_{\|}}{B}\nabla\hat{n}\cdot\vec{v}\right)+\frac{v_{\|}}{v_\perp^2}\frac{\partial\phi}{\partial\varphi}\nabla\hat{n}\cdot(\vec{v}\times\hat{n}). \qquad \text{(C.8)}$$

Finally, by inserting (C.8) into (C.6) we end up with

$$\nabla\phi\approx\frac{\partial\phi}{\partial\psi_*}(\nabla\psi)_*+\frac{\partial\phi}{\partial\theta_*}(\nabla\theta)_*+\frac{\partial\phi}{\partial\zeta_*}(\nabla\zeta)_*+\frac{Iv_{\|}}{\Omega}\left(\frac{\partial\phi}{\partial\psi_*}\frac{\partial(\nabla\psi)}{\partial\psi}+\frac{\partial\phi}{\partial\theta_*}\frac{\partial(\nabla\theta)}{\partial\psi}+\frac{\partial\phi}{\partial\zeta_*}\frac{\partial(\nabla\zeta)}{\partial\psi}\right)$$

$$+\frac{I}{\Omega v_{\|}}\frac{\partial\phi}{\partial\psi_*}\left(v_\perp^2\nabla(\ln B)+v_{\|}\nabla\hat{n}\cdot\vec{v}\right)+\mu_0\frac{\partial\phi}{\partial\mu}\nabla\ln B+\frac{\partial\phi}{\partial\varphi}\nabla\hat{e}_2\cdot\hat{e}_1-\frac{Mc}{Ze}\frac{\partial\phi}{\partial\psi_*}\nabla\left(v_{\|}R\hat{\zeta}\cdot\hat{n}\right)+\frac{Ze}{M}\frac{\partial\phi}{\partial E}\nabla\tilde{\phi}.$$

In the preceding expression the first three terms are one order larger than the rest.

Then, relating $v_{\|}$ and $v_{\|}^*$ and $\hat{n}$ and $\hat{n}_*$ using (A.82) and (B.5), noting that $\hat{n}_*\cdot(\nabla\psi)_*=(\hat{n}\cdot\nabla\psi)_*=0$, and observing that the $\left(\partial\phi/\partial E_*\right)v_{\|}\hat{n}\cdot\nabla\tilde{\phi}$ term is higher order, we evaluate $v_{\|}\hat{n}\cdot\nabla\phi$ to find

$$v_\parallel \hat{n}\cdot\nabla\phi \approx v_\parallel^* \hat{n}_*\cdot\left[\frac{\partial\phi}{\partial\zeta_*}(\nabla\zeta)_* + \frac{\partial\phi}{\partial\theta_*}(\nabla\theta)_*\right] + \frac{Iv_\parallel^2}{\Omega}\hat{n}\cdot\left(\frac{\partial\phi}{\partial\zeta_*}\frac{\partial(\nabla\zeta)}{\partial\psi} + \frac{\partial\phi}{\partial\theta_*}\frac{\partial(\nabla\theta)}{\partial\psi} + \frac{\partial\phi}{\partial\psi_*}\frac{\partial(\nabla\psi)}{\partial\psi}\right)$$
$$+\frac{I}{\Omega}\frac{\partial\phi}{\partial\psi_*}\left(v_\perp^2\hat{n}\cdot\nabla(\ln B) + v_\parallel\vec{\kappa}\cdot\vec{v}\right) + \mu_0 v_\parallel\frac{\partial\phi}{\partial\mu_*}\hat{n}\cdot\nabla\ln B + v_\parallel\frac{\partial\phi}{\partial\varphi_*}\hat{n}\cdot\nabla\hat{e}_2\cdot\hat{e}_1$$
$$-\frac{Mc}{Ze}\frac{\partial\phi}{\partial\psi_*}v_\parallel\hat{n}\cdot\nabla\left(v_\parallel R\hat{\zeta}\cdot\hat{n}\right) - v_\parallel\left(-\frac{\partial\hat{n}}{\partial\psi}\frac{Iv_\parallel}{\Omega} + \frac{\vec{v}\times\hat{n}}{\Omega}\cdot\nabla\hat{n}\right)\cdot\nabla\phi$$
$$-\left(\frac{\vec{v}\cdot\vec{v}_M}{v_\parallel} - \mu_*\frac{\vec{v}\times\hat{n}}{\Omega v_\parallel}\cdot\nabla B + \mu_*\frac{I}{\Omega}\frac{\partial B}{\partial\psi_*} + \frac{\vec{v}_\perp\vec{v}_\perp}{4\Omega} : (\hat{n}\times\nabla\hat{n} - \nabla\hat{n}\times\hat{n}) + \frac{v_\perp^2}{2\Omega}\hat{n}\cdot\nabla\times\hat{n}\right)\hat{n}\cdot\nabla\phi \quad \text{(C.9)}$$

Then, we use

$$v_\parallel^2\frac{\partial\hat{n}}{\partial\psi}\cdot\nabla\phi + v_\parallel^2\hat{n}\cdot\left[\frac{\partial\phi}{\partial\zeta_*}\frac{\partial(\nabla\zeta)}{\partial\psi} + \frac{\partial\phi}{\partial\theta_*}\frac{\partial(\nabla\theta)}{\partial\psi} + \frac{\partial\phi}{\partial\psi_*}\frac{\partial(\nabla\psi)}{\partial\psi}\right] - \mu_0\frac{\partial B}{\partial\psi}\hat{n}\cdot\nabla\phi =$$
$$v_\parallel\left[\frac{\partial\phi}{\partial\theta_*}\frac{\partial}{\partial\psi}\left(v_\parallel\hat{n}\cdot\nabla\theta\right) + \frac{\partial\phi}{\partial\zeta_*}\frac{\partial}{\partial\psi}\left(v_\parallel\hat{n}\cdot\nabla\zeta\right)\right]$$

and

$$\hat{n}\cdot\nabla\left(v_\parallel R\hat{\zeta}\cdot\hat{n}\right) = R\hat{\zeta}\cdot[\hat{n}\cdot\nabla(\vec{v}\cdot\hat{n}\hat{n})] = \frac{I}{B}\vec{v}\cdot\vec{\kappa} + v_\parallel R\hat{\zeta}\cdot\vec{\kappa}\,.$$

Gyroaveraging then gives

$$\left\langle v_\parallel\hat{n}\cdot\nabla\phi\right\rangle \approx v_\parallel^*\hat{n}_*\cdot\left[\frac{\partial\overline{\phi}}{\partial\zeta_*}(\nabla\zeta)_* + \frac{\partial\overline{\phi}}{\partial\theta_*}(\nabla\theta)_*\right] + \frac{Iv_\parallel}{\Omega}\left(\frac{\partial\overline{\phi}}{\partial\zeta_*}\frac{\partial\left(v_\parallel\hat{n}\cdot\nabla\zeta\right)}{\partial\psi} + \frac{\partial\overline{\phi}}{\partial\theta_*}\frac{\partial\left(v_\parallel\hat{n}\cdot\nabla\theta\right)}{\partial\psi}\right)$$
$$+\left(\frac{Iv_\perp^2}{\Omega}\frac{\partial\overline{\phi}}{\partial\psi_*} + \mu_0 v_\parallel\frac{\partial\overline{\phi}}{\partial\mu_*}\right)\hat{n}\cdot\nabla\ln B - \frac{Mc}{Ze}\frac{\partial\overline{\phi}}{\partial\psi_*}Rv_\parallel^2\hat{\zeta}\cdot\vec{\kappa} - \frac{v_\perp^2}{2\Omega}\left(\hat{n}\cdot\nabla\times\hat{n}\right)\left(\hat{n}\cdot\nabla\overline{\phi}\right)$$
$$-\left\langle v_\parallel\frac{\vec{v}\times\hat{n}}{\Omega}\cdot\nabla\hat{n}\cdot\nabla\phi\right\rangle. \quad \text{(C.10)}$$

First three terms. Next, we analyze $d\overline{\phi}/dt$. We start by writing

$$\frac{d\bar{\phi}}{dt} = \frac{\partial\bar{\phi}}{\partial t} + \dot{\psi}_* \frac{\partial\bar{\phi}}{\partial\psi_*} + \dot{\theta}_* \frac{\partial\bar{\phi}}{\partial\theta_*} + \dot{\zeta}_* \frac{\partial\bar{\phi}}{\partial\zeta_*} + \dot{E}_* \frac{\partial\bar{\phi}}{\partial E_*}, \tag{C.11}$$

where we insert (2.17) - (2.19) for $\dot{\psi}_*$, $\dot{\theta}_*$, and $\dot{\zeta}_*$, respectively, while for $\dot{E}_*$ we need only the leading order result

$$\dot{E}_* \approx -\frac{Ze}{M} v_\parallel \hat{n} \cdot \nabla\bar{\phi}. \tag{C.12}$$

To eliminate the terms quadratic in $\bar{\phi}$ we use (B.21) along with the observation that

$$\frac{\partial\bar{\phi}}{\partial\theta_*}\vec{v}_E \cdot \nabla\theta + \frac{\partial\bar{\phi}}{\partial\zeta_*}\vec{v}_E \cdot \nabla\zeta \approx -\frac{\partial\bar{\phi}}{\partial\psi_*}\vec{v}_E \cdot \nabla\psi,$$

where $\vec{v}_E \equiv \left(c/B\right)\hat{n} \times \nabla\bar{\phi}$. Then, (C.11) becomes

$$\frac{d\bar{\phi}}{dt} = \left(\frac{\partial\bar{\phi}}{\partial t}\right)_* + \frac{\partial\bar{\phi}}{\partial\zeta_*}\left[\left(v_\parallel^* \hat{n}_* + \vec{v}_M\right) \cdot \nabla\zeta + \frac{Iv_\parallel}{\Omega}\frac{\partial}{\partial\psi}\left(\frac{Iv_\parallel}{BR^2}\right)\right]$$

$$+\frac{\partial\bar{\phi}}{\partial\theta_*}\left[\left(v_\parallel^* \hat{n}_* + \vec{v}_M\right) \cdot \nabla\theta + \frac{Iv_\parallel}{\Omega}\frac{\partial\left(v_\parallel \hat{n} \cdot \nabla\theta\right)}{\partial\psi}\right]. \tag{C.13}$$

Combining (C.13) with (C.10) we obtain

$$\frac{d\bar{\phi}}{dt} - \left\langle\left(\frac{\partial\phi}{\partial t}\right)_r\right\rangle - \left\langle v_\parallel \hat{n} \cdot \nabla\phi\right\rangle \approx \vec{v}_M \cdot \nabla\zeta \frac{\partial\bar{\phi}}{\partial\zeta_*} + \vec{v}_M \cdot \nabla\theta \frac{\partial\bar{\phi}}{\partial\theta_*} - \left(\frac{Iv_\perp^2}{\Omega}\frac{\partial\bar{\phi}}{\partial\psi_*} + \mu_0 v_\parallel \frac{\partial\bar{\phi}}{\partial\mu_*}\right)\hat{n} \cdot \nabla \ln B$$
$$+\frac{Mc}{Ze} R v_\parallel^2 \hat{\zeta} \cdot \vec{\kappa}\frac{\partial\bar{\phi}}{\partial\psi_*} + \frac{v_\perp^2}{2\Omega}\left(\hat{n} \cdot \nabla \times \hat{n}\right)\left(\hat{n} \cdot \nabla\bar{\phi}\right) - \left\langle\frac{v_\parallel}{\Omega}\vec{v} \times \hat{n} \cdot \nabla\hat{n} \cdot \nabla\phi\right\rangle. \tag{C.14}$$

Remaining terms. Finally, we analyze the last two terms in (C.3). As in the conventional gyrokinetics we find

$$-B\nabla\phi\cdot\nabla_v\left(\mu_1\big|_{\vec{r},\vec{v}}\right)=\frac{\vec{v}_\perp\cdot\nabla\phi}{\Omega}(\vec{v}\times\hat{n})\cdot\nabla\ln B+\vec{v}_M\cdot\nabla\phi+\frac{v_\parallel}{2\Omega}(\nabla\phi\times\hat{n})\cdot\nabla\hat{n}\cdot\vec{v}_\perp$$
$$+\frac{v_\parallel}{2\Omega}(\vec{v}\times\hat{n})\cdot\nabla\hat{n}\cdot\nabla\phi+\frac{v_\parallel}{2\Omega}(\vec{v}_\perp\cdot\nabla\phi)(\hat{n}\cdot\nabla\times\hat{n})$$
$$+\left[\frac{2v_\parallel}{\Omega}(\vec{v}\times\hat{n})\cdot(\hat{n}\cdot\nabla\hat{n})+\frac{1}{4\Omega}[\vec{v}_\perp(\vec{v}\times\hat{n})+(\vec{v}\times\hat{n})\vec{v}_\perp]:\nabla\hat{n}+\frac{v_\perp^2}{2\Omega}\hat{n}\cdot\nabla\times\hat{n}\right]\hat{n}\cdot\nabla\phi.$$

Then, we notice that

$$\left\langle\frac{\vec{v}_\perp\cdot\nabla\phi}{\Omega}(\vec{v}\times\hat{n})\cdot\nabla\ln B\right\rangle=-\left\langle\frac{\partial\phi}{\partial\varphi}(\vec{v}\times\hat{n})\cdot\nabla\ln B\right\rangle=\langle\phi\vec{v}_\perp\rangle\cdot\nabla\ln B,$$

and therefore

$$\left\langle-\frac{\tilde{\phi}\vec{v}\cdot\nabla\ln B}{B}-\nabla\phi\cdot\nabla_v\left(\mu_1\big|_{\vec{r},\vec{v}}\right)\right\rangle=\frac{\vec{v}_M\cdot\nabla\phi}{B}+\frac{\mu_0}{\Omega}\left(\hat{n}\cdot\nabla\times\hat{n}\right)\left(\hat{n}\cdot\nabla\bar{\phi}\right)$$
$$+\left\langle\frac{v_\parallel}{2\Omega B}\left(\nabla\phi\times\hat{n}\right)\cdot\nabla\hat{n}\cdot\vec{v}_\perp+\frac{v_\parallel}{2\Omega B}\left(\vec{v}\times\hat{n}\right)\cdot\nabla\hat{n}\cdot\nabla\phi\right\rangle. \quad \text{(C.15)}$$

Next, we combine the terms in the triangle brackets from (C.15) with the $\left\langle v_\parallel\frac{\vec{v}\times\hat{n}}{\Omega}\cdot\nabla\hat{n}\cdot\nabla\phi\right\rangle$ term from (C.14). With the help of relation (A.91) and $\vec{v}_\perp\vec{v}_\perp+(\vec{v}\times\hat{n})(\vec{v}\times\hat{n})=v_\perp^2\left(\vec{I}-\hat{n}\hat{n}\right)$, we obtain

$$\left\langle\frac{v_\parallel}{2\Omega}\left(\nabla\phi\times\hat{n}\right)\cdot\nabla\hat{n}\cdot\vec{v}_\perp-\frac{v_\parallel}{2\Omega}\left(\vec{v}\times\hat{n}\right)\cdot\nabla\hat{n}\cdot\nabla\phi\right\rangle=$$

$$-v_{\|}\mu_0\left(\frac{\partial\bar{\phi}}{\partial\mu}+\frac{BI}{\Omega v_{\|}}\frac{Mc}{Ze}\frac{\partial\bar{\phi}}{\partial\psi_*}\right)\hat{n}\cdot\nabla\ln B\,. \tag{C.16}$$

Combining terms. Finally, we combine the results from the subsections of this appendix to obtain

$$\frac{MB}{Ze}(\dot{\mu})_\phi=\frac{\partial\bar{\phi}}{\partial\psi_*}\vec{v}_M\cdot\nabla\psi+\frac{Iv_\perp^2}{2\Omega}\frac{\partial\bar{\phi}}{\partial\psi_*}\hat{n}\cdot\nabla\ln B-\frac{\partial\bar{\phi}}{\partial\psi_*}\frac{Mc}{Ze}Rv_{\|}^2\hat{\zeta}\cdot\vec{\kappa}\,.$$

Noticing that $\vec{v}_{\nabla B}\cdot\nabla\psi=-\left(Iv_\perp^2/2\Omega\right)\hat{n}\cdot\nabla\ln B$ and $\vec{v}_\kappa\cdot\nabla\psi=\left(Mc/Ze\right)Rv_{\|}^2\hat{\zeta}\cdot\vec{\kappa}$ we find to the requisite order the desired result

$$(\dot{\mu})_\phi=0\,. \tag{C.17}$$

D Jacobian in the strong potential gradient case

To follow is the derivation of the leading order Jacobian of the transformation from the original set of variables to the one consisting of ψ_*, θ_*, ζ_*, ε, μ_*, and φ_*. We start by writing

$$\frac{1}{J}\equiv\left|\frac{\partial\left(\psi_*,\theta_*,\zeta_*,\varepsilon,\mu_*,\varphi_*\right)}{\partial\left(\vec{r},\vec{v}\right)}\right|=\left|\begin{array}{c|c|c|c|c|c}\nabla\psi_* & \nabla\theta_* & \nabla\zeta_* & \nabla\varepsilon & \nabla\mu_* & \nabla\varphi_* \\ \hline \nabla_v\psi_* & \nabla_v\theta_* & \nabla_v\zeta_* & \nabla_v\varepsilon & \nabla_v\mu_* & \nabla_v\varphi_*\end{array}\right|. \tag{D.1}$$

Keeping only the leading order terms in all the blocks yields

$$\frac{1}{J}=\left|\begin{array}{c|c|c|c|c|c} \nabla\psi & \nabla\theta & \nabla\zeta & \frac{Ze}{M}\nabla\phi & 0 & 0 \\ \hline -\frac{I}{\Omega}\hat{n} & 0 & 0 & \vec{v} & \frac{\vec{v}_\perp}{B} & -\frac{\vec{v}\times\hat{n}}{v_\perp^2} \end{array}\right|. \qquad \text{(D.2)}$$

In the absence of sharp potential gradient we would neglect the $\nabla\phi$ term in the upper-right block to obtain the usual expression for the leading order Jacobian, namely,

$$\frac{1}{J}=-\left[\left(\vec{v}\times\frac{\vec{v}_\perp}{B}\right)\cdot\frac{\vec{v}\times\hat{n}}{v_\perp^2}\right](\nabla\psi\times\nabla\theta\cdot\nabla\zeta)=\frac{v_\parallel}{B}\vec{B}\cdot\nabla\theta. \qquad \text{(D.3)}$$

To calculate the determinant for $w\sim\rho_{pol}$ we multiply the first column of matrix (D.2) by $\left(Ze/M\right)\left(\partial\phi/\partial\psi\right)$, the second by $\left(Ze/M\right)\left(\partial\phi/\partial\theta\right)$ and the third by $\left(Ze/M\right)\left(\partial\phi/\partial\zeta\right)$, add them together and subtract the resulting linear combination from the fourth column of matrix (D.2) to obtain

$$\frac{1}{J}=\left|\begin{array}{c|c|c|c|c|c} \nabla\psi & \nabla\theta & \nabla\zeta & 0 & 0 & 0 \\ \hline -\frac{I}{\Omega}\hat{n} & 0 & 0 & \vec{v}+\frac{cI}{B}\frac{\partial\phi}{\partial\psi}\hat{n} & \frac{\vec{v}_\perp}{B} & -\frac{\vec{v}\times\hat{n}}{v_\perp^2} \end{array}\right|. \qquad \text{(D.4)}$$

The preceding determinant is easily evaluated to find

$$\frac{1}{J}=\left(\frac{v_\parallel}{B}+\frac{cI}{B^2}\frac{\partial\phi}{\partial\psi}\right)\vec{B}\cdot\nabla\theta. \qquad \text{(D.4)}$$

Notice, that if $1/w\equiv\left|\left(e/T\right)\left(\partial\phi/\partial\psi\right)\nabla\psi\right|$ is of order $1/\rho_{pol}$ the two terms on the right side of (D.4) are comparable.

E The integral on the right side of (4.57)

When evaluating the parallel ion flow we used (4.58) to neglect one of the integrals on the right side of (4.58). Integrals of this type do not appear in the conventional case and require special treatment which is presented here.

We start by switching to W and λ variables,

$$\int d^3vg = 4\pi S \int \frac{dWd\lambda BW}{B_0\left(v_{\|}+u\right)} g = -4\pi \int dWd\lambda g \frac{\partial\left(v_{\|}+u\right)}{\partial\lambda}, \quad \text{(E.1)}$$

where (4.33) is used to obtain the integral in the expression on the right side of (E.1). Before integrating by parts it is convenient to rewrite (E.1) as

$$\int d^3vg = -4\pi \int dWd\lambda g \frac{\partial\left[\left(v_{\|}+u\right)-\sqrt{2W/S_0}\right]}{\partial\lambda} =$$

$$-4\pi \int dWd\lambda \sqrt{2SW} g \frac{\partial\left(\sqrt{1-\lambda B/B_0}-1\right)}{\partial\lambda}. \quad \text{(E.2)}$$

Then, observing that

$$\int_p d\lambda g \frac{\partial\left(\sqrt{1-\lambda B/B_0}-1\right)}{\partial\lambda} = \left(\sqrt{1-\lambda B/B_0}-1\right) g \Big|_{\text{freely passing}}^{\text{trapped-passing}} -$$

$$\int_p d\lambda \left(\sqrt{1-\lambda B/B_0}-1\right) \frac{\partial g}{\partial\lambda}, \quad \text{(E.3)}$$

and, using that $g = 0$ at the trapped-passing boundary as well as $\lambda \to 0$ for the freely passing particles, we transform (E.2) into

$$\int d^3vg = 4\pi \int dW d\lambda \sqrt{2SW}\left(\sqrt{1-\lambda B/B_0}-1\right)\frac{\partial g}{\partial \lambda}. \qquad \text{(E.4)}$$

Next, we insert (4.34) into (E.4) to find

$$\int d^3vg = \frac{4\pi IM\sqrt{S}}{\Omega_0 T^2}\frac{\partial T}{\partial \psi}\int dW d\lambda W\left(W - T\sigma/M\right)\left(\frac{\sqrt{1-\lambda B/B_0}-1}{\left\langle\sqrt{1-\lambda B/B_0}\right\rangle}\right). \qquad \text{(E.5)}$$

Replacing the λ variable with κ^2 using (4.6), along with the observation that

$$d\lambda = \frac{2\varepsilon d\kappa^2}{\kappa^2 + 2\varepsilon}, \qquad \text{(E.6)}$$

equation (E.5) becomes

$$\int d^3vg \approx \frac{8\pi IM\varepsilon S}{\Omega_0 T^2}\frac{\partial T}{\partial \psi}\int dW d\kappa^2 \frac{W\left(W - T\sigma/M\right)}{\kappa^2 + 2\varepsilon}\times$$

$$\frac{\left[\sqrt{1-\kappa^2\sin^2\left(\theta/2\right)}-\sqrt{1+\kappa^2/2\varepsilon S}\right]}{\left\langle\sqrt{1-\kappa^2\sin^2\left(\theta/2\right)}\right\rangle}, \qquad \text{(E.7)}$$

where (4.2) is used for $\left(v_{\|}+u\right)$ and the κ^2 integral is only over the passing$\left(0<\kappa^2<1\right)$ region.

To leading order

$$\frac{\left[\sqrt{1-\kappa^2\sin^2\left(\theta/2\right)}-\sqrt{1+\kappa^2/2\varepsilon}\right]}{\left\langle\sqrt{1-\kappa^2\sin^2\left(\theta/2\right)}\right\rangle}\approx\frac{\pi\left[1-\sqrt{1+\kappa^2/2\varepsilon}\right]}{2E\left(\kappa\right)}, \quad \text{(E.8)}$$

where the elliptic function in the denominator changes from $\pi/2$ at $\kappa=0$ to 1 $\kappa=1$. Our goal is to demonstrate that integral (E.1) is small in $\sqrt{\varepsilon S}$. For this purpose we can replace $E\left(\kappa\right)$ with $E\left(0\right)=\pi/2$ since this does not change the order of the estimate for (E.1). Thus, the integral over κ^2 in (E.7) is approximately evaluated to give

$$\int_0^1\frac{d\kappa^2}{\left(\kappa^2+2\varepsilon S\right)}\frac{\pi\left[1-\sqrt{1+\kappa^2/2\varepsilon S}\right]}{2E\left(\kappa\right)}\approx$$

$$-\frac{1}{\sqrt{2\varepsilon S}}\int_0^1\frac{d\kappa^2\left(\sqrt{2\varepsilon S}-\sqrt{\kappa^2+2\varepsilon S}\right)}{\left(\kappa^2+2\varepsilon S\right)}\approx 2\sqrt{2\varepsilon S}\,. \quad \text{(E.9)}$$

Hence, noticing that in (E.7) the integral (E.9) is preceded by a factor of εS we obtain the desired result (4.58) to leading order in the expansion parameter, $\int d^3vg\propto\sqrt{\varepsilon S}\ll 1$.

F Comparison to Shaing and Hazeltine

Here, using s streamlined notation that ignores all irrelevant functions (such as B, Ω, W, I, $\partial f_M/\partial\psi$, ...) we illustrate the subtle difference between our solution and that of Shaing and Hazeltine for the localized piece of the distribution function. To do so we define $\omega \equiv v_{\|} + u = S\left(v_{\|} + u_*\right) \equiv S\omega_*$, and employ $\omega^2/2S = \left(1-\lambda\right)$ to write $\omega\,\partial\omega/\partial\lambda = -S$ and $\partial/\partial\lambda = -\left(S/\omega\right)\partial/\partial\omega$. Then, the constraint equation to be solved in our variables is

$$\left\langle\omega\right\rangle\partial g/\partial\lambda = \left\langle\omega\,\partial\omega/\partial\lambda\right\rangle,$$

while in the variables of Shaing and Hazeltine our equation becomes

$$\left(\left\langle\omega\right\rangle/\omega\right)\partial g/\partial\omega = 1,$$

where the derivatives and averages are to be taken at fixed ψ_*, and we write $f = \psi_* - \psi - u + g = g - \omega$. In terms of f we find the localized piece of the distribution function to be

$$\partial f/\partial\omega = \left(\omega/\left\langle\omega\right\rangle\right) - 1.$$

Shaing and Hazeltine write $f_{SH} = -\psi + g_{SH}$ and solve

$$\left(\left\langle\omega\right\rangle/\omega\right)\partial g_{SH}/\partial\omega = C$$

and rewrite this equation in terms of f_{SH} to obtain

$$\partial f_{SH}/\partial\omega = C\left(\omega/\left\langle\omega\right\rangle\right) - \partial\psi/\partial\omega,$$

where C is a constant and the ω derivative of ψ must be performed holding $\psi_* = \psi - v_{\|}$ fixed. To perform this derivative Shaing and Hazeltine implicitly assume that they can replace ψ by $\psi + u_*$ since $\partial u_* / \partial \omega = 0$ as the use

$$\partial \psi / \partial \omega = \partial \left(\psi + u_* \right) / \partial \omega = \partial \left(v_{\|} + u \right) / \partial \omega = \partial \omega_* / \partial \omega = 1 / S .$$

As a result, they obtain

$$\partial f_{SH} / \partial \omega = C \left(\omega / \langle \omega \rangle \right) - 1 / S .$$

The boundary condition the give them $C = 1 / S$ and the localized piece of the distribution function becomes

$$\partial f_{SH} / \partial \omega = \left[\left(\omega / \langle \omega \rangle \right) - 1 \right] / S ,$$

which has the extra $1 / S$ factor. This extra $1 / S$ results from u_* being implicitly inserted, instead of including the u factor by employing $f_{SH} = -\psi - u + g_{SH}$ at the outset. By inserting the u at the start we are making use of the energy conservation property of the ion-ion collision operator, namely $C \left\{ u v^2 f_M \right\} = 0$. Inserting u_* later gives an error because $C \left\{ u_* v^2 f_M \right\} \neq 0$. The erroneous $1 / S$ factor gets squared in the Shaing and Hazeltine evaluation of the ion heat flux, thereby accounting for the difference between our result and theirs.